Fall 2015

# Improving understanding of haze pollution In the North China Plain via atmospheric modeling and data assimilation

Meng Gao
*University of Iowa*

# IMPROVING UNDERSTANDING OF HAZE POLLUTION IN THE NORTH CHINA PLAIN VIA ATMOSPHERIC MODELING AND DATA ASSIMILATION

by

Meng Gao

A thesis submitted in partial fulfillment
of the requirements for the Doctor of Philosophy
degree in Chemical and Biochemical Engineering in the
Graduate College of
The University of Iowa

December 2015

Thesis Supervisor: Professor Gregory R. Carmichael

Graduate College
The University of Iowa
Iowa City, Iowa

CERTIFICATE OF APPROVAL

_____

PH.D. THESIS

_____

This is to certify that the Ph.D. thesis of

Meng Gao

has been approved by the Examining Committee for
the thesis requirement for the Doctor of Philosophy degree
in Chemical and Biochemical Engineering at the December 2015 graduation.

Thesis Committee: _____
Gregory R. Carmichael, Thesis Supervisor

_____
Charles O. Stanier

_____
Scott N. Spak

_____
Patrick T. O'Shaughnessy

_____
David G. Rethwisch

To My Family

Everything has beauty, but not everyone sees it.

——Confucius

**ACKNOWLEDGEMENTS**

There are many people that I would like to thank. First and foremost, I would like to express my deepest gratitude to my Thesis Supervisor Professor Gregory Carmichael for taking me as his student and for his guidance, patience, encouragement, and support during my Ph.D. journey. He always respects and allows me to pursue what I want to do on research, and gives me insightful suggestions. He explained what a great scientist, a great advisor, and a great friend should be like in his words and deeds. I also want to acknowledge my mentor, Prof. Stanier, for his concern about my study and life at uiowa. Special thanks to Prof. Spak for his suggestions and help in my health impact assessment and remote sensing related studies. Thanks to Prof. O'Shaughnessy and Prof. Rethwisch for teaching interesting courses and being great thesis committee members. I thank all the CBE faculty members for providing me great education, and CGRER staff Jane Frank, Jeremie Moen, and Amy Parker for administrative and technical support. I would like to thank Dr. Pablo Saide, Dr. Man Yu, Dr. Ashish, and Dr. Pallavi Marrapu for their help and useful suggestions on research and life. Thanks to other CGRER members and other people I got to know in iowa city for being good friends.

Thanks to Dr. Zifang Wang and his group for help on the MICS-Asia project, and hospitality and friendship during my summer stay at LAPC. I appreciate the valuable measurements from Dr. Yuesi Wang and his group at LAPC/CERN-SCAS (Dr. Jinyuan Xin, Dr. Zirui Liu, and Dr. Dongsheng Ji), and emission inventory from Dr. David Streets, Dr. Qiang Zhang, and Dr. Zifeng Lu. I thank Prof. Sarath Guttikunda from DRI, Dr. Gabi Pfister and Dr. Rajesh Kumar from NCAR for sharing some important codes with me.

At last, I would like to express utmost thanks to my family in Nanjing for their unconditional love and support.

## ABSTRACT

Frequent haze events have been happening in the North China Plain (NCP) and the severity of these events has attracted massive attention from both the public and the scientific community. Extremely high aerosol loadings in these haze events significantly influence visibility, human health and climate. Thus, improving the scientific understanding of haze pollution is of great importance. Furthermore, air quality modeling remains challenging due to large uncertainties in the emission inventory and incomplete parameterizations in the current model. This thesis aims to improve the understanding of haze pollution in the NCP using a regional model called WRF-Chem and to improve performance of the WRF-Chem model through various strategies, including finding proper model settings, incorporating missing mechanism into the current model, and applying data assimilation techniques.

The analyses of the January 2010 haze event show that it was mainly caused by high emissions of air pollutants and stagnant winter weather (low wind speeds, strong temperature inversion). The importance of secondary aerosol formation and cloud chemistry in winter haze was also emphasized by calculating the increasing ratios of primary aerosols, secondary inorganic aerosols and secondary organic aerosols from non-haze days to haze days, and by quantifying the increase in $PM_{2.5}$ concentrations due to cloud chemistry. The contribution of regional transport to haze in Beijing was studied. It was found that non-local sources contributed about 47.8% to the $PM_{2.5}$ concentrations in Beijing in haze days and sources of the non-local contributions were primarily from south Hebei, Shandong and Henan provinces. The high aerosol loadings were shown to have important feedbacks to decrease boundary layer heights by more than 100 meters and increase $PM_{2.5}$ by about 20$\mu g/m^3$ in some areas.

The responses of $PM_{2.5}$ to emission changes suggest that increases in $SO_2$, OC and $NH_3$ emissions may be the main causes of increasing haze occurrences since surface sulfate and OC aerosols were estimated to increase by 30.8% and 26.5% due to emission changes from 1985 to 2010. Increasing $NH_3$ emissions also significantly increased $PM_{2.5}$ concentrations. These sensitivities are important supplements to previous studies conducted in Europe and the United States. In addition, the impacts of meteorology changes on $PM_{2.5}$ concentrations were also investigated using this online coupled model, which are closer to what is happening in the atmosphere compared with those results using offline models. It was found that increases in temperature lead to increases in sulfate, nitrate, and ammonium because of higher reaction rate, higher concentrations of OH radicals and lower boundary layer heights, and an increase in Relative Humidity (RH) promoted more water aerosols and clouds, but caused decreases in dry $PM_{2.5}$ concentrations because of higher wet deposition rate.

The WRF-Chem model was first applied to evaluate short-term health risks of haze events, which overcome the shortcomings of observations that have less spatial information. Health impacts assessments show that the $PM_{2.5}$ concentrations in January were estimated to cause 690 (95% Confidence Interval (CI): (490, 890)) premature deaths, 45350 (95% CI: (21640, 57860)) acute bronchitis and 23720 (95% CI: (17090, 29710)) asthma cases in Beijing area, leading to about 253.8 (95% CI: (170.2, 331.2)) million US$ losses. These results directly stressed the importance of implementing pollution control policies.

The laboratory measured RH dependent $SO_2$ uptake coefficients were used to incorporate heterogeneous sulfate formation into the WRF-Chem model, which substantially improved the model performance in simulating sulfate during haze. The newly developed data assimilation system for the WRF-Chem model was first applied to constrain anthropogenic aerosol radiative

forcing in China. The estimated daytime monthly mean anthropogenic aerosol radiative forcing was estimated to be -29.9W/$m^2$ at the surface, 27.0W/$m^2$ inside the atmosphere, and -2.9W/$m^2$ at the top of the atmosphere. This data assimilation system has been approved to be effective to reduce errors in aerosol modeling, and can be additionally applied in air quality forecasting and health impacts assessments.

This thesis elucidated the roles of meteorology, secondary aerosol formation, regional transport, and aerosol feedbacks in winter haze formation, clarified the impacts of emission changes and meteorology changes on $PM_{2.5}$ concentrations, directly emphasized the importance of implementing pollution control strategies using assessments of health and climate effects, and improved model performance in simulating sulfate and $PM_{2.5}$ via incorporating heterogeneous sulfate formation and assimilating surface $PM_{2.5}$ concentrations. This thesis also provided some implications for policy makers. Priorities should be given to control $SO_2$, $NH_3$, and OC emissions, which can be achieved by promoting the shift from coal/biofuel to cleaner energy, and by changing animal feeding and housing ways. In addition, more attention to greenhouse gases and absorbing aerosols is still necessary since absorbing aerosols play important roles in aerosol feedbacks, aerosol feedbacks can aggravate haze pollution, and increases in temperature may increase aerosol concentrations. To protect the public health, it is of great importance to predict air pollution episodes, release alerts of incoming severe haze episodes, and take emergency measures to reduce pollution levels.

## PUBLIC ABSTRACT

Frequent haze events have been happening in the North China Plain (NCP), and the severity of these events has attracted massive attention from both the public and the scientific community. Extremely high aerosol loadings in these haze events significantly influence visibility, human health and climate. Thus, improving understanding of haze pollution is of great importance. Furthermore, air quality modeling remains challenging.

This thesis elucidated the roles of meteorology, secondary aerosol formation, regional transport, and aerosol feedbacks in winter haze formation, clarified the impacts of emission changes and meteorology changes on $PM_{2.5}$ concentrations, directly emphasized the importance of implementing pollution control strategies using assessments of health and climate effects, and improved model performance in simulating sulfate and $PM_{2.5}$ via incorporating heterogeneous sulfate formation and assimilating surface $PM_{2.5}$ concentrations. This thesis also provided some implications for policy makers. Priorities should be given to control $SO_2$, $NH_3$, and OC emissions, which can be achieved by promoting the shift from coal/biofuel to cleaner energy, and by changing animal feeding and housing ways. In addition, more attention to greenhouse gases and absorbing aerosols is still necessary since absorbing aerosols play important roles in aerosol feedbacks, aerosol feedbacks can aggravate haze pollution, and increases in temperature may increase aerosol concentrations. To protect the public health, it is of great importance to predict air pollution episodes, release alerts of incoming severe haze episodes, and take emergency measures to reduce pollution levels.

**TABLE OF CONTENTS**

## LIST OF TABLES

## LIST OF FIGURES

# CHAPTER 1: GENERAL INTRODUCTION

## 1.1 Motivation and Importance of Work

Haze is defined as an air pollution phenomenon where horizontal visibility is less than 10 km caused by aerosol particles, such as dust and Black Carbon (BC), suspended in the atmosphere (CMA, 2010; Tao et al., 2012). China has been undergoing rapid industrialization and urbanization processes, leading to severe haze pollution, which is characterized by large amounts of fine particles ($PM_{2.5}$, particles with diameter less than or equal to 2.5 micrometers) in the air. Van Donkelaar et al. (2010) derived global map of $PM_{2.5}$ averaged over 2001-2006 by using total-column aerosol measurements from satellite and vertical distribution information from a global model. As shown in Van Donkelaar et al. (2010), $PM_{2.5}$ concentrations in east China are much higher than in most other countries.

Large amounts of $PM_{2.5}$ during haze efficiently reduce visibility, and accordingly affect land, sea and air traffic safety. It can also directly enter human body and adhere to lungs to cause respiratory and cardiovascular diseases (Liu et al., 2013). Pope et al. (2009) found that an increase of $10\mu g/m^3$ in the concentration of $PM_{2.5}$ contributed to an estimated decrease in mean life expectancy of 0.61±0.20 years in the United States. Time-series analysis showed that short-term increase in hospital admission rates is related to $PM_{2.5}$, especially for heart failure hospitalization, which increased 1.28% for every $10\mu g/m^3$ increase in daily mean $PM_{2.5}$ concentrations (Dominici et al., 2006). Lim et al. (2012) estimated that ambient particulate matter pollution is among the top global risk factors, and it is the $4^{th}$ risk factor in rapidly urbanizing East Asia (China). In addition to adverse physical health effects, it has been pointed out that pollution is also associated with stress and depression symptoms (Hyslop, 2009).

Moreover, haze affects climate and ecosystems via altering radiation (Sun, et al., 2006; Liu et al., 2013). Ramanathan et al. (2001) estimated that the great Indo-Asian haze has a large negative forcing (-20±4 $W/m^2$) at the surface and also significantly heats the atmosphere. It was also reported that aerosol pollution over Asia is impacting global air circulations and it is likely to change weather patterns over North America (Wang et al., 2014c).

A series of severe haze events have been frequently happening in city clusters (e.g., Beijing-Tianjin-Hebei (BTH), Yangtze River Delta, and Pearl River Delta clusters) in China and have become critical concerns due to its above-mentioned adverse influences on visibility, public health (both physical and psychological), and climate. Haze in Beijing and surrounding North China Plain (NCP) cities even attracts more attention because of extremely high $PM_{2.5}$ concentrations during haze and high occurrences, especially in winter. For example, in January 2013, a severe and long-lasting haze episode occurred over eastern and northern China. According to the monitoring data by the Chinese Academy of Sciences (CAS), downtown Beijing's daily mean $PM_{2.5}$ concentrations exceeded 35 $\mu g/m^3$ (the 24-hour $PM_{2.5}$ standard in the United States) for 27 days in January (He et al., 2014; Wang et al., 2014a) and the hourly maximum $PM_{2.5}$ was 680$\mu g/m^3$. Beijing is located at the northern tip of the NCP, with the Yanshan mountains range to the north, Taihang mountains range to the west, and with flat land to the east and south. This kind of topography is not favorable for diffusion of air pollutants under southerly winds conditions. The main causes of winter haze in the NCP include high anthropogenic emissions and unfavorable meteorological conditions, but their roles have still not been well understood.

The past decade has witnessed advances in air quality modeling, which are used to study the evolution and temporal and spatial variability of air pollutants. One notable improvement is the

inclusion of interactions between meteorology and chemistry in online coupled models and this kind of model will be employed in this research. Nevertheless, air quality modeling is still challenging due to large uncertainties related to: incomplete or inaccurate emissions data, inaccurate initial and boundary conditions due to lack of key measurements, poorly parameterized processes in models, and other factors (Carmichael et al., 2008). As a result, large discrepancies can exist between model and observations, and these discrepancies lead to large uncertainties in estimates of above-mentioned health and climate effects. Data assimilation has been proved to be promising to reduce these discrepancies, but its applications in air quality studies in China are quite limited. The concept of data assimilation is introduced in chapter 6, including literature review, and summary of the current state of the science.

## 1.2 Objectives

This thesis is focused on understanding the formation mechanism of winter haze in the NCP and its health and climate impacts using the chemistry version of the Weather Research and Forecasting model (WRF-Chem) and a newly developed data assimilation tool.

Specifically, five objectives are addressed:

1. Investigate the roles of meteorology, secondary aerosol formation, regional transport, and aerosol feedbacks in winter haze formation in the North China Plain (NCP).

2. Examine the responses of $PM_{2.5}$ concentrations to emission changes ($SO_2$, $NH_3$, $NH_4$, BC, and OC) and meteorology changes (temperature, relative humidity, and wind speeds) during winter haze.

3. Evaluate health impacts and health-related economic losses due to severe haze events.

4. Improve model's performance in simulating sulfate during haze via incorporating heterogeneous chemistry.

5. Apply new data assimilation technique to improve aerosol predictions and evaluate climate effects based on improved aerosol predictions.

## 1.3 WRF-Chem Overview

There are two types of models, namely online and offline, for air quality modeling. Offline models do not consider feedbacks between air quality and meteorology, causing losses of important processes (Zhang, 2008). For online models, there are also two types: online integrated and online access models. Online integrated models compute meteorological and chemical fields simultaneously on the same grid. Online access models may have different spatial grids, and meteorology and chemistry models are linked through a model interface (Baklanov et al., 2014). The WRF-Chem model is an online integrated model, which has treatments of aerosol direct and indirect effects. The flow chart of WRF-Chem is shown in Figure 1.1. Terrestrial data and gridded meteorological data are the main inputs for the WRF Preprocessing System (WPS) and outputs from WPS together with emissions (anthropogenic, biogenic and biomass burning emissions) are inputs for the WRF-Chem model. The most frequently used gridded meteorological data is the 1º x 1ºNCEP FNL final analyses. The emissions used in this thesis will be introduced in the next section. Programs like NCL, GrADS can be used to visualize the outputs from WRF-Chem, and are used in this study. MOZART-4 (Model for Ozone and Related chemical Tracers, version 4) forecasts can be used as chemical initial and boundary conditions.

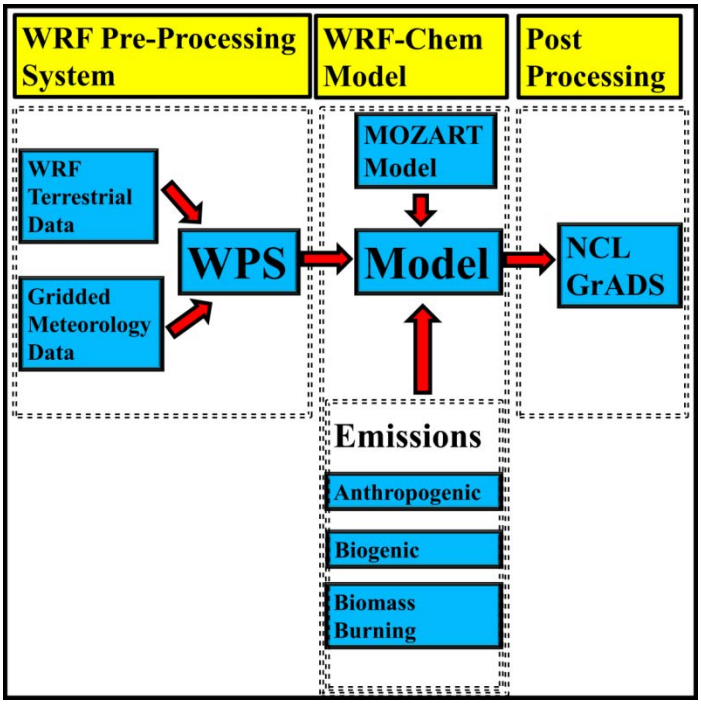


Figure 1.1. WRF-Chem flow chart

The WRF-Chem model considers various physical and chemical processes, such as transport, deposition, photolysis, and radiation. Each process has numerous scheme options. The standard gas phase chemistry options in WRF-Chem include the CBMZ, RADM2, MOZART and it is convenient to add mechanisms using a tool called KPP (Damian et al., 2002). More detailed descriptions of the WRF-Chem model can be found in Grell et al. (2005).

## 1.4 Emissions

The main difference between running WRF with and without chemistry is the inclusion of emission data, which include anthropogenic emissions, biogenic emissions and biomass burning emissions. In this research, "Mix for Model Inter-Comparison Study-Asia (MICS-Asia)" emissions are used. The anthropogenic inventory for China is from the Multi-resolution

Emission Inventory for China (MEIC, http://www.meicmodel.org/) database developed by Tsinghua University. This combined emission inventory includes emissions of sulfur dioxide ($SO_2$), nitrogen oxides ($NO_x$), CO, non-methane volatile organic compounds (NMVOC), $NH_3$, BC, OC, $PM_{2.5}$, $PM_{10}$, and carbon dioxide ($CO_2$) by five sectors (power, industry, residential, transportation and agriculture) in 2008 and 2010. Spatial resolution is 0.25×0.25 degree and temporal resolution is one month.

Biogenic emissions are predicted hourly by the MEGAN algorithm (Guenther et al., 2006) using information provided by WRF. MEGAN was developed for estimating the net emission of aerosols and gases from terrestrial ecosystems into atmosphere and land cover, weather and chemical composition of atmosphere are considered to be the driving variables (http://lar.wsu.edu/megan/). Since the study periods are winter, biomass burning is not significant, particularly in the NCP, so it is not included in this research.

## 1.5 Thesis Organization

Details of this research are shown in the following chapters. Chapter 2 focuses on the formation mechanism of the 2010 regional winter haze in the NCP. This study explains the causes of this haze event from several aspects, including roles of meteorology, secondary aerosol formation, regional transport, and aerosol feedbacks. In addition, the role of BC in the aerosol feedbacks has also been studied. This chapter is based on the results published in Gao et al. (2015a). Chapter 3 focuses on the responses of winter $PM_{2.5}$ to emission and meteorology changes. The causes of the increasing haze frequency are still unknown, which may result from huge emission changes due to rapid industrialization and urbanization processes that happened in

the past three decades. In addition, it may be also related to meteorology changes. This study was designed to investigate how these factors are related. Chapter 4 is focused on the assessment of health impacts and economic losses of the 2013 January haze event in Beijing. Beijing is one of the most populated cities in the world and numerous lives are endangered when pollution hazard happens. Therefore, health impacts and health-related economic losses are needed to be quantified to provide the basis for air pollution control. This chapter is based on the results published in Gao et al. (2015b). Chapter 5 is focused on the incorporation of heterogeneous sulfate formation since sulfate aerosols are largely underestimated by current models in many previous studies. It was pointed out that the missing heterogeneous sulfate formation can probably explain these underestimations (He et al., 2014; Y. Wang et al., 2014b; Zheng et al., 2015). This study also examines the sensitivity of simulated sulfate aerosol to $SO_2$ emissions. Chapter 6 focuses on assimilating surface $PM_{2.5}$ measurements to constrain anthropogenic radiative forcing estimates. Although there have been great advances in air quality modeling in the past several decades, disagreements between model results and observations still exist, which will lead to uncertainties in estimates of health and climate impacts. This study applies data assimilation technique to constrain the estimate of aerosol climate impacts. Chapter 7 is a summary of this thesis and discussion of future research directions.

## 1.6 References


Baklanov, a., Schlünzen, K., Suppan, P., Baldasano, J., Brunner, D., Aksoyoglu, S., Carmichael, G., Douros, J., Flemming, J., Forkel, R., Galmarini, S., Gauss, M., Grell, G., Hirtl, M., Joffre, S., Jorba, O., Kaas, E., Kaasik, M., Kallos, G., Kong, X., Korsholm, U., Kurganskiy, a., Kushta, J., Lohmann, U., Mahura, a., Manders-Groot, a., Maurizi, a., Moussiopoulos, N., Rao, S.T., Savage, N., Seigneur, C., Sokhi, R.S., Solazzo, E., Solomos, S., Sørensen, B., Tsegas, G., Vignati, E., Vogel, B., Zhang, Y., 2014. Online coupled regional meteorology chemistry models in Europe: Current status and prospects. Atmos. Chem. Phys. 14, 317–398. doi:10.5194/acp-14-317-2014

Carmichael, G.R., Sandu, A., Chai, T., Daescu, D.N., Constantinescu, E.M., Tang, Y., 2008. Predicting air quality: Improvements through advanced methods to integrate models and measurements. J. Comput. Phys. 227, 3540–3571. doi:10.1016/j.jcp.2007.02.024

China, M.A., 2010. Observation and forecasting levels of haze.

Damian, V., Sandu, A., Damian, M., 2002. The kinetic preprocessor KPP-a software environment for solving chemical kinetics. Comput. Chem. … 26, 1567–1579.

Dominici, F., Peng, R.D., Bell, M.L., Pham, L., McDermott, A., Zeger, S.L., Samet, J.M., 2006. Fine particulate air pollution and hospital admission for cardiovascular and respiratory diseases. JAMA-J. Am. Med. Assoc. 295, 1127–34. doi:10.1001/jama.295.10.1127

Ezzati, M., Dockery, D.W., 2009. Fine-Particulate Air Pollution and Life Expectancy in the United States. N. Engl. J. Med.

Gao, M., Carmichael, G.R., Wang, Y., Saide, P.E., Yu, M., Xin, J., Liu, Z., Wang, Z., 2015a. Modeling study of the 2010 regional haze event in the North China Plain. Atmos. Chem. Phys. Discuss. 15, 22781–22822. doi:10.5194/acpd-15-22781-2015

Gao, M., Guttikunda, S.K., Carmichael, G.R., Wang, Y., Liu, Z., Stanier, C.O., Saide, P.E., Yu, M., 2015b. Health impacts and economic losses assessment of the 2013 severe haze event in Beijing area. Sci. Total Environ. 511, 553–561. doi:10.1016/j.scitotenv.2015.01.005

Grell, G. a., Peckham, S.E., Schmitz, R., McKeen, S. a., Frost, G., Skamarock, W.C., Eder, B., 2005. Fully coupled "online" chemistry within the WRF model. Atmos. Environ. 39, 6957–6975. doi:10.1016/j.atmosenv.2005.04.027

Guenther, a., Karl, T., Harley, P., Wiedinmyer, C., Palmer, P.I., Geron, C., 2006. Estimates of global terrestrial isoprene emissions using MEGAN (Model of Emissions of Gases and Aerosols from Nature). Atmos. Chem. Phys. Discuss. 6, 107–173. doi:10.5194/acpd-6-107-2006

He, H., Tie, X., Zhang, Q., Liu, X., Gao, Q., Li, X., Gao, Y., 2014. Analysis of the causes of heavy aerosol pollution in Beijing, China: A case study with the WRF-Chem model. Particuology. doi:10.1016/j.partic.2014.06.004

Hyslop, N.P., 2009. Impaired visibility: the air pollution people see. Atmos. Environ. 43, 182–195. doi:10.1016/j.atmosenv.2008.09.067

Lim, S.S., Vos, T., Flaxman, A.D., Danaei, G., Shibuya, K., Adair-Rohani, H., Amann, M., Anderson, H.R., Andrews, K.G., Aryee, M., Atkinson, C., Bacchus, L.J., Bahalim, A.N., Balakrishnan, K., Balmes, J., Barker-Collo, S., Baxter, A., Bell, M.L., Blore, J.D., Blyth, F., Bonner, C., Borges, G., Bourne, R., Boussinesq, M., Brauer, M., Brooks, P., Bruce, N.G., Brunekreef, B., Bryan-Hancock, C., Bucello, C., Buchbinder, R., Bull, F., Burnett, R.T., Byers, T.E., Calabria, B., Carapetis, J., Carnahan, E., Chafe, Z., Charlson, F., Chen, H., Chen, J.S., Cheng, A.T.-A., Child, J.C., Cohen, A., Colson, K.E., Cowie, B.C., Darby, S., Darling, S., Davis, A., Degenhardt, L., Dentener, F., Des Jarlais, D.C., Devries, K., Dherani, M., Ding, E.L., Dorsey, E.R., Driscoll, T., Edmond, K., Ali, S.E., Engell, R.E., Erwin, P.J., Fahimi, S., Falder, G., Farzadfar, F., Ferrari, A., Finucane, M.M., Flaxman, S., Fowkes, F.G.R., Freedman, G., Freeman, M.K., Gakidou, E., Ghosh, S., Giovannucci, E., Gmel, G., Graham, K., Grainger, R., Grant, B., Gunnell, D., Gutierrez, H.R., Hall, W., Hoek, H.W., Hogan, A., Hosgood, H.D., Hoy, D., Hu, H., Hubbell, B.J., Hutchings, S.J., Ibeanusi, S.E., Jacklyn, G.L., Jasrasaria, R., Jonas, J.B., Kan, H., Kanis, J. a, Kassebaum, N., Kawakami, N., Khang, Y.-H., Khatibzadeh, S., Khoo, J.-P., Kok, C., Laden, F., Lalloo, R., Lan, Q., Lathlean, T., Leasher, J.L., Leigh, J., Li, Y., Lin, J.K., Lipshultz, S.E., London, S., Lozano, R., Lu, Y., Mak, J., Malekzadeh, R., Mallinger, L., Marcenes, W., March, L., Marks, R., Martin, R., McGale, P., McGrath, J., Mehta, S., Mensah, G. a, Merriman, T.R., Micha, R., Michaud, C., Mishra, V., Mohd Hanafiah, K., Mokdad, A. a, Morawska, L., Mozaffarian, D., Murphy, T., Naghavi, M., Neal, B., Nelson, P.K., Nolla, J.M., Norman, R., Olives, C., Omer, S.B., Orchard, J., Osborne, R., Ostro, B., Page, A., Pandey, K.D., Parry, C.D.H., Passmore, E., Patra, J., Pearce, N., Pelizzari, P.M., Petzold, M., Phillips, M.R., Pope, D., Pope, C.A., Powles, J., Rao, M., Razavi, H., Rehfuess, E. a, Rehm, J.T., Ritz, B., Rivara, F.P., Roberts, T., Robinson, C., Rodriguez-Portales, J. a, Romieu, I., Room, R., Rosenfeld, L.C., Roy, A., Rushton, L., Salomon, J. a, Sampson, U., Sanchez-Riera, L., Sanman, E., Sapkota, A., Seedat, S., Shi, P., Shield, K., Shivakoti, R., Singh, G.M., Sleet, D. a, Smith, E., Smith, K.R., Stapelberg, N.J.C., Steenland, K., Stöckl, H., Stovner, L.J., Straif, K., Straney, L., Thurston, G.D., Tran, J.H., Van Dingenen, R., Van Donkelaar, A., Veerman, J.L., Vijayakumar, L., Weintraub, R., Weissman, M.M., White, R. a, Whiteford, H., Wiersma, S.T., Wilkinson, J.D., Williams, H.C., Williams, W., Wilson, N., Woolf, A.D., Yip, P., Zielinski, J.M., Lopez, A.D., Murray, C.J.L., Ezzati, M., AlMazroa, M. a, Memish, Z. a, 2012. A comparative risk assessment of burden of disease and injury attributable to 67 risk factors and risk factor clusters in 21 regions, 1990-2010: a systematic analysis for the Global Burden of Disease Study 2010. Lancet 380, 2224–60. doi:10.1016/S0140-6736(12)61766-8

Liu, X.G., Li, J., Qu, Y., Han, T., Hou, L., Gu, J., Chen, C., Yang, Y., Liu, X., Yang, T., Zhang, Y., Tian, H., Hu, M., 2013. Formation and evolution mechanism of regional haze: a case study in the megacity Beijing, China. Atmos. Chem. Phys. 13, 4501–4514. doi:10.5194/acp-13-4501-2013

Ramanathan, V., Crutzen, P.J., Lelieveld, J., Mitra, A.P., Althausen, D., Anderson, J., Andreae, M.O., Cantrell, W., Cass, G.R., Chung, C.E., Clarke, A.D., Coakley, J.A., Collins, W.D., Conant, W.C., Dulac, F., Heintzenberg, J., Heymsfield, A.J., Holben, B., Howell, S., Hudson, J., Jayaraman, A., Kiehl, J.T., Krishnamurti, T.N., Lubin, D., Mcfarquhar, G., Novakov, T., Ogren, J.A., Podgorny, I.A., Prather, K., Priestley, K., Prospero, J.M., Quinn, P.K., Rajeev, K., Rasch, P., Rupert, S., Sadourny, R., Satheesh, S.K., Shaw, G.E., Sheridan, P., Valero, F.P.J., 2001. Indian Ocean Experiment : An integrated analysis of the climate forcing and effects of the great Indo-Asian haze. J. Geophys. Res. 106.

Sun, Y., Zhuang, G., Tang, a A., Wang, Y., An, Z., 2006. Chemical characteristics of PM2.5 and PM10 in haze-fog episodes in Beijing. Environ. Sci. Technol. 40, 3148–55.

Tao, M., Chen, L., Su, L., Tao, J., 2012. Satellite observation of regional haze pollution over the North China Plain. J. Geophys. Res. Atmos. 117, n/a–n/a. doi:10.1029/2012JD017915

Van Donkelaar, A., Martin, R. V., Brauer, M., Kahn, R., Levy, R., Verduzco, C., Villeneuve, P.J., 2010. Global estimates of ambient fine particulate matter concentrations from satellite-based aerosol optical depth: Development and application. Environ. Health Perspect. 118, 847–855. doi:10.1289/ehp.0901623

Wang, Y., Yao, L., Wang, L., Liu, Z., Ji, D., Tang, G., Zhang, J., Sun, Y., Hu, B., Xin, J., 2014a. Mechanism for the formation of the January 2013 heavy haze pollution episode over central and eastern China. Sci. China Earth Sci. 57, 14–25. doi:10.1007/s11430-013-4773-4

Wang, Y., Zhang, Q., Jiang, J., Zhou, W., Wang, B., He, K., Duan, F., Zhang, Q., Philip, S., Xie, Y., 2014b. Enhanced sulfate formation during China's severe winter haze episode in January 2013 missing from current models. J. Geophys. Res. Atmos. 425–440. doi:10.1002/2013JD021426.Received

Wang, Y., Zhang, R., Saravanan, R., 2014c. Asian pollution climatically modulates mid-latitude cyclones following hierarchical modelling and observational analysis. Nat. Commun. 5, 3098. doi:10.1038/ncomms4098

Zhang, Y., 2008. Online-coupled meteorology and chemistry models : history , current status , and outlook. Atmos. Chem. Phys. 2895–2932.

Zheng, B., Zhang, Q., Zhang, Y., He, K.B., Wang, K., Zheng, G.J., Duan, F.K., Ma, Y.L., Kimoto, T., 2014. Heterogeneous chemistry: a mechanism missing in current models to explain secondary inorganic aerosol formation during the January 2013 haze episode in North China. Atmos. Chem. Phys. Discuss. 14, 16731–16776. doi:10.5194/acpd-14-16731-2014

# CHAPTER 2: MODELING STUDY OF THE 2010 REGIONAL HAZE EVENT IN THE NORTH CHINA PLAIN[21]

## 2.1 Abstract

The online coupled Weather Research and Forecasting-Chemistry (WRF-Chem) model was applied to simulate a haze event that happened in January 2010 in the North China Plain (NCP), and was validated against various types of measurements. The evaluations indicate that WRF-Chem provides reliable simulations for the 2010 haze event in the NCP. This haze event is mainly caused by high emissions of air pollutants in the NCP and stable weather conditions in winter. Secondary inorganic aerosols also played an important role and cloud chemistry had important contributions. Air pollutants outside Beijing contributed about 47.8% to the $PM_{2.5}$ levels in Beijing during this haze event, and most of them are from south Hebei, Shandong and Henan provinces. In addition, aerosol feedback has important impacts on surface temperature, Relative Humidity (RH) and wind speeds, and these meteorological variables affect aerosol distribution and formation in turn. In Shijiazhuang, Planetary Boundary Layer (PBL) decreased about 300m and $PM_{2.5}$ increased more than 20μg/$m^3$ due to aerosol feedback. Feedbacks associated to Black Carbon (BC) account for about 50% of the $PM_{2.5}$ increases and 50% of the PBL decreases in Shijiazhuang, indicating more attention should be paid to BC from both air pollution control and climate change perspectives.

[21] This work has been published as Gao et al. (2015).

## 2.2 Introduction

The North China Plain (NCP) is one of the most densely populated areas in the world and it has been the Chinese center of culture and politics since early times. Beijing, the capital of China, Tianjin, Shijiazhuang and other big cities with active economic developments are located in the NCP. This region is experiencing heavy haze pollution with record-breaking high concentrations of particulate matters (L. T. Wang et al., 2014). Haze is defined as an air pollution phenomenon where horizontal visibility is less than 10 km caused by aerosol particles, such as dust and Black Carbon (BC), suspended in the atmosphere (Tao et al., 2012). Its formation is highly related to meteorological conditions, emissions of pollutants and gas-to-particle conversion (Sun et al., 2006; Watson, 2002). Haze has attracted much attention for its adverse impacts on visibility and human health. During haze periods, reduced visibility affects land, sea and air traffic safety and the fine particles can directly enter the human body and adhere to lungs to cause respiratory and cardiovascular diseases (Liu et al., 2013). Moreover, haze affects climate and ecosystems via aerosol-cloud-radiation interactions (Sun, et al., 2006; Liu et al., 2013).

Because haze influences visibility, human health and climate (Gao et al., 2015b), numerous studies have used multiple methods to investigate physical, chemical and seasonal characteristics of aerosols during haze. The increase of secondary inorganic aerosols is considered to be an attribute of the haze pollution in east China (Tan et al., 2009; Zhao et al., 2013). Tan et al. (2009) studied the characteristics of aerosols in non-haze and haze days in Guangzhou, China and found that secondary pollutants (OC, $SO4^{2-}$, $NO^{3-}$ and $NH^{4+}$) were the major components of haze aerosols and they showed a remarkable increase from non-haze to haze days. Similar conclusions were drawn by Zhao et al. (2013) after studying the chemical characteristics of haze aerosols in

the NCP. Secondary Organic Aerosol (SOA) formation can also be significant during haze (Tan et al., 2009; Zhao et al., 2013). Studies of aerosol optical properties show that fine-mode aerosols were dominant during haze (Yu et al., 2011; Li et al., 2013). In addition, contributions of diverse factors to haze formation, such as biomass burning and regional transport, have been investigated. Chen et al. (2007) used MM5-CMAQ to reproduce the haze pollution in September 2004 in the Pearl Region Delta (PRD) region and discovered that sea-land breeze played an important role. Wang et al. (2009) discovered that almost 30-90 percent of the organics during the haze happened in June 2007 in Nanjing were from wheat straw burning. Cheng et al. (2014) concluded that biomass burning could cause haze issues and they found biomass burning contributed 37% of $PM_{2.5}$, 70% of Organic Carbon (OC) and 61% of Elemental Carbon (EC) based upon both modeling and measurement results of case study in summer 2011 in the Yangtze River Delta (YRD) region. These biomass burning events mainly occurred in summer and autumn in east and south China (Cheng et al., 2013, 2014; Li et al., 2010; Wang et al., 2007, 2009). To evaluate regional contributors to the haze in southern Hebei, Wang et al. (2012) simulated from 2001 to 2010 and concluded that Shanxi province and the northern Hebei were two major contributors, and winter was the worst season, followed by autumn and summer. X. Han et al. (2014) pointed out that the haze formation mechanism in winter in Beijing was different from that in summer and mass concentrations of $PM_{2.5}$ in winter were relatively higher and the compositions were different than in summer. The extreme winter haze in the NCP has attracted enormous scientific interests. It has been found the stagnant meteorological conditions (weak surface wind speed and low Planetary Boundary Layer (PBL) height) and secondary aerosol formation are the main causes of winter haze formation (S. Han et al., 2014; He et al., 2014b; K. Huang et al., 2014; Sun et al., 2014; Wang et al., 2014a; Zhao et al., 2013; Zheng et

al., 2014, 2015). Other causes proposed include high local emissions (He et al., 2014b; Zheng et al., 2014), enhanced coal combustion in winter (K. Huang et al., 2014; Sun et al., 2014), heterogeneous chemistry (He et al., 2014a; X. Huang et al., 2014b; Quan et al., 2014; Wang et al., 2014a, b; Zheng et al., 2014, 2015) and regional transport (Tao et al., 2014; Sun et al., 2014; L. T. Wang et al., 2014; Z. Wang et al., 2014; Zheng et al.,2014). It was also pointed out that fog processing (K. Huang et al., 2014), aerosol-radiation interactions (J. Wang et al., 2014; Z. Wang et al., 2014; B. Zhang et al., 2015) and nucleation events (Guo et al., 2014) may play important roles in winter haze formation.

Although previous studies have revealed characteristics and possible causes of winter haze in China, complex haze formation mechanisms still need further studies. Li et al. (2015) emphasized that regional transport of $PM_{2.5}$ is a major cause of severe haze in Beijing, but R. Zhang et al. (2015) pointed out that the evidence provided by Li et al. (2015) is insufficient and regional transport should be evaluated using chemical transport models. Furthermore, the contribution of aerosol feedbacks to $PM_{2.5}$ levels is controversial. Therefore, the roles of regional transport and aerosol-radiation interactions in haze events need to be better understood. In this study, the online coupled model WRF-Chem, which is capable of simulating aerosols' effects on meteorology and climate, is used to reproduce the severe haze event that happened in the NCP from 16 to 19 January 2010. During this haze event, the highest hourly $PM_{2.5}$ concentration reached 445.6 and 318.1 $\mu g/m^3$ in Beijing and Tianjin and the areas with low visibility covered most eastern China regions (Zhao et al., 2013). In this study, we address the following important questions: (1) what is the performance of the model configurations in representing the meteorological variables, and the physical and chemical characteristics of the aerosols during the selected study period?; (2) How does the haze build up and dissipate?; (3) How do the chemical

species of $PM_{2.5}$ change during haze period?; (4) Does regional transport play an import role in the 2010 haze event in Beijing?; (5) What is the contribution of aerosol feedback mechanisms to $PM_{2.5}$ levels during the haze event?; and (6) What is the role of BC absorption in the feedback mechanism? In section 2.3, we describe the model we use and model configuration, including emissions and used parameterization schemes. In section 2.4, surface meteorological, chemical observations, atmospheric sounding products, as well as remote sensing products are used to evaluate the model performance. In section 2.5, questions from (2) to (6) are answered in detail. Conclusions are provided in the section 2.6.

## 2.3 Model description and configuration

The WRF-Chem model version 3.5.1 was employed to simulate the 2010 haze event in the NCP region and aerosol-radiation interactions were included (Chapman et al., 2006; Fast et al., 2006). Domain settings are the same as those of Jing-Jin-Ji modeled area of Yu et al. (2012). As shown in Figure 2.1, three domains with two-way nesting were used and grid resolutions were 81km × 81km (domain 1), 27km × 27km (domain 2) and 9km × 9km (domain 3). The number of vertical grids used was 27 and the number of horizontal grids was 81×57, 49×49, and 55×55, respectively. The first domain covers most areas of the East Asia region, including China, Korea, Japan and Mongolia. Beijing was set to be the center of the innermost nested domain. The chemical and aerosol mechanism used was gas-phase chemical mechanism CBMZ (Zaveri and Peters, 1999) coupled with the 8-bin sectional MOSAIC model with aqueous chemistry (Zaveri et al., 2008). MOSAIC treats all the important aerosol species, including sulfate, nitrate, chloride, ammonium, sodium, BC, primary organic mass, liquid water and other inorganic mass (Zaveri et

al., 2008). Some of the physics configuration options include Lin cloud-microphysics (Lin et al., 1983), RRTM long wave radiation (Mlawer et al., 1997), Goddard short wave radiation (Chou et al., 1998), Noah land surface model, and the Yonsei University planetary boundary layer parameterization (Hong et al., 2006).

Emissions are key factors in the accuracy of air quality modeling results. Monthly 2010 Multi-resolution Emission Inventory for China (MEIC) (http://www.meicmodel.org/) was used as the anthropogenic emissions. This inventory includes emissions of sulfur dioxide ($SO_2$), nitrogen oxides ($NO_x$), Carbon Monoxide (CO), non-methane volatile organic compounds (NMVOC), $NH_3$, BC, organic carbon (OC), $PM_{2.5}$, $PM_{10}$, and carbon dioxide ($CO_2$) by several sectors (power generation, industry, residential, transportation, etc.). Biogenic emissions were calculated on an online way by the MEGAN model (Guenther et al., 2006). Meteorological initial and boundary conditions were obtained from the National Centers for Environmental Prediction (NCEP) Final Analysis (FNL) data set. Chemical initial and boundary conditions were taken from MOZART-4 forecasts (Emmons et al., 2010). The period from 11 to 24 January 2010 was chosen as the modeling period, covering the 2010 NCP haze period (from 16 to 19 January 2010). To overcome the impacts of initial conditions, three days were simulated and considered as spin-up time.

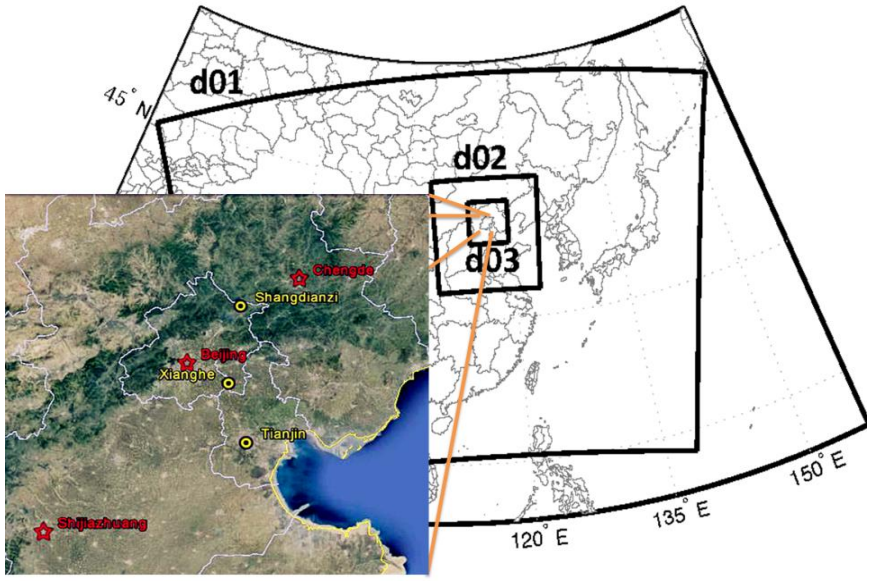


Figure 2.1. WRF-Chem modeling domain settings and locations of observations

## 2.4 Model evaluation

### 2.4.1 Observation data sets and evaluation metrics

Model evaluation was conducted in terms of both temporal variation and spatial distribution. Table 2.1 gives a summary of the observation data and variables used in the model evaluation. The meteorological variables, including 2 meter temperature (T2), 2 meter relative humidity (RH2) and 10 meter wind speed (WS10), at four stations (Beijing, Tianjin, Baoding and Chengde) were used. Surface concentrations of $PM_{2.5}$, $NO_2$, $SO_2$ at three sites (Beijing, Tianjin and Xianghe, shown in Figure 2.1), and Aerosol Optical Depth (AOD) at four sites (Beijing city, Beijing forest, Baoding city, Cangzhou city) were also used in the evaluation against measurements. $PM_{2.5}$ and AOD are typical variables to represent severity of haze pollution. To evaluate how model performs in simulating horizontal and vertical distributions of

meteorological and chemical variables, soundings of temperature and RH at Beijing, and AODs derived from CALIPSO were used in this study. The statistical metrics calculated include correlation coefficient R, mean bias (MB), mean error (ME), the root mean square error (RMSE), the normalized mean bias (NMB), the normalized mean error (NME), the mean fractional bias (MFB) and the mean fractional error (MFE). The definitions of these metrics can be found in Morris et al. (2005) and Willmott and Matsuura (2005).

Table 2.1. Observation data and variables used in this study

| Data sets [a] | Variables [b] | Data frequency | Number of sites used | Data sources |
|---|---|---|---|---|
| CMDSSS | T2, RH2, WS10 | Daily | 4 | http://cdc.cma.gov.cn/home.do |
| Atmospheric Sounding | T, RH | 12 hours | 1 | http://weather.uwyo.edu/upperair/sounding.html |
| CARE-China | $PM_{2.5}$, $NO_2$, $SO_2$ | Hourly | 3 | |
| CSHNET | AOD | Hourly | 4 | |
| SDZ | T1.5, RH1.5, WS10, $PM_{2.5}$, $NO_2$, CO | Hourly | 1 | Zhao et al. (2013) |
| CALIPSO | AOD | N/A | N/A | http://www-calipso.larc.nasa.gov/ |
| MODIS | AOD | Daily | N/A | http://ladsweb.nascom.nasa.gov/data/search.html |

[a]CMDSSS—China Meteorological Data Sharing Service System; CARE-China—Campaign on the atmospheric Aerosol Research network of China; CSHNET—Chinese Sun Hazemeter Network; SDZ—Observation data at Shangdianzi site are extracted from paper Zhao et al. (2013); CALIPSO—The Cloud-Aerosol Lidar and Infrared Pathfinder Satellite Observation; MODIS—the Moderate Resolution Imaging Spectroradiometer. [b]T2— temperature at 2m; RH2—relative humidity at 2m; WS10—wind speed at 10m; T1.5—temperature at 1.5m; RH1.5—relative humidity at 1.5m; AOD—Aerosol Optical Depth.

### 2.4.2 Meteorology simulations

Figure 2.2 shows the temporal variations of simulated and observed 24-h average temperature (a-d), relative humidity (e-h) and wind speed (i-l) at Beijing, Tianjin, Baoding and

Chengde stations. These observations were collected from the China Meteorological Data Sharing Service System (CMDSSS) data set. From normal days to haze days (gray shaded), temperature and relative humidity increased and wind speeds decreased. Generally, the variations of surface temperature, RH and wind speeds are captured by model, although overestimations of wind speed occur at the Chengde station throughout the whole period. Model mean, observation mean, MB, ME and RMSE were calculated and summarized in Table 2.2. The MB and RMSE for surface temperature vary from -2.0 to 2.0 K and from 1.5 to 3.2 K, respectively. The model underestimates temperature at Beijing, Tianjin and Baoding stations, and overestimates temperature at the Chengde station. RH agrees well with observations, with MB varying from -4.4% to 8.1% and RMSE varying from 6.4% to 11.1%. The magnitudes of MB and RMSE are comparable with those of L. T. Wang et al. (2014). The model shows good performance in simulating wind speed, with RMSE ranging from 1.1 to 1.6 m/s at Beijing, Tianjin and Baoding stations, below the level of "good" model performance criteria for wind speed prediction proposed by Emery et al. (2001). Wind speeds at the Chengde station were overestimated, with RMSE larger than the proposed criteria (2m/s).

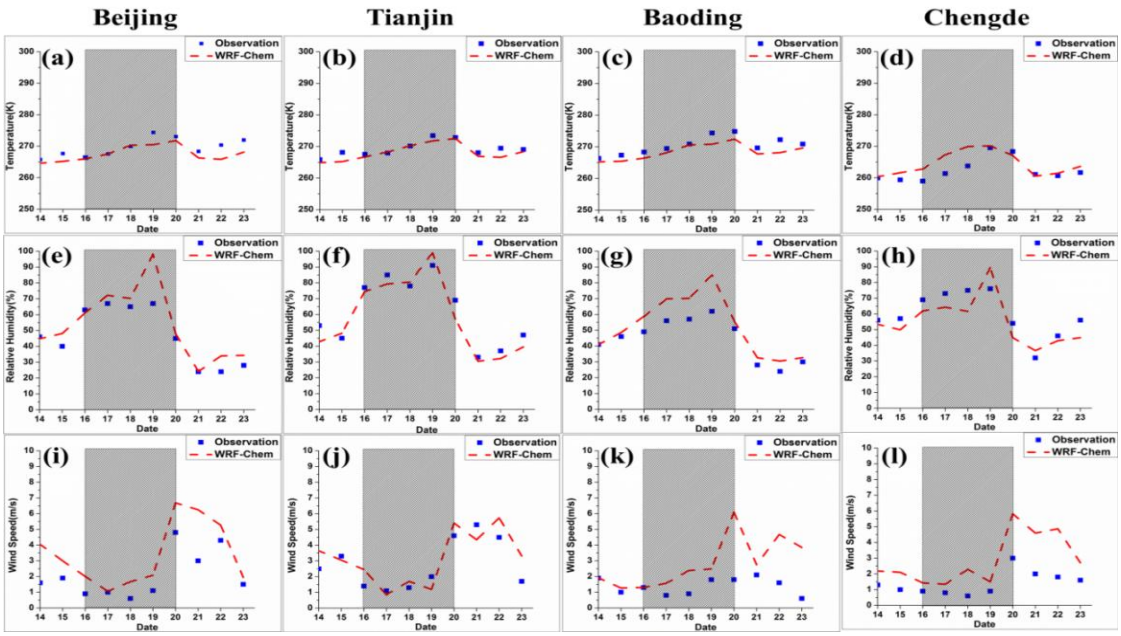


Figure 2.2. The temporal variations of observed and simulated 24-h average temperature (a-d), relative humidity (e-h) and wind speed (i-l) in the Beijing, Tianjin, Baoding, and Chengde stations

Table 2.2. Performance statistics for meteorological variables

| Variables | Beijing | | | | | Tianjin | | | | | Baoding | | | | | Chengde | | | | |
|---|---|---|---|---|---|---|---|---|---|---|---|---|---|---|---|---|---|---|---|---|
| | Obs. | Mod. | MB | ME | RMSE | Obs. | Mod. | MB | ME | RMSE | Obs. | Mod. | MB | ME | RMSE | Obs. | Mod. | MB | ME | RMSE |
| T2(K) | 269.5 | 267.6 | -1.9 | 2.0 | 2.5 | 269.3 | 268.1 | -1.1 | 1.2 | 1.5 | 270.4 | 268.5 | -2.0 | 2.0 | 2.3 | 262.5 | 264.5 | 2.0 | 2.4 | 3.2 |
| RH2 (%) | 46.9 | 53.4 | 6.6 | 7.2 | 11.1 | 61.5 | 58.4 | -3.1 | 5.9 | 6.4 | 44.4 | 52.5 | 8.1 | 8.1 | 10.4 | 59.4 | 55.0 | -4.4 | 8.0 | 8.8 |
| WS10(m/s) | 2.1 | 3.4 | 1.3 | 1.3 | 1.6 | 2.8 | 3.2 | 0.4 | 1.0 | 1.1 | 1.4 | 2.8 | 1.4 | 1.4 | 2.1 | 1.4 | 2.9 | 1.5 | 1.5 | 1.8 |

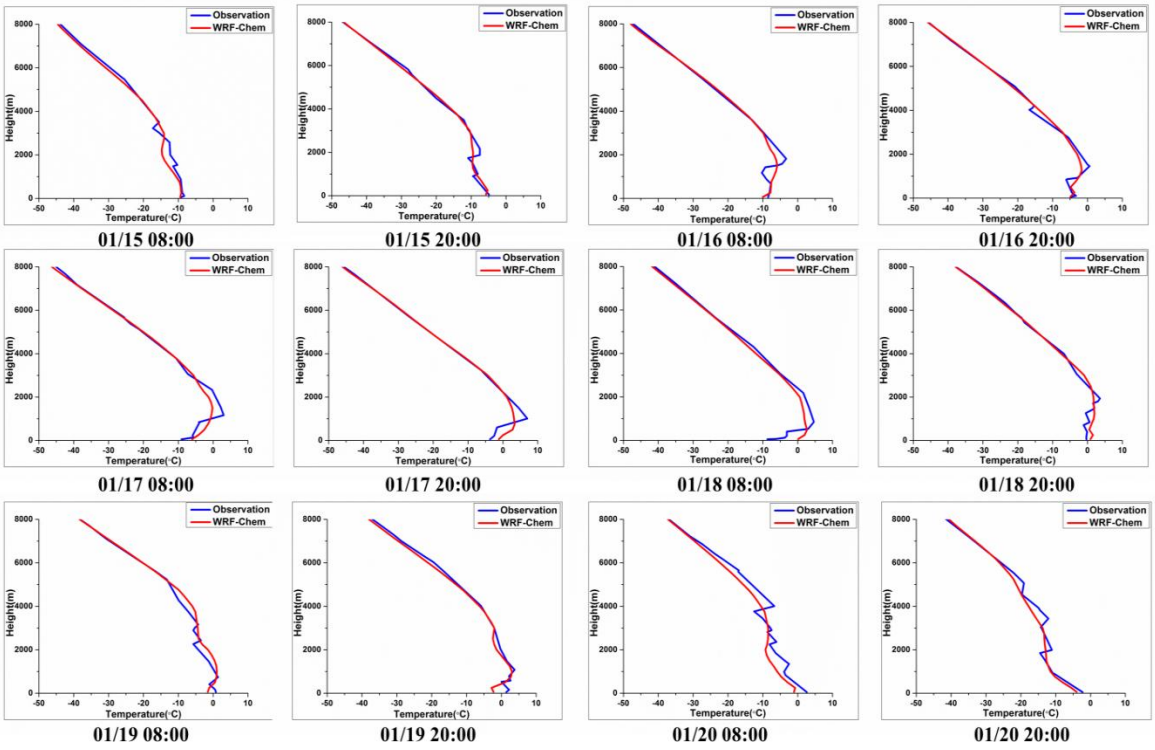


Figure 2.3. Simulated and observed vertical temperature profiles at 0800 and 2000 (China Standard Time, CST) from 15 January to 20 January

Figure 2.3 compares simulated and observed vertical temperature profiles at 0800 and 2000 (CST) from January 15 to January 20 at Beijing city. These atmospheric sounding data are from the NCAR Earth observing laboratory atmospheric sounding data set. The model captures the vertical profiles of temperature well. Obvious strong temperature inversions existed during the haze period (from 01/16 08:00 to 01/19 20:00) and the lapse rate during this period was about 5-15°C/km, indicating unfavorable conditions for diffusion of pollutants. Figure 2.4 shows the vertical profiles of RH. The model captures the general profiles of RH, although the performance is not as good as for temperature. Simulated RH deviates largely away from observations on January 18 and 19, when RH was high near the surface.

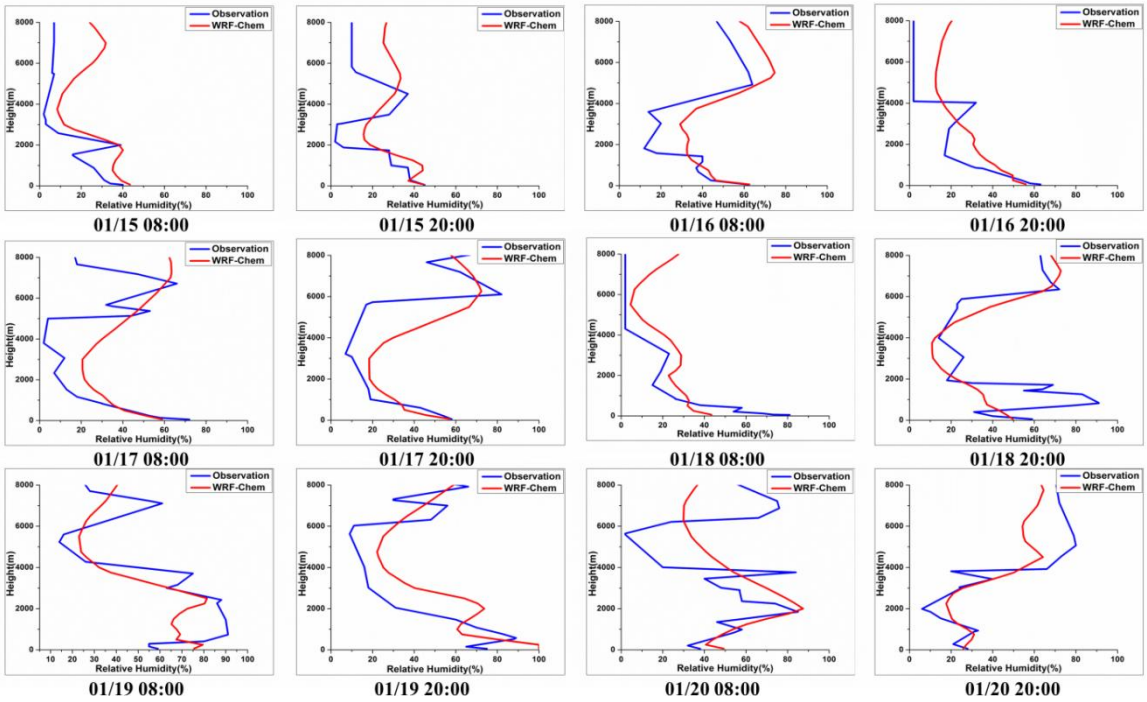


Figure 2.4. Simulated and observed vertical RH profiles at 0800 and 2000 (CST) from 15 January to 20 January

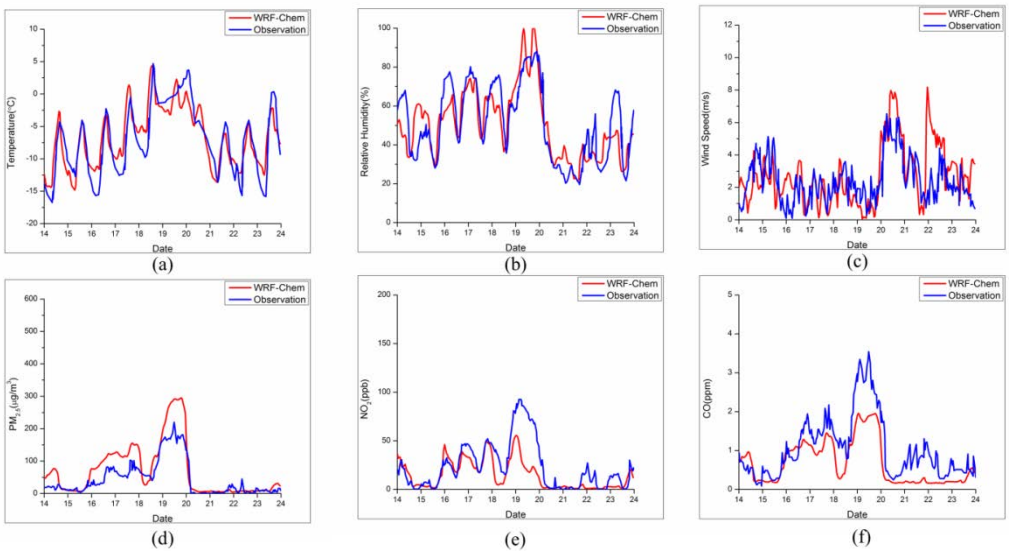


Figure 2.5. Simulated and observed hourly temperature, RH, wind speed, $PM_{2.5}$, $NO_2$ and CO in the Shangdianzi (SDZ) station

Figure 2.5(a-c) compares simulated and observed hourly temperature, RH and wind speed at SDZ station (shown in Figure 2.1) using observations from Zhao et al. (2013). Simulated variations of meteorological variables agree well with observations, despite RH was overestimated on January 19 and 20 (Figure 2.5(b)) and wind speed was overestimated on January 22 (Figure 2.5(c)), which is similar to the comparisons shown in Figure 2.2.

### 2.4.3 Chemical simulations

Figure 2.5(d-f) shows variations of simulated and observed hourly $PM_{2.5}$, $NO_2$ and CO at the SDZ station. The haze event started from 16 January with rapid increase of $PM_{2.5}$, $NO_2$, and CO concentrations and ended on 20 January. The magnitudes and trends over time of the simulated $PM_{2.5}$, $NO_2$ and CO are generally consistent with measurements, although overestimation of $PM_{2.5}$ and underestimations of $NO_2$ and CO exist during the haze days. Figure 2.6 shows the temporal variations of the simulated and observed $PM_{2.5}$, $NO_2$ and $SO_2$ at Beijing (a-c), Tianjin (d-f) and Xianghe (g-i) stations. $SO_2$ was overestimated in Beijing, but other simulations agree well with observations, especially for $PM_{2.5}$. Observation mean, model mean, MB, ME, NMB, NME, MFB, and MFE were calculated for 24-h average simulated and observed $PM_{2.5}$ at these three stations and summarized in Table 2.3. As shown in Table 2.3, the model underestimates $PM_{2.5}$ concentrations at all stations. NMBs for $PM_{2.5}$ are -8.5%, -26.9% and -39.1% at Beijing, Tianjin and Xianghe, respectively. MFBs at these three stations range from -21.8% to 0.4% and MFEs range from 26.3% to 50.7%. They are all within the criteria proposed by Boylan et al. (2006) that model performance is "satisfactory" when MFB is within ±60% and MFE is below 75%. Although the model performance for $PM_{2.5}$ is satisfactory, biases still exist, especially

during severe haze days. Reasons for the biases might be errors in meteorological variables, large uncertainties of emission inventory, effects of horizontal and vertical resolutions, and incomplete treatments of atmospheric chemistry. Many atmospheric chemistry reactions have been and are being proposed for PM formation in winter haze. For example, He et al. (2014a) proposed that mineral dust and $NO_x$ could promote the formation of sulfate in heavy pollution days. The sensitivity of the simulations to some of these factors will be discussed in future studies.

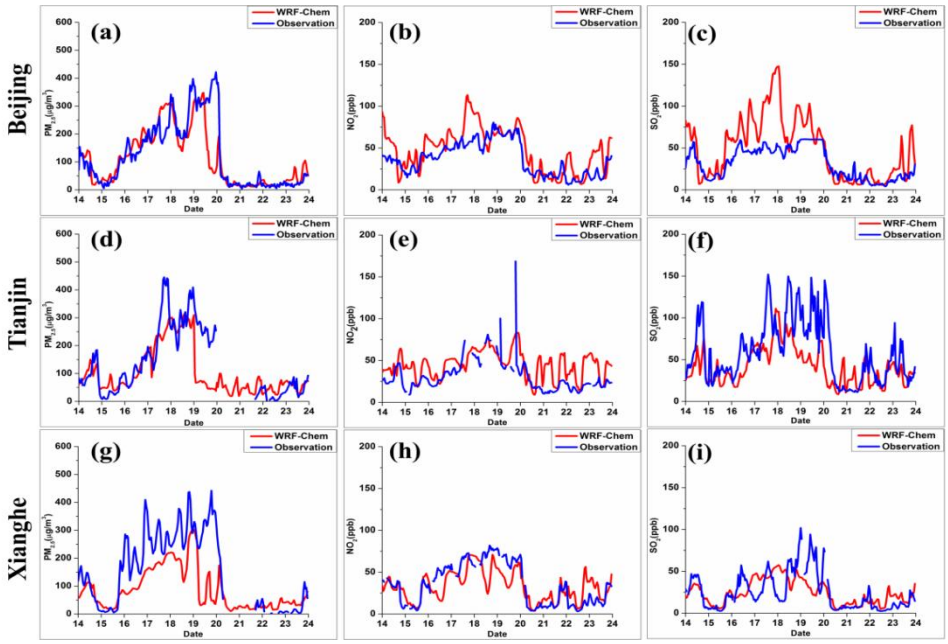


Figure 2.6. Temporal variations of the simulated and observed $PM_{2.5}$, $NO_2$ and $SO_2$ at Beijing (a-c), Tianjin (d-f) and Xianghe (g-i) stations

Table 2.3. Performance statistics of $PM_{2.5}$

| | Obs. (μg/m$^3$) | Model (μg/m$^3$) | R | MB (μg/m$^3$) | ME (μg/m$^3$) | NMB (%) | NME (%) | MFB (%) | MFE (%) |
|---|---|---|---|---|---|---|---|---|---|
| Beijing | 111.7 | 122.1 | 0.77 | -10.4 | 30.4 | -8.5 | 24.9 | 0.4 | 26.3 |
| Tianjin | 103.3 | 141.2 | 0.75 | -37.9 | 56.1 | -26.9 | 39.7 | -7.8 | 49.6 |
| Xianghe | 93.0 | 152.6 | 0.69 | -59.7 | 68.0 | -39.1 | 44.5 | -21.8 | 50.7 |

### 2.4.4 Simulations of optical properties

In WRF-Chem, aerosol optical properties are calculated at four specific wavelengths, 300nm, 400nm, 600nm, and 1000nm, while AOD observations from CSHNET, CALIPSO are not at these four wavelengths. To evaluate model performance of simulating AOD, we derived AOD at observation wavelengths based on Angstrom exponent relation (Schuster et al., 2006). Figure 2.7 compares simulated and observed AOD at 500nm in Beijing city (a), Beijing forest (b), Baoding city (c) and Cangzhou city (d). In severe haze days, AOD could not be retrieved , so the observerd AOD data in some days are missing. At all four stations, model agrees very well with observations.

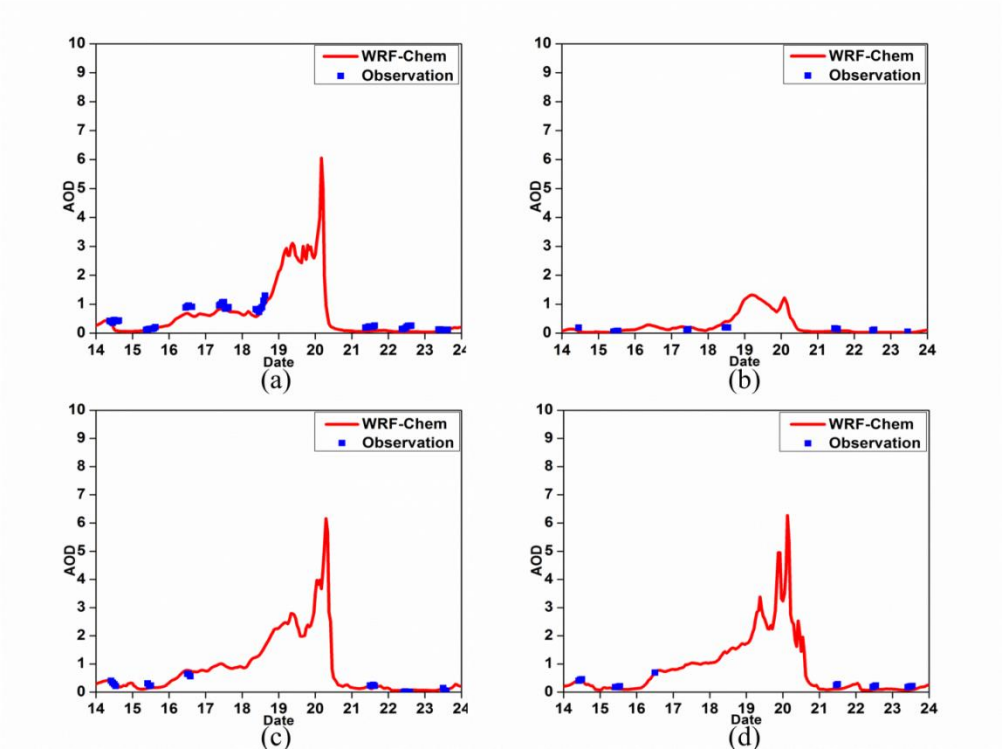


Figure 2.7. Simulated and measured AOD at 500nm at Beijing city (a), Beijing forest (b), Baoding city (c) and Cangzhou city

CALIPSO retrievals provide vertical curtains of aerosol and clouds. Figure 2.8 shows paths of the CALIPSO satellite, simulated extinction coefficient and observed plume top, and simulated AOD and CALIPSO retrieved AOD at 532nm at three moments: January 14 12:00(CST) (a-c), January 21 02:00(CST) (d-f), and January 21 12:00(CST) (g-i), respectively. There were no retrievals in the NCP during haze days. Figure 2.8(a), (d) and (g) show that CALIPSO satellite passed over the NCP region at these three moments. Simulated extinction coefficient matches observed plume top (Figure 2.8(b), (e) and (h)), indicating that the model captures the vertical distributions of aerosols. The model also has good performance in

simulating AOD at 532nm, although underestimations happen around latitude 36°N (Figure 2.8(c), (f) and (i)).

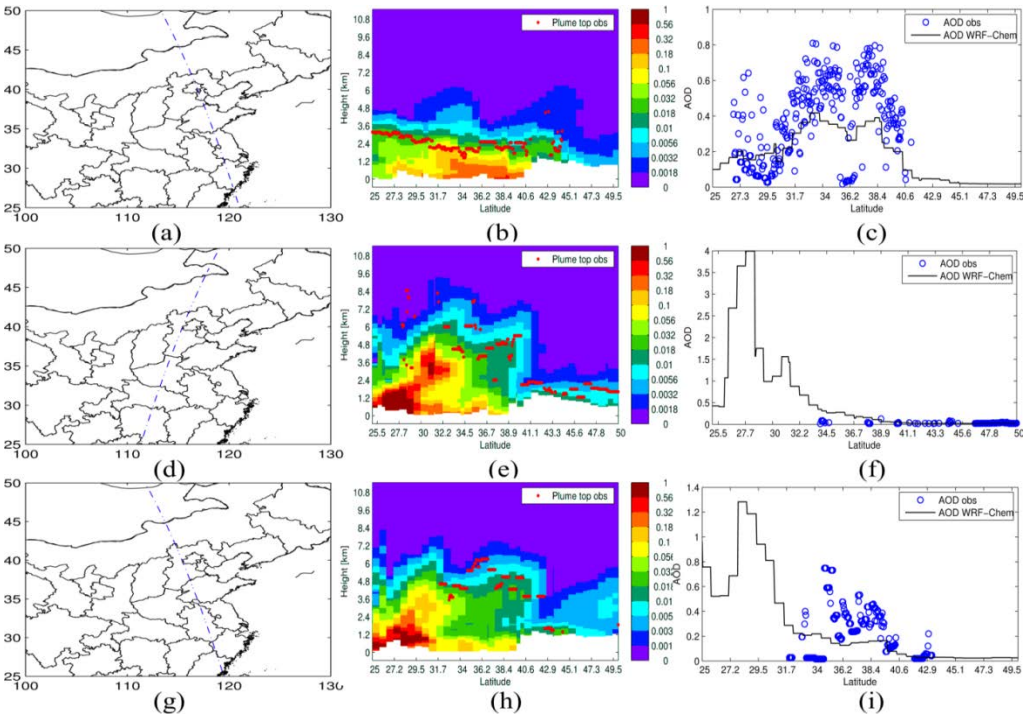


Figure 2.8. Routes of CALIPSO satellite, simulated extinction coefficient and observed plume top, and simulated AOD and CALIPSO retrieved AOD at 532nm at three moments: January 14 12:00(CST) (a-c), January 21 02:00(CST) (d-f), and January 21 12:00(CST) (g-i)

The model is shown to be capable of simulating the major meteorological and chemical evolution of this haze event. As spatial and vertical profiles of the haze period are incomplete or missing in the satellite retrievals and ground stations only provide point estimates, we can use the model to understand the haze spatial, vertical and temporal evolution, as discussed in the following sections.

## 2.5 Results and Discussions

### 2.5.1 Meteorological conditions and evolution of air pollutants

The evolution of the spatial distributions of the haze event is shown in Figure 2.9, where the horizontal distributions of $PM_{2.5}$ and wind vectors are plotted every 12 hours from January 14 00:00 to January 21 00:00. In the second plot (January 14 12:00), NCP surface areas were controlled by a low pressure system and air flows converged, resulting in a small increase of $PM_{2.5}$ concentration. From January 14 00:00 to January 16 00:00, $PM_{2.5}$ concentration over the NCP was generally below 120μg/m$^3$. From January 16 to January 18, Beijing and surrounding areas were controlled by a weak high pressure system. During this period, large amounts of emissions in the NCP accumulated and the persistent southerly winds brought some air pollutants upwards to Beijing and southern Hebei areas. The weak high pressure system was replaced by a low pressure system that lasted until January 20. The weak high pressure system was too weak to disperse air pollutants and the replaced low pressure system aggravated the accumulation of air pollutants. On January 19, the NCP haze was in the worst state, with $PM_{2.5}$ concentrations above 350μg/m$^3$ in south NCP. From January 20, strong northerly winds dispersed the accumulated air pollutants and the haze ended.

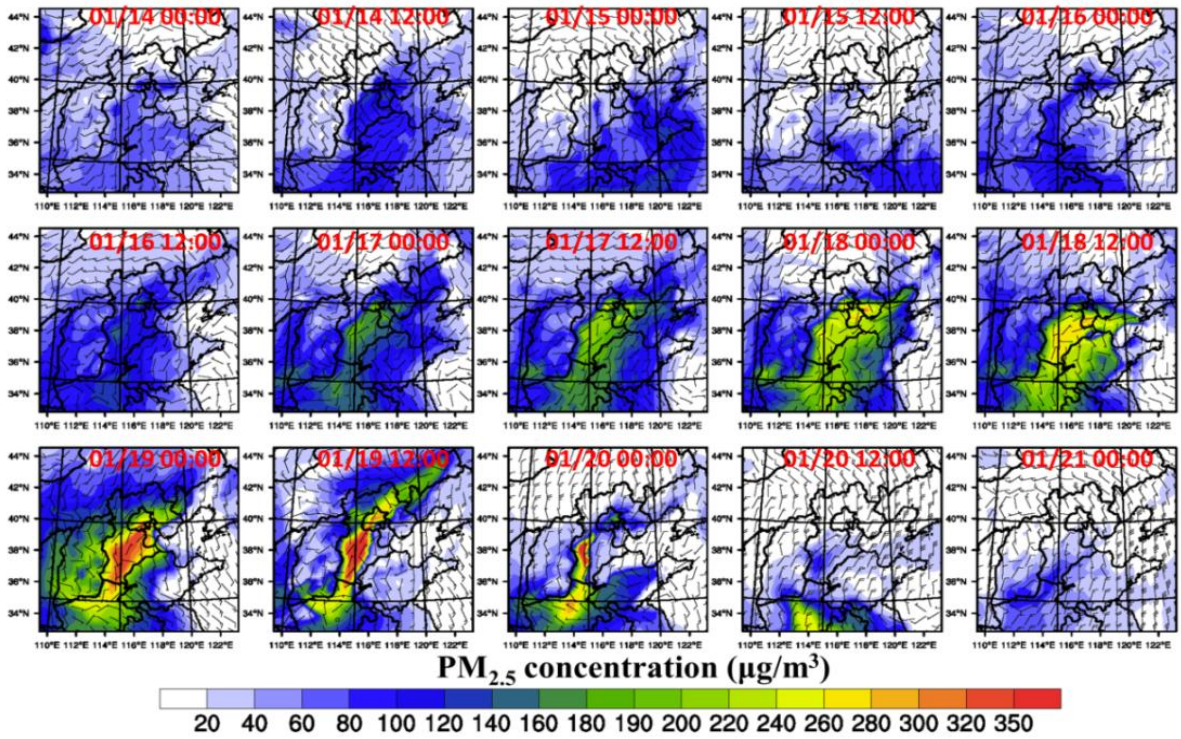


Figure 2.9. $PM_{2.5}$ concentration from 14 January 00:00 to 21 00:00 January, plotted every 12 hours

To illustrate the vertical structure of the haze, vertical cross sections of $PM_{2.5}$ concentration and clouds are presented in Figure 2.11. The cross section location is shown in Figure 2.10. There were two highly polluted points (around latitude 35 and 39) and they started merging as one from January 18 12:00 (Figure 2.11). At that time, southerly winds blew air pollutants northwards (Figure 2.9) and the polluted region was expanded. On January 19, there were fog and/or clouds near the surface and the impacts of fog and/or clouds will be discussed in section 2.5.2.

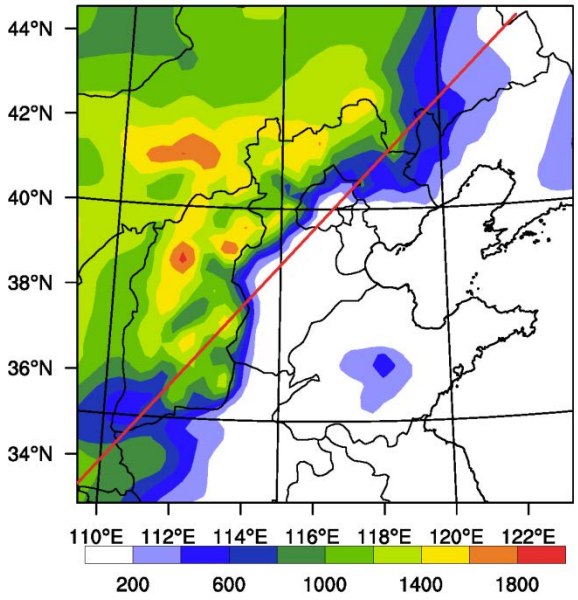


Figure 2.10. Terrain heights and direction of cross section plots

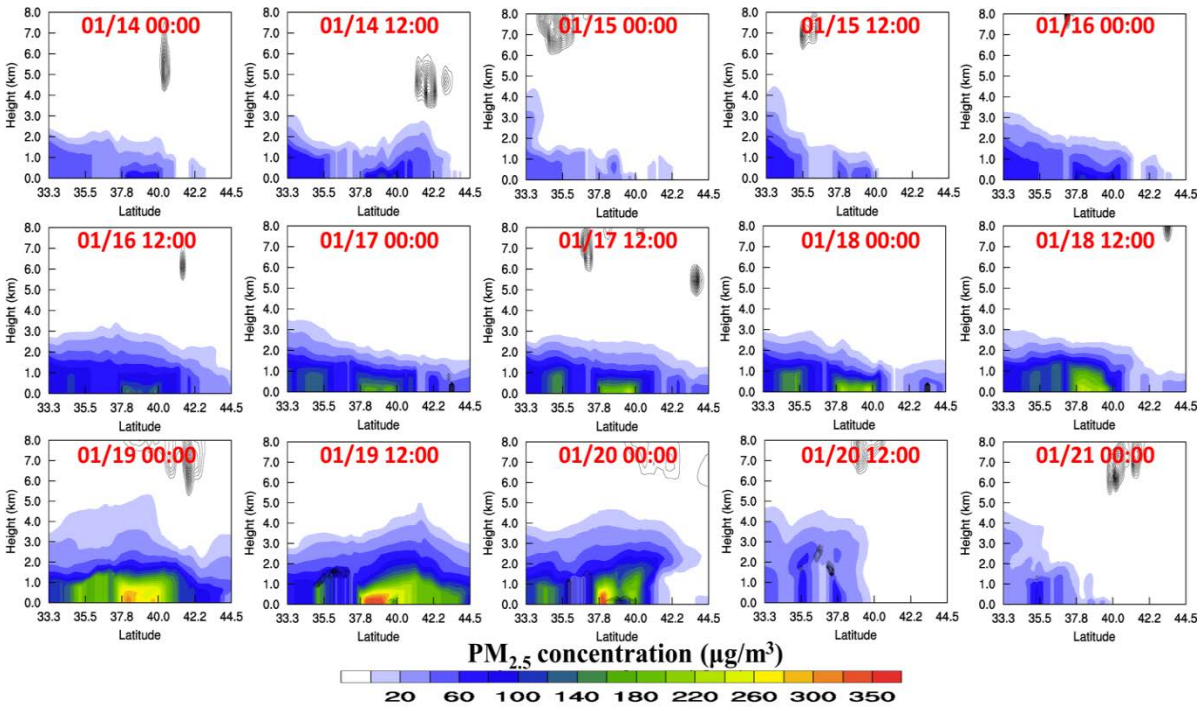

Figure 2.11. Cross section plots of $PM_{2.5}$ concentration and clouds from 14 January 00:00 to 21 00:00 January every 12 hours

Further details of the evolution of the haze are shown in the temporal variations of $PM_{2.5}$ concentrations in Shijiazhuang, Tianjin and Chengde (marked in Figure 2.1) in Figure 2.12. All three sites show similar temporal variations. Around noon of January 15, $PM_{2.5}$ concentrations in Shijiazhuang, Chengde and Beijing increased at nearly the same time, labeled by red arrow in Figure 2.12. Air pollutants started accumulating when the NCP was controlled by the weak and stable weather conditions. Compared to Shijiazhuang and Beijing, the capital city of Hebei province and the capital of China, $PM_{2.5}$ concentrations in Chengde were lower (Figure 2.12). It was estimated that there are more than 8100 coal-fired boilers and industrial kilns in Shijiazhuang city (Peng et al., 2002), resulting in high intensity of emissions in Shijiazhuang. On January 20, Chengde was the first to show sharp decrease of $PM_{2.5}$ concentrations, followed by Beijing and Shijiazhuang, corresponding to the northerly wind impacts discussed above.

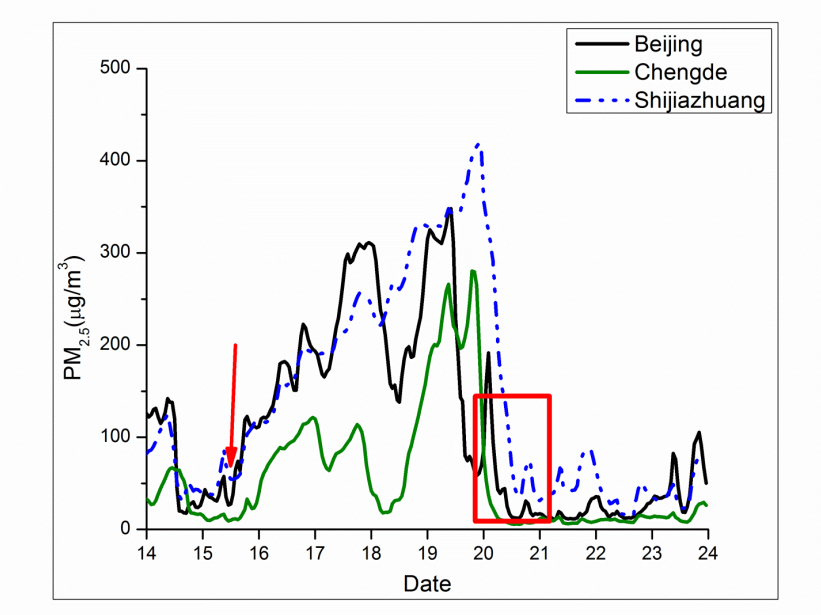

Figure 2.12. Temporal variations of simulated $PM_{2.5}$ at Shijiazhuang, Beijing and Chengde

To better understand the relationships between meteorological factors and pollution levels, time series of different pairs of variables are shown in Figure 2.13. CO shows very high correlation with $PM_{2.5}$ (Figure 2.13(a)), which is consistent with the observation and modeling results in Santiago, Chile (Perez et al., 2004; Saide et al., 2011), and shows the large contribution of primary sources (including gaseous precursors) to $PM_{2.5}$. Secondary aerosol formation also plays a role as $PM_{2.5}$ peaks on the 19$^{th}$ while CO peaks on the 18$^{th}$. RH and wind speed are two important factors affecting the concentrations of aerosols. RH has similar variations as $PM_{2.5}$ concentration (shown in Figure 2.13(a) and 2.13(b)). The NCP is close to the sea and under the slow southerly flows, temperature and RH increase along with $PM_{2.5}$. During the haze event, RH values were generally above 40% and wind speeds were below 2 m/s (Figure 2.13(b)). Low wind speed is unfavorable for the dilution of air pollutants and high RH would accelerate the formation of secondary species, such as sulfate and nitrate, to aggravate the pollution level (Sun et al., 2006). $NO_X$ concentrations show similar variations as $PM_{2.5}$, indicating the buildup of concentrations during the wind speed stagnation. Ozone shows lower concentrations during haze event (Figure 2.13(c)) because high aerosol loadings produce low photochemical activity due to decrease in UV radiation. The concentrations have an inverse relationship with PBL Height (PBLH) as shown in Figure 2.13(d). Diurnal maximums of PBLHs were mostly below 400m and PBL collapsed at night during the haze event, indicating aerosols were trapped near the surface. On January 21 and 22, PBLHs were between 800 and 1000 meters, which helped diffuse and dilute the air pollutants, resulting in a decrease in concentration. The relationships between these variables are further discussed with respect to the influences of aerosol feedback mechanism in section 4.4.

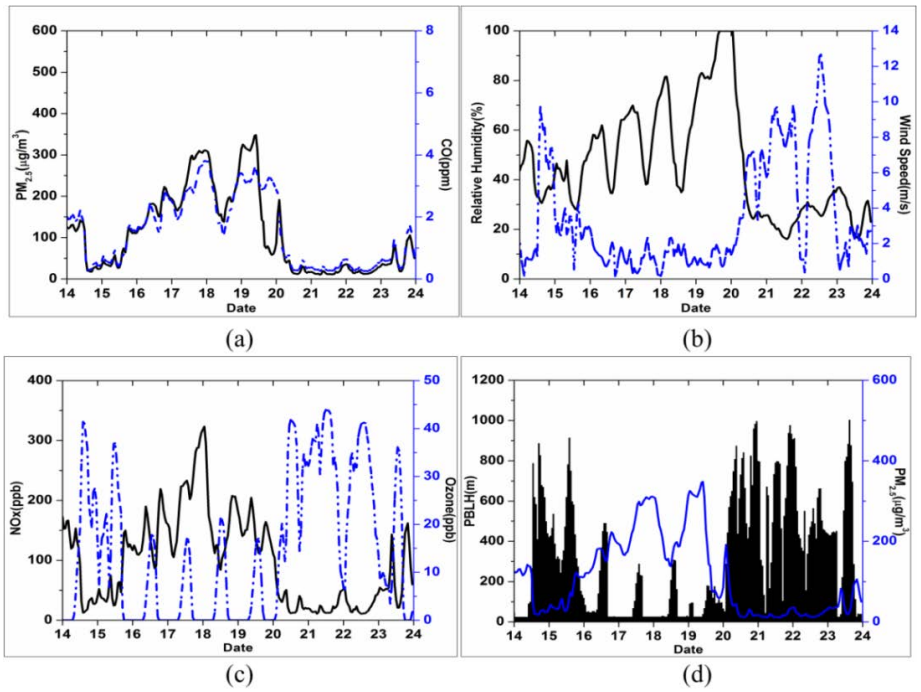


Figure 2.13. Simulated temporal variations of meteorological and chemical variables in Beijing

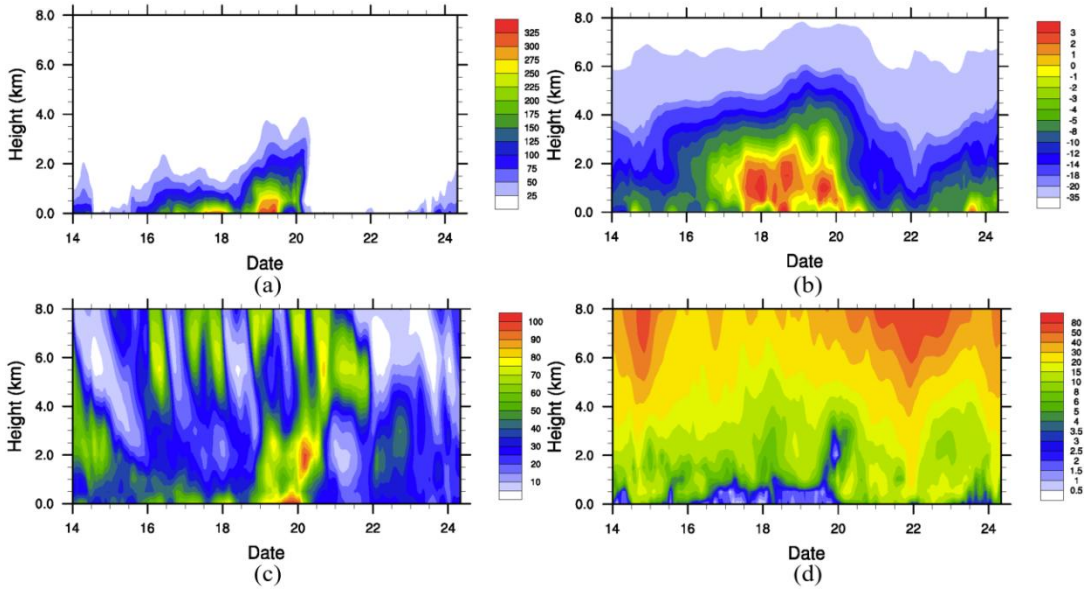


Figure 2.14. Temporal variations of vertical profiles of simulated (a) $PM_{2.5}$ (unit: $\mu g/m^3$) (b) temperature (unit: °C) (c) RH (unit: %) (d) wind speeds (unit: m/s) in Beijing

Figure 2.14 shows the temporal variations of vertical profiles of simulated $PM_{2.5}$ concentration (a), temperature (b), RH (c) and wind speeds (d) at the Beijing site. $PM_{2.5}$ was accumulated below 500m and concentrations reached peak values around January 18 00:00 (Figure 2.14(a)), when a strong temperature inversion happened over Beijing (Figure 2.14(b)), which inhibited vertical atmospheric mixing. A strong temperature inversion also happened on January 19 (Figure 2.14(b)). From January 16 to 19, RH was mostly higher than 50% and reached a peak on the night of January 19 (Figure 2.14(c)). As a result, air pollutants released into the atmosphere were trapped in the moist atmosphere and accumulated as near surface horizontal winds were very weak (below 1.5m/s) during the haze period (Figure 2.14(d)). As mentioned above, the high RH enhances the formation of secondary species, which will be discussed in the following section.

### 2.5.2 Evolution of aerosol composition during haze

As shown above, during haze events, aerosols build up due to low mixing heights and low wind speeds. An important question is what is the role of secondary aerosol formation during such events? Previous measurement studies have found that the increase of secondary inorganic pollutants could be considered as a common property of haze pollution in East China (Zhao et al., 2013). However, few modeling studies have focused on the chemical characteristics, especially the secondary aerosol formation during haze. The observed and simulated chemical species of $PM_{2.5}$ in Beijing are shown in Figure 2.15(a) and 2.15(b), respectively. Observed secondary inorganic aerosols (SIA) ($NH_4^+$, $SO_4^{2-}$, $NO^{3-}$) increased significantly during the haze episode and accounted for 37.7% of $PM_{2.5}$ mass concentration (Zhao et al., 2013). Primary OC,

BC, sulfate, nitrate and ammonium accounted for the major parts of the simulated $PM_{2.5}$ during haze. Table 2.4 summarizes the mean concentrations of primary aerosols (primary OC and BC) and SIA ($NH_4^+$, $SO_4^{2-}$, $NO^{3-}$) in non-haze days, and in the most serious haze day. The primary aerosols increased by a factor of 4.0 from non-haze days to haze days. The SIA also increased from non-haze days to haze days, which agrees with the observation (Tan et al., 2009; Zhao et al., 2013). The SIA increased by a factor of 7.6 from non-haze days to haze days. However, the amounts of sulfate are underestimated by WRF-Chem, compared with the observation in Figure 7(a) from Zhao et al. (2013). Tuccella et al. (2012) pointed out that the underestimation of simulated sulfate could be due to the underestimation of $SO_2$ gas phase oxidation, errors in nighttime boundary layer height predicted by WRF-Chem, and/or the uncertainties in aqueous-phase chemistry. It could also be caused by the missing heterogeneous sulfate formation in current model (He et al., 2014a; Wang et al., 2014b; Zheng et al., 2015). As discussed earlier, the $SO_2$ gas phase concentrations at this site were overestimated. Adding reaction pathways to produce sulfate aerosol would improve both the predictions of sulfate (increase) and $SO_2$ (decrease) (He et al., 2014a; Wang et al., 2014c; Zheng et al., 2015).

We investigated the role of aqueous phase chemistry during the haze event. Figure 2.16 shows the contribution of aqueous chemistry to $PM_{2.5}$ (calculated as the difference between with and without cloud chemistry scenarios). The aqueous phase pathway can reach a level of over 50 $\mu g/m^3$ around Beijing area, accounting for a significant part (about 14.3%) of total $PM_{2.5}$ concentration. As shown in Figure 2.11, fog/clouds existed near the surface on January 19 and this corresponds to the $PM_{2.5}$ difference on that day in Figure 2.16. The sulfate production in aqueous phase may be higher than shown here after adding missing aqueous-phase reactions.

The impacts of heterogeneous reactions on sulfate production will be investigated in future studies.

As shown in Figure 2.15(a) and 2.15(b), the model underestimates OC. To evaluate the formation of Secondary Organic Aerosol (SOA) during the haze event, the RADM2/MADE-SORGAM model was used. The CBMZ/MOSAIC version used is not capable of simulating SOA formation because CBMZ was hard-wired with a numerical solver in WRF-Chem and thus SOA condensable precursors could not be directly added into it (Zhang et al., 2012). RADM2 is an upgrade of RADM1 and it gives more realistic predictions of $H_2O_2$ (Stockwell et al., 1990), and Schell et al., (2001) incorporated SOA into the Modal Aerosol Dynamics Model for Europe (MADE) (Ackermann et al., 1998) by means of the Secondary Organic Aerosol Model (SORGAM). SORGAM treats anthropogenic and biogenic aerosol precursors separately and eight SOA compounds are considered, of which four are anthropogenic and the other four are biogenic (Schell et al., 2001). Predicted Anthropogenic SOA (ASOA), biogenic SOA (BSOA) and Primary Organic Aerosol (POA) in Beijing are shown in Figure 2.15(c). SOA indeed shows a marked increase from non-haze days to haze days, but the amount of SOA is very small compared with POA. The highest SOA concentrations in China are usually found in summer and in Central China (Jiang et al., 2012). In addition, almost all of the simulated SOA are ASOA. Jiang et al. (2012) also concluded that in winter, the fractions of ASOA are larger than 90% in north China. Biogenic emissions are usually controlled by solar radiation and temperature, and solar radiation is weaker and temperature is lower in winter compared with summer. Moreover, the high isoprene, API (a-pinene and other cyclic terpenes with one double bond) and LIM (limonene and other cyclic diene terpenes) emissions are located below 30 °N and in Northeast China (Jiang et al., 2012), not in the NCP, so the SOA concentrations are not high in this winter

haze event period in the NCP. As shown in Table 2.4, the mean SOA concentration in non-haze days is 0.3μg/m$^3$ and in the haze days is 1.1μg/m$^3$. The factor increase of SOA from non-haze days to haze day is 3.7, which is close to that of primary aerosols and much lower than that of SIA. The SOA formation in winter has not been well studied and it might be underestimated by the model as it could have missing pathways to SOA formation. Further work is needed to improve the underestimation of SOA formation in the winter.

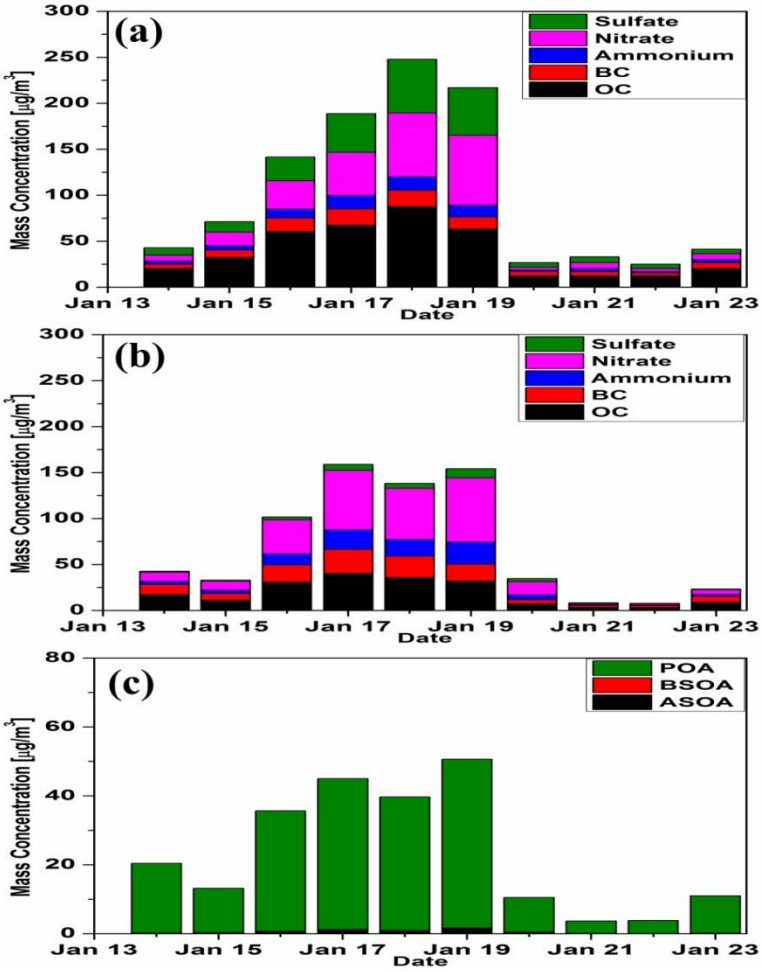


Figure 2.15. Observed (a) and simulated (b) chemical species of $PM_{2.5}$ and simulated SOA (c) in the Beijing site

Table 2.4. Primary aerosol, SIA and SOA (μg/m$^3$) during haze days and non-haze days in Beijing

| | Primary | SIA | SOA |
|---|---|---|---|
| Haze days | 56.4 | 81.9 | 1.1 |
| Non-haze days | 14.2 | 10.8 | 0.3 |
| Ratio | 4.0 | 7.6 | 3.7 |

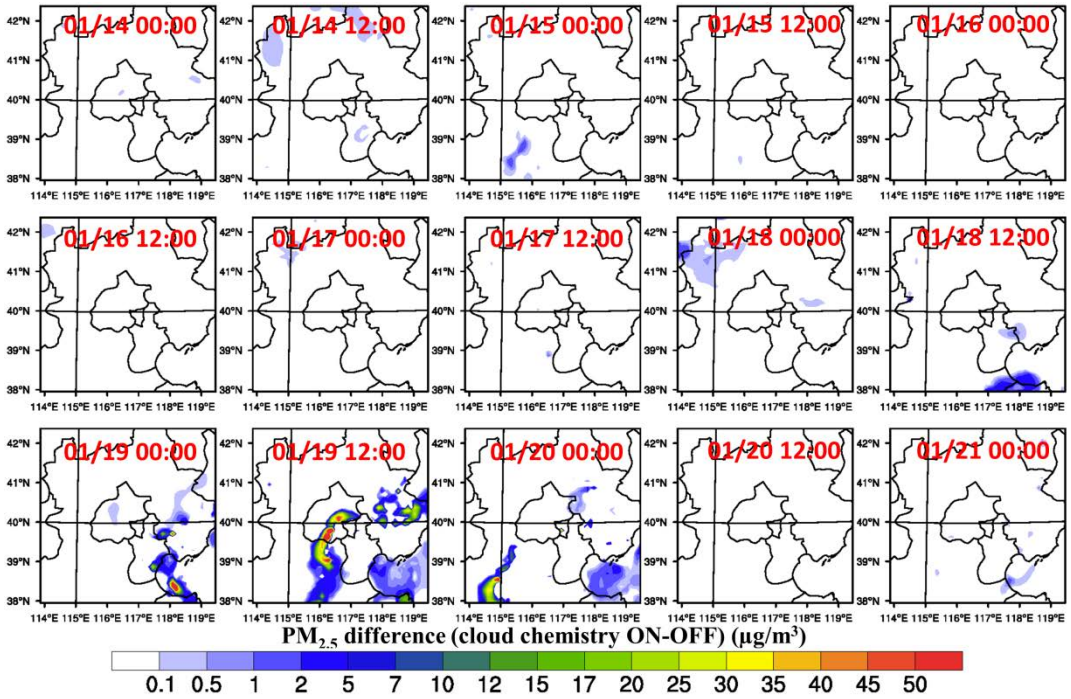


Figure 2.16. $PM_{2.5}$ concentration difference due to cloud chemistry from 14 January 0000 to 21 January 0000, plotted every 12 hours

### 2.5.3 Impacts of surrounding areas on haze in Beijing

Previous studies found that both local emissions and regional transport have significant contributions to the high fine particle levels in Beijing (Yang et al., 2011). In section 4.1, we mentioned that there exists a high correlation between CO and $PM_{2.5}$ concentrations. Figure 2.17

shows the correlations of $PM_{2.5}$ and CO concentrations in Beijing (a) and SDZ (b). The correlation coefficients are 0.91 and 0.96, respectively. According to these high correlations, we can use CO transport to represent $PM_{2.5}$ transport to quantify the local and regional contributions to the Beijing haze. CO tracer tests were conducted in two simulations: one with Beijing local CO emissions on and the other one with Beijing local emissions off. The ratio of CO in Beijing when Beijing emissions are turned off to CO in Beijing when Beijing emissions are on represents the non-local contributions. It can reach above 70% during haze (Figure 2.18) and the average contribution is about 47.8% from January 16 to January 19. These contribution values can be used to represent the non-local contributions to the $PM_{2.5}$ levels in Beijing during haze.

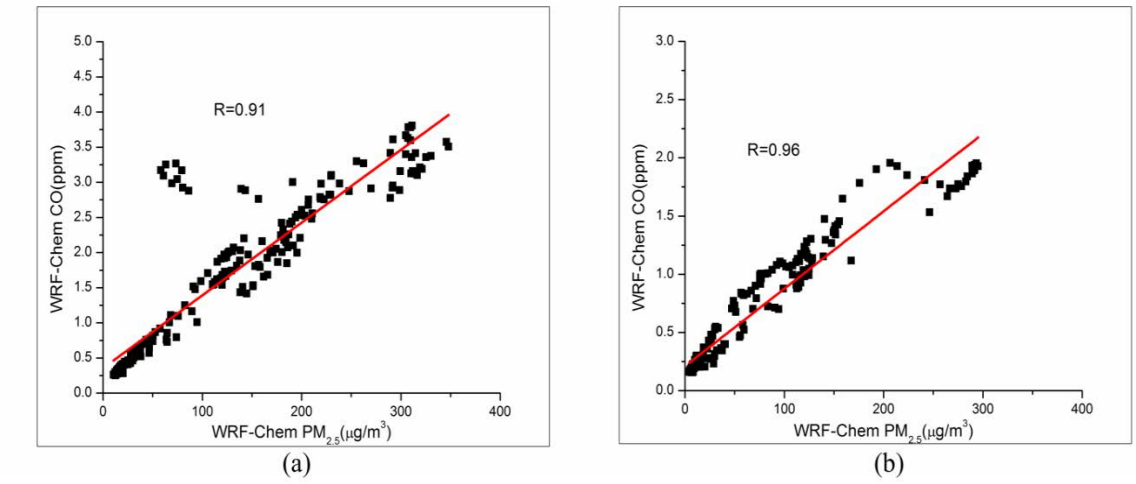


Figure 2.17. Correlation between CO and $PM_{2.5}$ at Beijing (a) Shangdianzi (b)

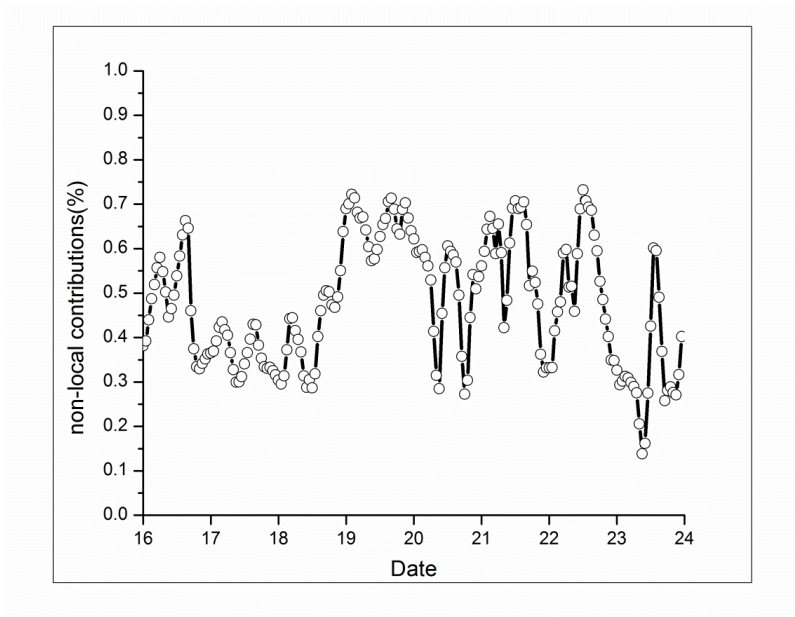


Figure 2.18. Non-local contributions to CO in Beijing

To figure out the dominant transport paths, FLEXPART-WRF (Stohl et al., 1998; Fast and Easter, 2006) was used to generate 72-hour backward dispersions around the Beijing area. 50000 particles were released backwards from a box (1 degree×1 degree×400m), the center of which is Beijing urban area, from January 19 00:00. The number concentrations of particles were plotted at 6 hours before, 12 hours before, 24 hours before and 48 hours before the released time (Figure 2.19). For 12 hours, Beijing was influenced by sources to the south, including sources from south Hebei and Shandong. For 2 days, more sources contributed to the haze buildup in Beijing, including sources from Henan and Inner Mongolia. A number of coal mines are located in Hebei, Shandong and Henan provinces and Inner Mongolia areas have high emissions of primary aerosols.

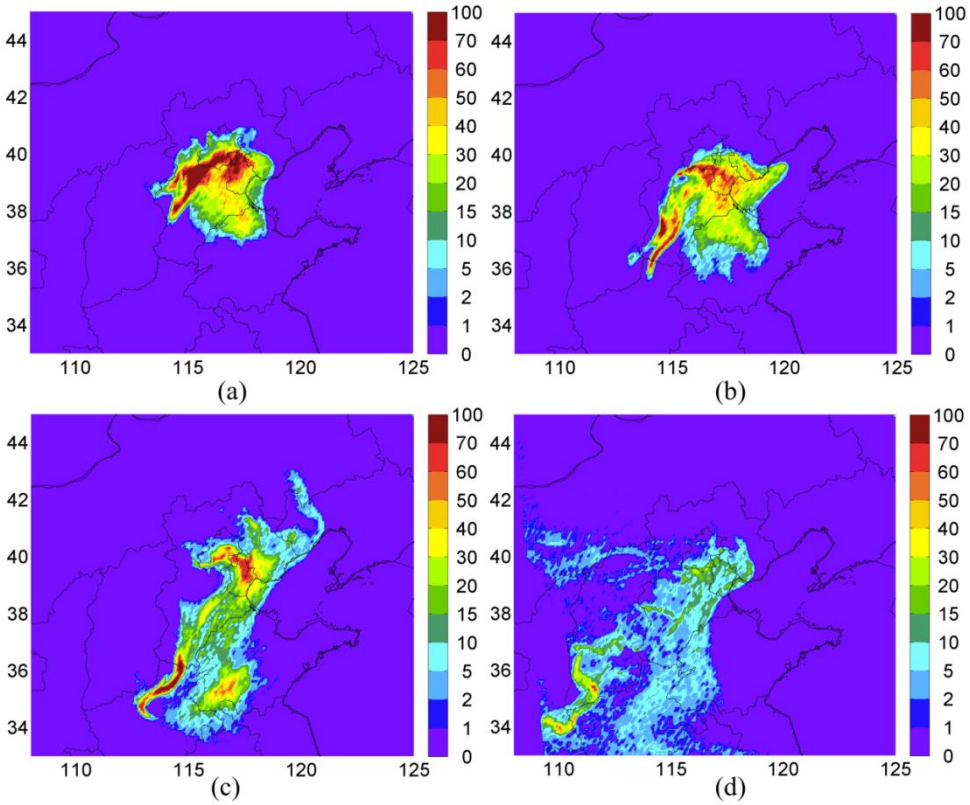


Figure 2.19. Backward dispersion of particles released on January 19 00:00, plotted 6, 12, 24, and 48 hours before being released (unit: number/grid cell)

### 2.5.4 The impact of aerosol feedback

Aerosols affect weather and climate through many pathways, including reducing downward solar radiation through absorption and scattering (direct effect), changing temperature, wind speed, RH and atmospheric stability due to absorption by absorbing aerosols (semi-direct effect), serving as cloud condensation nuclei (CCN) and thus impacting optical properties of clouds (first indirect effect), and affecting cloud coverage, lifetime of clouds and precipitation (second indirect effect) (Zhang et al., 2010; Forkel et al., 2012). The feedback mechanisms are complex and many aspects of them are not well understood. Although previous studies have investigated

aerosol-radiation-meteorology interactions (Zhang et al., 2010; Forkel et al., 2012), the studies on short time scale events with high aerosol loadings, such as haze events, are limited. This section focuses on evaluating the impacts of aerosol feedback mechanism on meteorology and air quality. The feedback discussed in this paper only includes aerosols' direct and semi-direct effects.

#### 2.5.4.1 Impact of feedback on meteorology and $PM_{2.5}$ distribution

Figure 2.20(a) shows the observed daily maximum surface solar radiation and simulated surface solar radiation in with feedback (WF) and without feedback (NF) scenarios in Beijing. Simulated daily surface maximum surface shortwave radiations in NF feedback scenario are higher than observations and the overestimations are reduced by implementing aerosol feedback (Figure 2.20(a)). In NF scenario, the correlation coefficient R between simulated and observed daily maximum surface shortwave radiation is 0.84 in Beijing; in WF scenario, simulated and observed surface shortwave radiation are highly correlated, with 0.93 R value in Beijing, proving that high concentrations of aerosols can significantly affect radiative transfer. Ding et al. (2013) investigated the influence of aerosols on weather during biomass burning episodes using radiation measurements and drew similar conclusions. However, their study did not include the evaluation of aerosol feedbacks from a modeling perspective.

The changes in radiation have impacts on the environment. Simulated PBLH and $PM_{2.5}$ concentration at Shijiazhuang in WF and NF scenarios are shown in Figure 2.20(b) and 2.20(c). In non-haze days, PBLH differences between the two scenarios are negligible due to low aerosol loadings. In haze days, PBLHs in the WF scenario are generally lower than in the NF scenario.

As shown in Figure 2.20(c), $PM_{2.5}$ concentration at Shijiazhuang in WF scenario is higher than it in the NF scenario and the difference reaches about 50μg/$m^3$ on January 19. Aerosols affect PBLHs in two ways: (1) radiation is scattered back to sky and absorbed, as a result, radiation reaching the surface is reduced (Figure 2.20(a)) and so is temperature; and (2) suspended aerosols like BC absorb radiation to heat the upper PBL (Ding et al., 2013). Both of these ways increase temperature inversion and atmospheric stability, and thus exacerbate $PM_{2.5}$ pollution.

Figure 2.21 shows temporal variations of vertical profiles of (a) $PM_{2.5}$ (c) RH (e) temperature (g) wind speeds differences in Beijing between WF and NF scenarios. When aerosol feedback is included, $PM_{2.5}$ concentrations near Beijing surface are mostly increased, except on the morning of January 17, on the afternoon of January 18 and on January 19 (Figure 2.21(a)). The increases of $PM_{2.5}$ are caused by the above mentioned increases of temperature inversion (shown in Figure 2.21(e)) and atmospheric stability. Apart from these, $PM_{2.5}$ concentrations are also affected by RH and wind speeds. In WF scenario, RH is generally increased near surface, especially on January 19 (Figure 2.21(c)), while horizontal wind speeds are also increased on January 19, which is the main cause of decreases of $PM_{2.5}$ concentrations in Beijing.

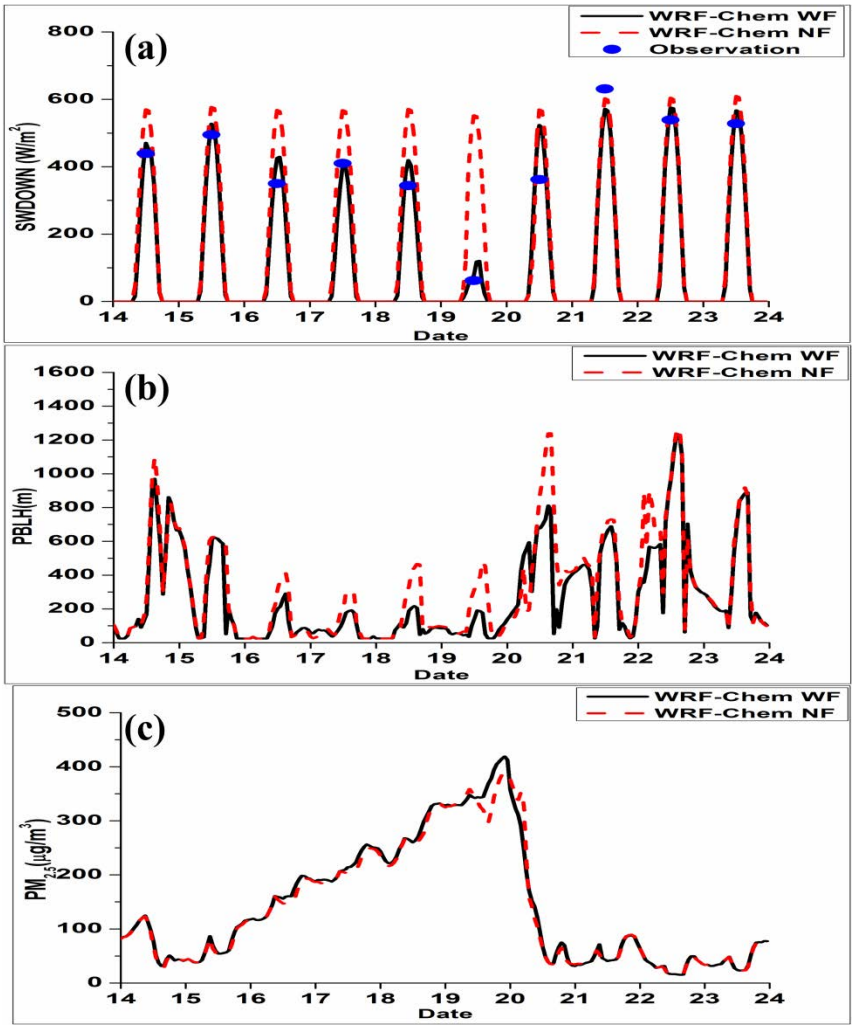


Figure 2.20. Observed daily maximum surface solar radiation and simulated surface shortwave radiation in with feedback (WF) and without feedback (NF) scenarios in Beijing (a), simulated PBLH (b) in WF and NF scenarios at Shijiazhuang, and simulated $PM_{2.5}$ concentration (c) in WF and NF scenarios at Shijiazhuang

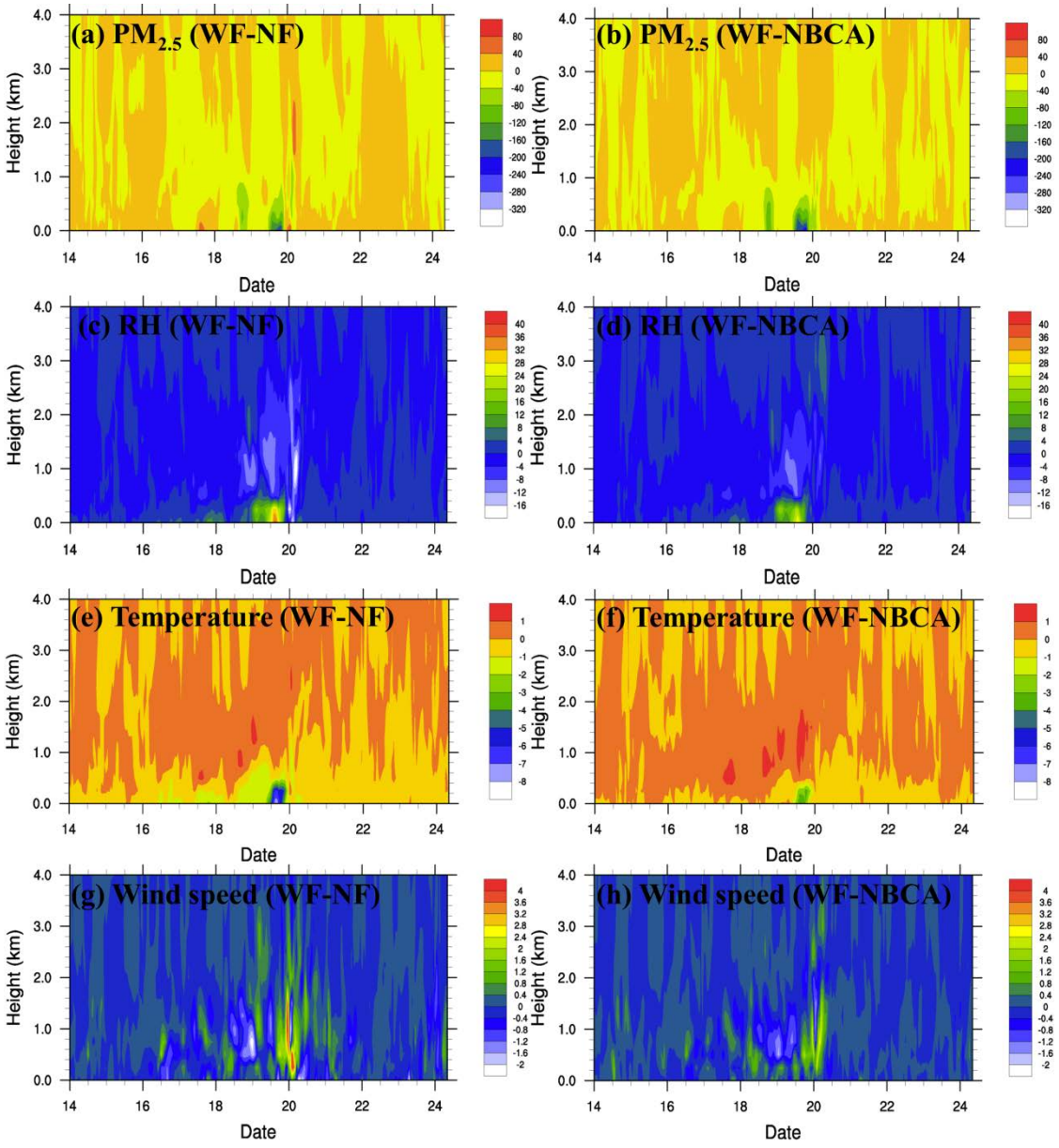


Figure 2.21. Temporal variations of vertical profiles of (a) $PM_{2.5}$ (unit: $\mu g/m^3$) (c) RH (unit: %) (e) temperature (unit: °C) (g) wind speeds (unit: m/s) differences in Beijing between WF and NF scenarios; (b), (d), (f) and (h) are $PM_{2.5}$ , RH, temperature and wind speeds differences in Beijing between WF and NBCA (BC absorptions are teased out) scenarios

To evaluate impact of aerosol feedback on horizontal meteorological fields and $PM_{2.5}$ distributions, averaged differences of $PM_{2.5}$ concentrations, temperature, PBLHs and horizontal winds between WF and NF scenarios at 2p.m. and 2a.m. in haze days (from January 16 to 19) were calculated and are shown in Figure 2.22. Figure 2.22(c) shows that PBLHs are reduced in almost all NCP areas when aerosol feedbacks are considered at 2p.m.. At 2p.m., $PM_{2.5}$ concentrations are increased about 20μg/$m^3$ at Shijiazhuang (114.53°E, 38.03°N). In a few locations (the areas below Beijing (Figure 2.22(a))), PM levels are decreased, although PBLHs are suppressed in those areas. The decreases of $PM_{2.5}$ concentrations in the areas below Beijing are due to big horizontal wind changes, shown in Figure 2.22(g). When aerosol feedback is included, surface temperature is reduced in areas where there are high aerosol loadings (Figure 2.22(e)). Figure 2.22(d) shows that PBLHs are enhanced in east and southwest NCP areas at 2a.m. with aerosol feedback. Aerosol feedback mechanism at night time is more complex compared to it at day time. At night, there is no incoming shortwave radiation from the sun and major radiation is the long wave radiation emitted from the earth. The presence of clouds and some kinds of aerosols can trap outgoing long wave radiation, and as a result, the surface atmosphere is warmed. Different aerosols show different effects on long wave radiation. Greenhouse gases (GHGs) absorb long wave radiation, while large particles like dust scatter long wave radiation. As a result, the upper atmosphere temperature is likely to be warmer or cooler than surface atmosphere temperature. If the upper atmosphere is warmer than the surface, a stable PBL will form. This can explain why aerosol feedbacks increase PBL heights in some regions and decrease in some other regions of NCP. Changes of $PM_{2.5}$ concentrations at 2a.m. are mainly caused by changed PBLHs (Figure 2.22 (b)), showing decreasing trends in areas where

PBLHs are enhanced, because changes of winds are relatively small (Figure 2.22(h)). Temperature changes at 2a.m. are similar to it at 2p.m., but the magnitudes are smaller.

### 2.5.4.2 Impact of BC absorption on meteorology and $PM_{2.5}$ distribution

To investigate BC's influence on meteorology and air quality, sensitivity tests were conducted by removing BC absorption in WRF-Chem (i.e., imaginary refractive index set to zero). Figure 2.21 shows temporal variations of vertical profiles of (b) $PM_{2.5}$ (d) RH (f) temperature and (h) wind speeds differences in Beijing between WF and NBCA scenarios. The differences between WF and NBCA can be used to represent impacts of BC absorption since in WF scenario both scattering and absorbing are considered while in NBCA scenario only scattering is considered. It is obvious from Figure 2.21(f) that upper atmosphere is heated by BC, especially at 1.5km, which increases temperature inversion and atmospheric stability. BC absorption's impacts on $PM_{2.5}$, RH and wind speeds are similar to the impacts of both scattering and absorption, but the magnitudes are smaller (Figure 2.21(b), (d) and (g)).

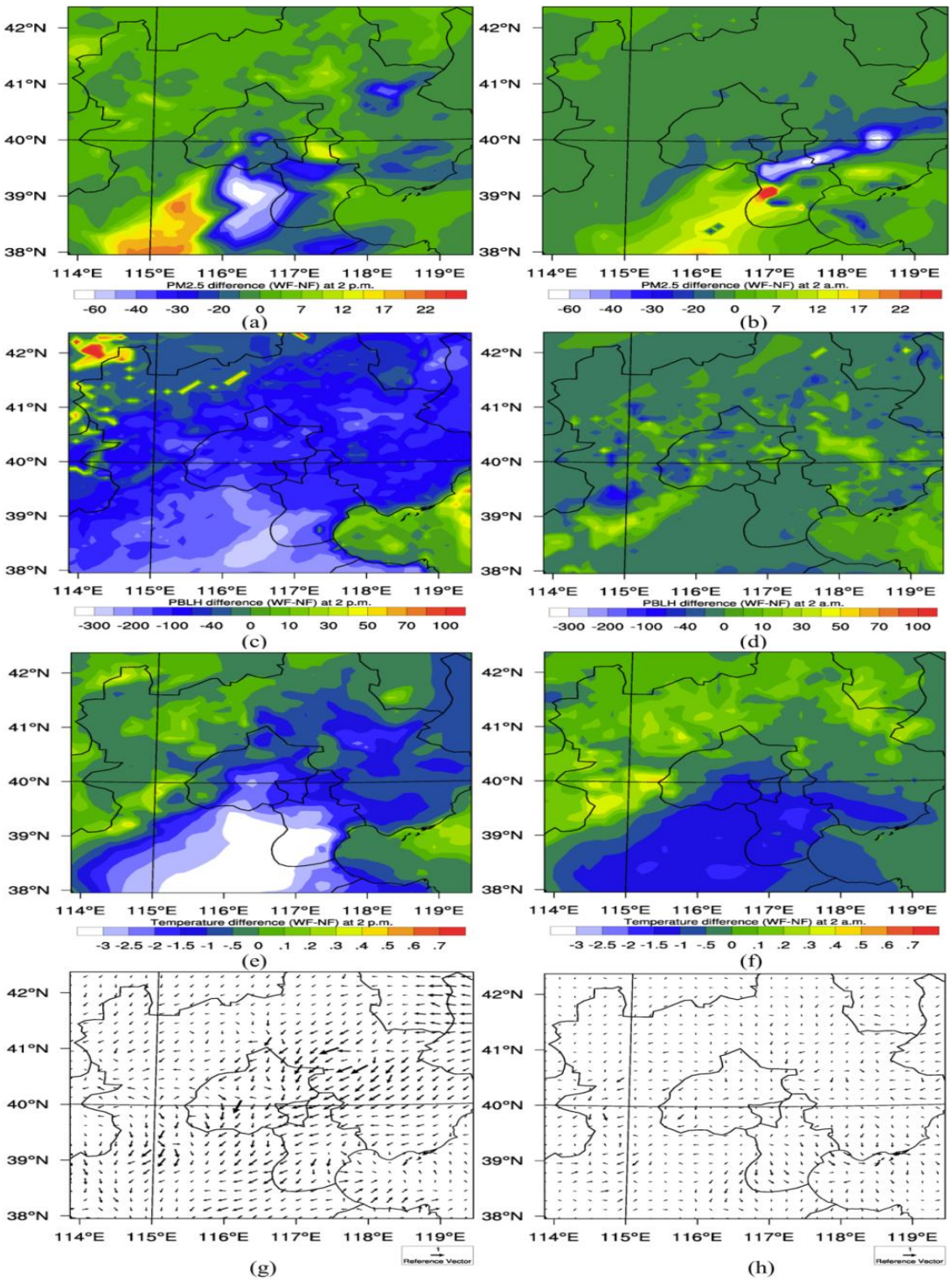


Figure 2.22. Differences of $PM_{2.5}$ concentration (unit: $\mu g/m^3$), temperature (unit: °C), PBLH (unit: m) and horizontal wind (unit: m/s) at 2p.m. (a, c, e, g) and 2a.m. (b, d, f, h) between WF and NF scenarios

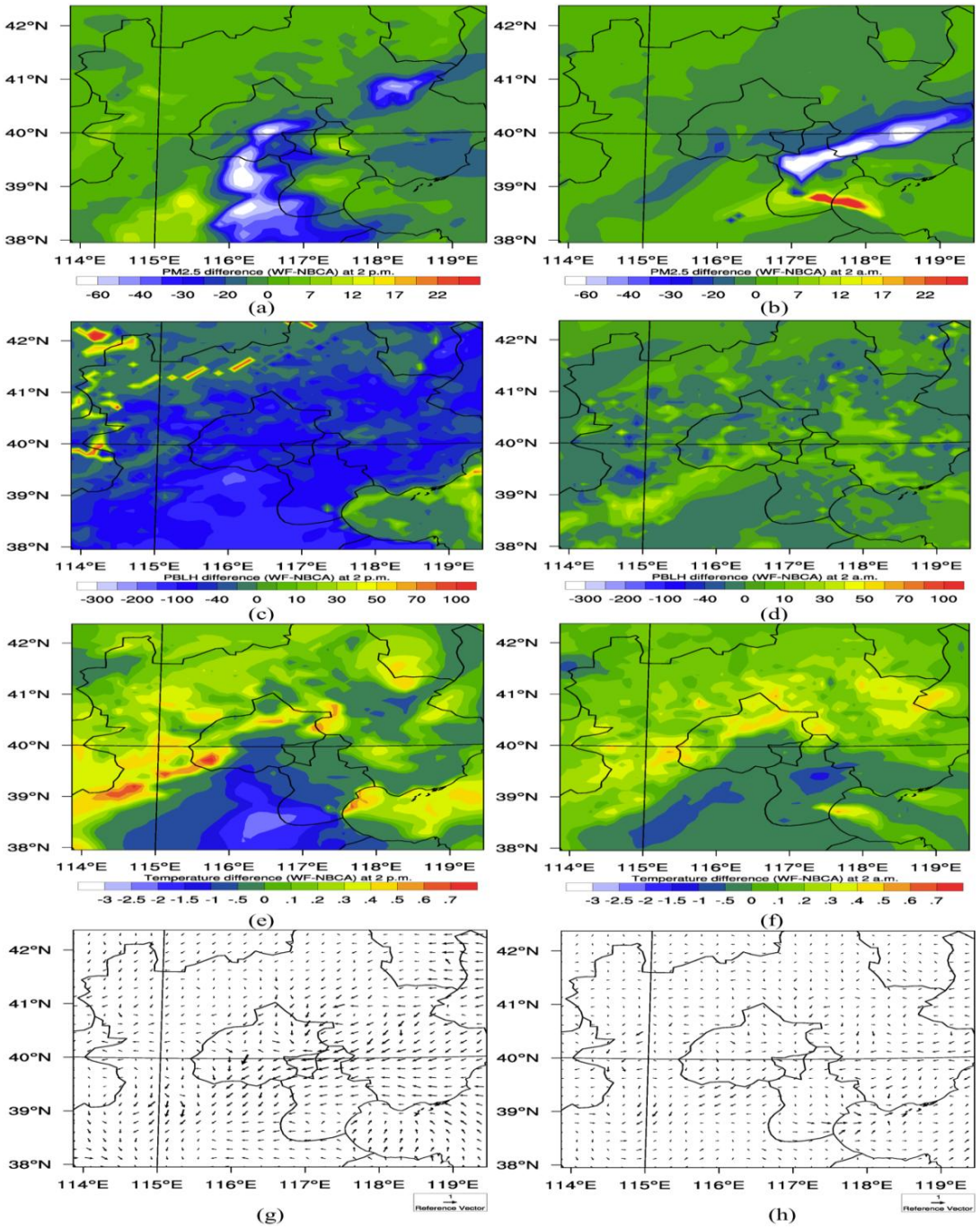


Figure 2.23. Differences of $PM_{2.5}$ concentration (unit: $\mu g/m^3$), temperature (unit: °C), PBLH (unit: m) and horizontal wind (unit: m/s) at 2p.m. (a, c, e, g) and 2a.m. (b, d, f, h) between WF and NBCA scenarios

Figure 2.23 is similar to Figure 2.22 except that the differences are between WF and NBCA scenarios. At 2p.m., $PM_{2.5}$ concentration is increased about 10μg/$m^3$ in Shijiazhuang (114.53°E, 38.03°N), accounting for about 50% of $PM_{2.5}$ changes due to the total aerosol feedback (Figure 2.23(a)). At 2p.m., PBL heights are decreased about 40-150m (Figure 2.23(c)), accounting for about 50% of those changes in Figure 2.22(c). At 2p.m., surface temperature in high aerosol loading areas are decreased about 0-2 °C (Figure 2.23(e)), while the temperature decreases in the same areas are above 2°C in Figure 2.23(e). At 2a.m., changes of $PM_{2.5,}$ PBLHs, surface temperature and wind speeds are similar to Figure 2.22, with smaller magnitudes.

## 2.6 Conclusions

In this study, the online coupled WRF-Chem model was used to reproduce the haze event happened in January, 2010 in the NCP. The model was evaluated against multiple observations, including surface observations of meteorological variables and air pollutants, atmospheric sounding products, surface AOD measurements, and satellite AOD measurements. The correlation coefficients between simulated and observed $PM_{2.5}$ concentrations in Beijing, Tianjin and Xianghe stations are 0.77, 0.75 and 0.69, indicating that WRF-Chem provides reliable representation for the 2010 haze event in the NCP.

This haze event is mainly caused by high emissions of air pollutants in the NCP region and stable weather conditions in winter. The haze built up almost simultaneously in major cities in the NCP and dissipated from north to south. During haze days, horizontal wind speeds and mixing heights were low, temperature inversion happened above surface and RH values were above 40%. Photochemistry was not significant during haze days due to weak UV radiation. In

addition, secondary inorganic aerosols played an important role in the haze event. The role of cloud chemistry in this haze event cannot be ignored.

CO was used to represent $PM_{2.5}$ to quantify non-local contributions to $PM_{2.5}$ in Beijing based on high correlations between them. The average contribution is about 47.8% in haze days. The FLEXPART model was implemented to investigate the sources of the non-local contributions and results show that air pollutants from south Hebei, Shandong and Henan provinces are the major contributors to the $PM_{2.5}$ in Beijing.

Impacts of high aerosols in haze days on radiation, boundary layer heights and $PM_{2.5}$ have been demonstrated. When aerosol feedback is considered, simulated surface radiation agrees well with observations. In haze days, aerosol feedback has important impacts on surface temperature, RH and wind speeds, and these meteorological variables affect aerosol distribution and formation in turn. The role of BC in aerosol feedback loop has also been investigated. It can account for about 50 % of the $PM_{2.5}$ increases and 50% of the PBLH decreases in Shijiazhuang. More attention should be paid to BC from both air pollution control and climate change perspectives.

This study still has some limitations. First, underestimation of sulfate and OC is a problem of WRF-Chem model. Further studies are needed to improve the simulation of sulfate and organic aerosols. Second, emissions have large uncertainties in Asia, which affect air quality simulations determinedly. Some advanced techniques, such as data assimilation, can be applied to reduce uncertainties in the future.

## 2.7 References


Ackermann, I. J., Hass, H., Memmesheimer, M., Ebel, A., Binkowski-, F. S. and Shankar, U. M. A.: Modal aerosol dynamics model for Europe: development and first applications, Atmos. Environ., 32(17), 2981–2999, 1998.

Boylan, J. W. and Russell, A. G.: PM and light extinction model performance metrics, goals, and criteria for three-dimensional air quality models, Atmos. Environ., 40(26), 4946–4959, doi:10.1016/j.atmosenv.2005.09.087, 2006.

Chapman, E. G., Jr, W. I. G., Easter, R. C., Barnard, J. C., Ghan, S. J., Pekour, M. S. and Fast, J. D.: and Physics Coupling aerosol-cloud-radiative processes in the WRF-Chem model : Investigating the radiative impact of elevated point sources, Atmos. Chem. Phys., 945–964, 2009.

Chen, Xun-lai; Feng, Ye-rong; Li, Jiang-nan; Lin, Wen-shi; Fan, Shao-jia; Wang, An-yu; Fong, Soikun; Lin, H.: Numerical Simulations on the Effect of Sea–Land Breezes on Atmospheric Haze over the Pearl River Delta Region, Environ. Model. Assess., 14(3), 351–363, doi:10.1007/s10666-007-9131-5, 2007.

Cheng, Y., Engling, G., He, K.-B., Duan, F.-K., Ma, Y.-L., Du, Z.-Y., Liu, J.-M., Zheng, M. and Weber, R. J.: Biomass burning contribution to Beijing aerosol, Atmos. Chem. Phys., 13(15), 7765–7781, doi:10.5194/acp-13-7765-2013, 2013.

Cheng, Z., Wang, S., Fu, X., Watson, J. G., Jiang, J., Fu, Q., Chen, C., Xu, B., Yu, J., Chow, J. C. and Hao, J.: Impact of biomass burning on haze pollution in the Yangtze River delta, China: a case study in summer 2011, Atmos. Chem. Phys., 14(9), 4573–4585, doi:10.5194/acp-14-4573-2014, 2014.

Chou, Ming-Dah; Suarez, Max J.; Ho, Chang-Hoi; Yan, Michael M.-H.; Lee, K.-T.: Parameterizations for Cloud Overlapping and Shortwave Single-Scattering Properties for Use in General Circulation and Cloud Ensemble Models, J. Clim., 11(2), 202–214, 1998.

Csavina, J., Field, J., Félix, O., Corral-Avitia, A. Y., Sáez, a E. and Betterton, E. a: Effect of wind speed and relative humidity on atmospheric dust concentrations in semi-arid climates., Sci. Total Environ., 487, 82–90, doi:10.1016/j.scitotenv.2014.03.138, 2014.

Ding, a. J., Fu, C. B., Yang, X. Q., Sun, J. N., Petäjä, T., Kerminen, V.-M., Wang, T., Xie, Y., Herrmann, E., Zheng, L. F., Nie, W., Liu, Q., Wei, X. L. and Kulmala, M.: Intense atmospheric pollution modifies weather: a case of mixed biomass burning with fossil fuel combustion pollution in eastern China, Atmos. Chem. Phys., 13(20), 10545–10554, doi:10.5194/acp-13-10545-2013, 2013.

Emery, Chris;Tai, Edward;Yarwood, G.: Enhanced Meteorological Modeling and Performance Evaluation for Two Texas Ozone Episodes, in Prepared for the Texas Natural Resource Conservation Commission, ENVIRON International Corporation, Novato, CA., 2001.

Emmons, L. K., Walters, S., Hess, P. G., Lamarque, J.-F., Pfister, G. G., Fillmore, D., Granier, C., Guenther, a., Kinnison, D., Laepple, T., Orlando, J., Tie, X., Tyndall, G., Wiedinmyer, C., Baughcum, S. L. and Kloster, S.: Description and evaluation of the Model for Ozone and Related chemical Tracers, version 4 (MOZART-4), Geosci. Model Dev., 3(1), 43–67, doi:10.5194/gmd-3-43-2010, 2010.

Fast, J. D. and Easter, R. C.: A Lagrangian Particle Dispersion Model Compatible with WRF, in 7th Annual WRF User's Workshop, Boulder, CO., 2006.

Fast, J. D., Gustafson, W. I., Easter, R. C., Zaveri, R. a., Barnard, J. C., Chapman, E. G., Grell, G. a. and Peckham, S. E.: Evolution of ozone, particulates, and aerosol direct radiative forcing in the vicinity of Houston using a fully coupled meteorology-chemistry-aerosol model, J. Geophys. Res. Atmos., 111, 1–29, doi:10.1029/2005JD006721, 2006.

Forkel, R., Werhahn, J., Hansen, A. B., McKeen, S., Peckham, S., Grell, G. and Suppan, P.: Effect of aerosol-radiation feedback on regional air quality – A case study with WRF/Chem, Atmos. Environ., 53, 202–211, doi:10.1016/j.atmosenv.2011.10.009, 2012.

Gao, M., Carmichael, G.R., Wang, Y., Saide, P.E., Yu, M., Xin, J., Liu, Z., Wang, Z., 2015a. Modeling study of the 2010 regional haze event in the North China Plain. Atmos. Chem. Phys. Discuss. 15, 22781–22822. doi:10.5194/acpd-15-22781-2015

Gao, M., Guttikunda, S. K., Carmichael, G. R., Wang, Y., Liu, Z., Stanier, C. O., Saide, P. E. and Yu, M.: Health impacts and economic losses assessment of the 2013 severe haze event in Beijing area, Sci. Total Environ., 511(January 2013), 553–561, doi:10.1016/j.scitotenv.2015.01.005, 2015b.

Guenther, a., Karl, T., Harley, P., Wiedinmyer, C., Palmer, P. I. and Geron, C.: Estimates of global terrestrial isoprene emissions using MEGAN (Model of Emissions of Gases and Aerosols from Nature), Atmos. Chem. Phys. Discuss., 6(1), 107–173, doi:10.5194/acpd-6-107-2006, 2006.

Guo, S., Hu, M., Zamora, M. L., Peng, J., Shang, D., Zheng, J., Du, Z., Wu, Z., Shao, M., Zeng, L., Molina, M. J. and Zhang, R.: Elucidating severe urban haze formation in China, Proc. Natl. Acad. Sci., 111, 17373–17378, doi:10.1073/pnas.1419604111, 2014.

Han, S., Wu, J., Zhang, Y., Cai, Z., Feng, Y., Yao, Q., Li, X., Liu, Y. and Zhang, M.: Characteristics and formation mechanism of a winter haze-fog episode in Tianjin, China, Atmos. Environ., 98, 323–330, doi:10.1016/j.atmosenv.2014.08.078, 2014a.

Han, X., Zhang, M., Gao, J., Wang, S. and Chai, F.: Modeling analysis of the seasonal characteristics of haze formation in Beijing, Atmos. Chem. Phys., 14(18), 10231–10248, doi:10.5194/acp-14-10231-2014, 2014b.

He, H., Tie, X., Zhang, Q., Liu, X., Gao, Q., Li, X. and Gao, Y.: Analysis of the causes of heavy aerosol pollution in Beijing, China: A case study with the WRF-Chem model, Particuology, doi:10.1016/j.partic.2014.06.004, 2014a.

He, H., Wang, Y., Ma, Q., Ma, J., Chu, B., Ji, D., Tang, G., Liu, C., Zhang, H. and Hao, J.: Mineral dust and NOx promote the conversion of SO2 to sulfate in heavy pollution days., Sci. Rep., 4(2), 4172, doi:10.1038/srep04172, 2014b.

Hong, Song-You; Noh, Yign; Dudhia, J.: A New Vertical Diffusion Package with an Explicit Treatment of, Mon. Weather Rev., 134(9), 2318–2341, 2006.

Huang, K., Zhuang, G., Wang, Q., Fu, J. S., Lin, Y., Liu, T., Han, L. and Deng, C.: Extreme haze pollution in Beijing during January 2013: chemical characteristics, formation mechanism and role of fog processing, Atmos. Chem. Phys. Discuss., 14(6), 7517–7556, doi:10.5194/acpd-14-7517-2014, 2014a.

Huang, X., Song, Y., Zhao, C., Li, M., Zhu, T., Zhang, Q. and Zhang, X.: Journal of Geophysical Research : Atmospheres, J. Geophys. Res. Atmos., 165–179, doi:10.1002/2014JD022301.Received, 2014b.

Li, P., Yan, R., Yu, S., Wang, S., Liu, W. and Bao, H.: Reinstate regional transport of PM 2 . 5 as a major cause of severe haze in Beijing, Proc. Natl. Acad. Sci., 2–3, doi:10.1073/pnas.1502596112, 2015.

Li, Z., Gu, X., Wang, L., Li, D., Xie, Y., Li, K., Dubovik, O., Schuster, G., Goloub, P., Zhang, Y., Li, L., Ma, Y. and Xu, H.: Aerosol physical and chemical properties retrieved from ground-based remote sensing measurements during heavy haze days in Beijing winter, Atmos. Chem. Phys., 13(20), 10171–10183, doi:10.5194/acp-13-10171-2013, 2013.

Li, W.J.; Shao, L.Y., and Buseck, P. R.: Haze types in Beijing and the influence of agricultural biomass.pdf, Atmos. Chem. Phys., 10, 8119–8130, 2010.

Lin Yuh-Lang;Farley, Richard D.;Orville, H. D.: Bulk Parameterization of the Snow Field in a Cloud Model, J. Clim. Appl. Meteorol., 22(6), 1065–1092, 1983.

Liu, X. G., Li, J., Qu, Y., Han, T., Hou, L., Gu, J., Chen, C., Yang, Y., Liu, X., Yang, T., Zhang, Y., Tian, H. and Hu, M.: Formation and evolution mechanism of regional haze: a case study in the megacity Beijing, China, Atmos. Chem. Phys., 13(9), 4501–4514, doi:10.5194/acp-13-4501-2013, 2013.

Mlawer, E. J., Taubman, S. J., Brown, P. D., Iacono, M. J. and Clough, S. a.: Radiative transfer for inhomogeneous atmospheres: RRTM, a validated correlated-k model for the longwave, J. Geophys. Res., 102(D14), 16663, doi:10.1029/97JD00237, 1997.

Morris, R. E., McNally, D. E., Tesche, T. W., Tonnesen, G., Boylan, J. W. and Brewer, P.: Preliminary Evaluation of the Community Multiscale Air Quality Model for 2002 over the Southeastern United States, J. Air Waste Manage. Assoc., 55, 1694–1708, doi:10.1080/10473289.2005.10464765, 2005.

Paciorek, C. J., Liu, Y., Moreno-Macias, H. and Kondragunta, S.: Spatiotemporal associations between GOES aerosol optical depth retrievals and ground-level $PM_{2.5}$., Environ. Sci. Technol., 42(15), 5800–6 (online) Available from: http://www.ncbi.nlm.nih.gov/pubmed/18754512, 2008.

Peng, C., Wu, X., Liu, G., Johnson, T. and Shah, J.: Urban Air Quality and Health in China, Urban Stud., 39(12), 2283–2299, doi:10.1080/00420980220003387, 2002.

Perez, P., Palacios, R. and Castillo, A.: Carbon Monoxide Concentration Forecasting in Santiago, Chile, J. Air Waste Manage. Assoc., 54(8), 908–913, doi:10.1080/10473289.2004.10470966, 2004.

Quan, J., Tie, X., Zhang, Q., Liu, Q., Li, X., Gao, Y. and Zhao, D.: Characteristics of heavy aerosol pollution during the 2012–2013 winter in Beijing, China, Atmos. Environ., 88, 83–89, doi:10.1016/j.atmosenv.2014.01.058, 2014.

Saide, P. E., Carmichael, G. R., Spak, S. N., Gallardo, L., Osses, A. E., Mena-Carrasco, M. a. and Pagowski, M.: Forecasting urban PM10 and $PM_{2.5}$ pollution episodes in very stable nocturnal conditions and complex terrain using WRF–Chem CO tracer model, Atmos. Environ., 45(16), 2769–2780, doi:10.1016/j.atmosenv.2011.02.001, 2011.

Schell, B., Ackermann, I. J., Hass, H. and Carolina, N.: Modeling the formation of secondary organic aerosol within a comprehensive air quality model system, J. Geophys. Res., 106(D22), 28275–28293, 2001.

Schuster, G. L., Dubovik, O. and Holben, B. N.: Angstrom exponent and bimodal aerosol size distributions, J. Geophys. Res., 111(April), 1–14, doi:10.1029/2005JD006328, 2006.

Stockwell, W. R., Middleton, P. and Chang, J. S.: The Second Generation Regional Acid Deposition Model Chemical Mechanism for Regional Air Quality Modeling The most important in the gas Alkanes with between, J. Geophys. Res., 95(D10), 16343–16367, 1990.

Stohl, a., Hittenberger, M. and Wotawa, G.: Validation of the lagrangian particle dispersion model FLEXPART against large-scale tracer experiment data, Atmos. Environ., 32(24), 4245–4264, doi:10.1016/S1352-2310(98)00184-8, 1998.

Sun, Y., Zhuang, G., Tang, a A., Wang, Y. and An, Z.: Chemical characteristics of $PM_{2.5}$ and PM10 in haze-fog episodes in Beijing., Environ. Sci. Technol., 40(10), 3148–55 (online) Available from: http://www.ncbi.nlm.nih.gov/pubmed/16749674, 2006.

Sun, Yele; Jiang, Qi; Wang, Zifa; Fu, Pingqing; Li, Jie; Yang, Ting; Yin, Y.: Investigation of the sources and evolution processes of severe haze pollution in Beijing in January 2013, J. Geophys. Res. Atmos., 119, 4380–4398, doi:10.1002/2014JD021641.Received, 2014.

Tan, J.-H., Duan, J.-C., Chen, D.-H., Wang, X.-H., Guo, S.-J., Bi, X.-H., Sheng, G.-Y., He, K.-B. and Fu, J.-M.: Chemical characteristics of haze during summer and winter in Guangzhou, Atmos. Res., 94(2), 238–245, doi:10.1016/j.atmosres.2009.05.016, 2009.

Tao, M., Chen, L., Su, L. and Tao, J.: Satellite observation of regional haze pollution over the North China Plain, J. Geophys. Res. Atmos., 117(D12), n/a–n/a, doi:10.1029/2012JD017915, 2012.

Tao, M., Chen, L., Xiong, X., Zhang, M., Ma, P., Tao, J. and Wang, Z.: Formation process of the widespread extreme haze pollution over northern China in January 2013: Implications for regional air quality and climate, Atmos. Environ., 98, 417–425, doi:10.1016/j.atmosenv.2014.09.026, 2014.

Wang, G., Kawamura, K., Xie, M., Hu, S., Cao, J., An, Z., Waston, J. G. and Chow, J. C.: Organic molecular compositions and size distributions of chinese summer and autumn aerosols from nanjing: characteristic haze event caused by wheat straw burning., Environ. Sci. Technol., 43(17), 6493–9 (online) Available from: http://www.ncbi.nlm.nih.gov/pubmed/19764207, 2009.

Wang, J., Wang, S., Jiang, J., Ding, A., Zheng, M., Zhao, B., Wong, D. C., Zhou, W., Zheng, G., Wang, L., Pleim, J. E. and Hao, J.: Impact of aerosol–meteorology interactions on fine particle pollution during China's severe haze episode in January 2013, Environ. Res. Lett., 9(9), 094002, doi:10.1088/1748-9326/9/9/094002, 2014a.

Wang, L. T., Wei, Z., Yang, J., Zhang, Y., Zhang, F. F., Su, J., Meng, C. C. and Zhang, Q.: The 2013 severe haze over southern Hebei, China: model evaluation, source apportionment, and policy implications, Atmos. Chem. Phys., 14(6), 3151–3173, doi:10.5194/acp-14-3151-2014, 2014b.

Wang, L., Xu, J., Yang, J., Zhao, X., Wei, W., Cheng, D., Pan, X. and Su, J.: Understanding haze pollution over the southern Hebei area of China using the CMAQ model, Atmos. Environ., 56, 69–79, doi:10.1016/j.atmosenv.2012.04.013, 2012.

Wang, Q., Shao, M., Liu, Y., William, K., Paul, G., Li, X., Liu, Y. and Lu, S.: Impact of biomass burning on urban air quality estimated by organic tracers: Guangzhou and Beijing as cases, Atmos. Environ., 41(37), 8380–8390, doi:10.1016/j.atmosenv.2007.06.048, 2007.

Wang, Y., Yao, L., Wang, L., Liu, Z., Ji, D., Tang, G., Zhang, J., Sun, Y., Hu, B. and Xin, J.: Mechanism for the formation of the January 2013 heavy haze pollution episode over central and eastern China, Sci. China Earth Sci., 57(1), 14–25, doi:10.1007/s11430-013-4773-4, 2014c.

Wang, Y., Zhang, Q., Jiang, J., Zhou, W., Wang, B., He, K., Duan, F., Zhang, Q., Philip, S. and Xie, Y.: Enhanced sulfate formation during China's severe winter haze episode in January 2013 missing from current models, J. Geophys. Res. Atmos., 1–16, doi:10.1002/2013JD021426.Received, 2014d.

Wang, Z., Li, J., Wang, Z., Yang, W., Tang, X., Ge, B., Yan, P., Zhu, L., Chen, X., Chen, H., Wand, W., Li, J., Liu, B., Wang, X., Zhao, Y., Lu, N. and Su, D.: Modeling study of regional severe hazes over mid-eastern China in January 2013 and its implications on pollution prevention and control, Sci. China Earth Sci., 57(1), 3–13, doi:10.1007/s11430-013-4793-0, 2014e.

Watson, J. G.: Visibility: Science and Regulation, J. Air Waste Manage. Assoc., 52(6), 628–713, doi:10.1080/10473289.2002.10470813, 2002.

Willmott, C. J. and Matsuura, K.: Advantages of the mean absolute error ( MAE ) over the root mean square error ( RMSE ) in assessing average model performance, Clim. Res., 30, 79–82, 2005.

Yang, F., Tan, J., Zhao, Q., Du, Z., He, K., Ma, Y., Duan, F. and Chen, G.: Characteristics of $PM_{2.5}$ speciation in representative megacities and across China, Atmos. Chem. Phys., 11(11), 5207–5219, doi:10.5194/acp-11-5207-2011, 2011.

Yu, M., Carmichael, G. R., Zhu, T. and Cheng, Y.: Sensitivity of predicted pollutant levels to urbanization in China, Atmos. Environ., 60, 544–554, doi:10.1016/j.atmosenv.2012.06.075, 2012.

Yu, X., Zhu, B., Yin, Y., Yang, J., Li, Y. and Bu, X.: A comparative analysis of aerosol properties in dust and haze-fog days in a Chinese urban region, Atmos. Res., 99(2), 241–247, doi:10.1016/j.atmosres.2010.10.015, 2011.

Zaveri, R. a., Easter, R. C., Fast, J. D. and Peters, L. K.: Model for Simulating Aerosol Interactions and Chemistry (MOSAIC), J. Geophys. Res., 113(D13), D13204, doi:10.1029/2007JD008782, 2008.

Zaveri, R. a. and Peters, L. K.: A new lumped structure photochemical mechanism for large-scale applications, J. Geophys. Res., 104(D23), 30387, doi:10.1029/1999JD900876, 1999.

Zhang, B., Wang, Y. and Hao, J.: Simulating aerosol–radiation–cloud feedbacks on meteorology and air quality over eastern China under severe haze conditionsin winter, Atmos. Chem. Phys., 15, 2387–2404, doi:10.5194/acp-15-2387-2015, 2015.

Zhang, Y., Chen, Y., Sarwar, G. and Schere, K.: Impact of gas-phase mechanisms on Weather Research Forecasting Model with Chemistry (WRF/Chem) predictions: Mechanism implementation and comparative evaluation, J. Geophys. Res., 117(D1), D01301, doi:10.1029/2011JD015775, 2012.

Zhang, Y., Wen, X.-Y. and Jang, C. J.: Simulating chemistry–aerosol–cloud–radiation–climate feedbacks over the continental U.S. using the online-coupled Weather Research Forecasting Model with chemistry (WRF/Chem), Atmos. Environ., 44(29), 3568–3582, doi:10.1016/j.atmosenv.2010.05.056, 2010.

Zhang, Renyi; Guo, Song; Zamora, Misti Levy; Hu, M.: Reply to Li et al .: Insufficient evidence for the contribution of regional transport to severe haze formation in Beijing, Proc. Natl. Acad. Sci., (1), 1073, doi:10.1073/pnas.1503855112, 2015.

Zhao, X. J., Zhao, P. S., Xu, J., Meng, W., Pu, W. W., Dong, F., He, D. and Shi, Q. F.: Analysis of a winter regional haze event and its formation mechanism in the North China Plain, Atmos. Chem. Phys., 13(11), 5685–5696, doi:10.5194/acp-13-5685-2013, 2013.

Zheng, B., Zhang, Q., Zhang, Y., He, K. B., Wang, K., Zheng, G. J., Duan, F. K., Ma, Y. L. and Kimoto, T.: Heterogeneous chemistry: a mechanism missing in current models to explain secondary inorganic aerosol formation during the January 2013 haze episode in North China, Atmos. Chem. Phys. Discuss., 14(11), 16731–16776, doi:10.5194/acpd-14-16731-2014, 2014a.

Zheng, G. J., Duan, F. K., Ma, Y. L., Cheng, Y., Zheng, B., Zhang, Q., Huang, T., Kimoto, T., Chang, D., Su, H., Pöschl, U., Cheng, Y. F. and He, K. B.: Exploring the severe winter haze in Beijing, Atmos. Chem. Phys. Discuss., 14(12), 17907–17942, doi:10.5194/acpd-14-17907-2014, 2014b.

# CHAPTER 3: RESPONSES OF WINTER $PM_{2.5}$ TO EMISSION AND METEOROLOGY CHANGES IN THE NORTH CHINA PLAIN[31]

## 3.1 Abstract

The winter haze is a growing problem in the North China Plain (NCP), but the causes have not been well understood. The changes in emissions and global warming might be the possible reasons. The chemistry version of the Weather Research and Forecasting model (WRF-Chem) was applied in the NCP to examine how the $PM_{2.5}$ concentrations change in response to changes in emissions (sulfur dioxide ($SO_2$), black carbon (BC), organic carbon (OC), ammonia ($NH_3$), and nitrogen oxides ($NO_x$)), as well as meteorology (temperature, relative humidity (RH), and wind speeds) changes in winter. The historical detailed $SO_2$, BC and OC emissions from Argonne National Laboratory (ANL), and inferred $NH_3$, $NO_x$ emission changes, as well as perturbations of temperature, RH, and wind speeds in model initial and boundary conditions were used to simulate a winter month (January 2010) in the NCP. From 1985 to 2010, the 25.7% increases in $SO_2$ surface emissions cause about 30.8% increases in surface sulfate aerosols. Monthly domain mean BC and OC aerosols increased about 9.8% and 26.8% from 1985 to 2010, due to 6.6% and 26.5% increases in BC and OC emissions. Due to $SO_2$, BC, and OC emission changes from 1985 to 2010, the domain maximum monthly $PM_{2.5}$ changes can reach 14.9μg/m3, and OC accounted for more than half this change. Increasing $NH_3$ emissions significantly increases $PM_{2.5}$ concentrations in the NCP and increasing $NO_x$ emissions also increases $PM_{2.5}$ concentrations but to a lesser extent. The increases in $NO_x$ emissions actually leads to 27.5% decrease in surface ozone concentration and 44.7% decrease in surface OH radical concentration because the NCP region is VOC-limited in winter and the reduced oxidants decrease sulfate

[31] This work is under preparation to be submitted.

aerosol. The sensitivity results indicate $SO_2$, OC and $NH_3$ emissions should be controlled preferentially to control winter haze. Based on the major sources of $SO_2$, OC and $NH_3$ emissions, natural gas should be promoted to take the place of coal and biofuel, and some animal feeding and animal housing strategies should be taken to control $NH_3$ emissions. Because of temperature increase, the predicted monthly $PM_{2.5}$ concentration increases 2.6μg/$m^3$ on domain average, and the domain peak increase is about 6.0μg/$m^3$. The increases of sulfate, nitrate, and ammonium are mostly due to increasing OH radicals and higher chemical reaction rate under enhanced temperature. The other causes of the increased $PM_{2.5}$ concentrations are the large changes in surface wind fields and Planetary Boundary Layer Heights (PBLHs) after temperature perturbations. Increases in RH lead to lower dry $PM_{2.5}$, but more water aerosols and clouds. Due to 5.3% decrease in wind speeds, monthly mean $PM_{2.5}$ increase by 1.25% on domain average.

## 3.2 Introduction

$PM_{2.5}$ (particulate matter with diameter equal to or less than 2.5μm) is a main air pollution concern due to its adverse effects on public health (Gao et al., 2015b; Pope et al., 2009). Pope et al. (2009) estimated that a decrease of 10μg $PM_{2.5}$ is related to about 0.61 year mean life expectancy increase. $PM_{2.5}$ is also associated with visibility reduction and regional climate (Cheung et al., 2005). Many cities in the North China Plain (NCP) are experiencing severe haze pollution with exceedingly high $PM_{2.5}$ concentrations. In January 2010, a regional haze occurred in the NCP and maximum hourly $PM_{2.5}$ concentration in Tianjin was over 400μg/m3 (Zhao et al., 2013). In January 2013, another unprecedented haze event happened, and the daily $PM_{2.5}$ concentrations in some areas of Beijing and Shijiazhuang reached over 500μg/m3 (Wang et al.,

2014a), and instantaneous $PM_{2.5}$ concentration at some urban measurement sites were over 1000μg/m3 (Zheng et al., 2015). It is well known that particulate matter levels are strongly influenced by emissions and meteorological conditions (Steiner et al., 2006). The PM in the atmosphere can be directly emitted from sources like wildfires, or formed from emitted gases through secondary aerosol formation mechanism. Meteorology affects PM levels via changing emissions, chemical reactions, transport and deposition processes (Mu and Liao, 2014). Increasing wildfire emission in North America is mainly caused by warmer temperatures and precipitation changes (Dawson et al., 2014), and increased temperature leads to higher biogenic emissions, which are important precursors of secondary organic aerosols (Dawson et al., 2014; Heald et al., 2008; Jacob and Winner, 2009). Increasing temperature also increases sulfate concentration due to higher $SO_2$ oxidation rate (Aw and Kleeman, 2003; Dawson et al., 2007) and semi-volatile aerosols may decrease due to evaporation under higher temperature (Sheehan and Bowman, 2001; Dawson et al., 2007; Tsigaridis and Kanakidou, 2007). Higher relative humidity favors the formation of nitrate and increasing precipitation decreases all PM species via wet scavenging (Dawson et al., 2007; Tai et al., 2010). Increasing clouds promote in-cloud sulfate production (Tai et al., 2010) and changes in wind speed and mixing height determines the dilution of primary and secondary PM (Jimenez-Guerrero et al., 2012; Megaritis et al., 2014; Pay et al., 2012).

With rapid economic boom and industrial developments, emissions in China changed enormously during the past years. It is estimated that $NO_x$ emissions in China increased by 70% from 1995 to 2004 (Zhang et al., 2007), Black Carbon (BC) increased by 46% from 2000 to 2010 (Lu et al., 2011), Organic Carbon (OC) increased by 33% from 2000 to 2010 (Lu et al., 2011), and $SO_2$ increased by 61% from 2000 to 2006 (Lu et al., 2011). Apart from emission changes, it

was observed that the winter is warming up in China, especially in the northern part (Hu et al., 2003; Ren et al., 2012).

Many studies have tried to investigate the impacts of emission changes on aerosol formation in Europe and in the United States (Aksoyoglu et al., 2011; Andreani-Aksoyoglu et al., 2008; Megaritis et al., 2013; Tsimpidi et al., 2012a; Tsimpidi et al., 2012b). Andreani-Aksoyoglu et al. (2008) applied the CAMx model to study the influences of reducing $NH_3$ and $NO_x$ emissions on secondary aerosol formation in Switzerland and northern Italy in summer and found that secondary aerosol formation in northern Switzerland is mainly limited by $HNO_3$ and aerosol formation around Milan is mostly dependent on $HNO_3$ and $NH_3$. Aksoyoglu et al. (2011) conducted similar studies in Europe in both summer and winter periods and concluded that aerosol formation in winter is more sensitive to ammonia emissions in most European areas, but it is $NO_x$-sensitive in Switzerland. Megaritis et al. (2013) applied the PMCAMx model to study the sensitivities of $PM_{2.5}$ to emissions ($SO_2$, $NH_3$, $NO_x$, anthropogenic VOCs and anthropogenic POA) in Europe, and found that reduction of $NH_3$ emissions is the most effective way to reduce $PM_{2.5}$ in both summer and winter, but reductions of $NO_x$ increases $PM_{2.5}$ in winter because more oxidants are available. Tsimpidi et al. (2012a, 2012b) applied the same model to quantify the response of inorganic $PM_{2.5}$ to emission changes of $SO_2$, $NH_3$, $NO_x$ and anthropogenic VOCs in the eastern United States in both summer and winter. They found that $SO_2$ control measure is better in July, $NH_3$ control strategy is better in January and coupled reduction of $SO_2$ and $NO_x$ emissions is more effective to reduce $PM_{2.5}$ in both summer and winter.

In addition, there have been a number of studies concerning the effects of climate/meteorology changes on $PM_{2.5}$ concentrations in the United States and in Europe (Dawson et al., 2007; Megaritis et al., 2013; Megaritis et al., 2014; Tagaris et al., 2007; Tai et al.,

2012a; Tai et al., 2012b). Tagaris et al. (2007) investigated the impacts of possible global climate change on $PM_{2.5}$ concentrations over the United States using Global Climate Model simulations and chemical transport model and found that major decreases in sulfate, nitrate and ammonium and minor organic carbon will make organic carbon be the dominant $PM_{2.5}$ component in the future. Tai et al. (2012a) also studied the influence of climate change on $PM_{2.5}$ concentration in the United States using general circulation models (GCMs) and concluded that effects of 2000-2050 climate change will affect annual $PM_{2.5}$ by less than $0.5\mu g/m^3$. Dawson et. (2007) applied PMCAMx model to study the sensitivities of $PM_{2.5}$ to various meteorological variables and concluded that wind speed, mixing height and precipitation affect all PM species, temperature increased sulfate formation and decreased nitrate and organic carbon, and absolute humidity increased nitrate formation. The effects of meteorology on $PM_{2.5}$ concentrations were also studied over Europe (Megaritis et al., 2013), and they concluded that increasing temperature decreases $PM_{2.5}$ concentrations due to evaporation of ammonium nitrate, increases organic aerosol and sulfate due to higher gas-phase reaction rates. It was also found that increasing absolute humidity increases nitrate aerosols and decreases sulfate in winter (Megaritis et al., 2014). Tai et al. (2012b) used a multiple linear regression model to explore the relationships between $PM_{2.5}$ and meteorological variables in the United States and found that temperature and $PM_{2.5}$ components are highly correlated in most of the US areas and relative humidity is negatively correlated with organic carbon but positively correlated with sulfate and nitrate. They also found that the overall correlations of temperature and RH with $PM_{2.5}$ are mainly driven by synoptic transport modes (Tai et al., 2012b).

Although the impacts of emission, climate/meteorology changes on $PM_{2.5}$ concentrations have been topics of many studies conducted in the Europe and the United States, similar studies

are still limited in China. The haze pollution is growing in China, especially in the NCP, but the causes of the growth have not been well understood. The large emission changes in the last 2 to 3 decades may be a cause and the observed winter warming in the NCP could be another cause. The main objective of this study is to quantify the responses of $PM_{2.5}$ and its major species to changes in emissions, including $SO_2$, BC, OC, $NO_x$ and $NH_3$, and to temperature, Relative Humidity (RH) and wind speed changes in the NCP region. Winter haze in the NCP has a large contribution from secondary inorganic aerosols and secondary inorganic aerosols are influenced by emissions, temperature and RH. The models used in previous similar studies referenced above are all offline models, which are not capable of considering the feedbacks of changing temperature on other meteorological variables, and the impacts of aerosols on meteorology. Wang et al. (2014b) pointed out that aerosol feedbacks should not be neglected when modeling aerosol in China, so we considered aerosols feedbacks using a fully online coupled model WRF-Chem in this study.

This chapter is organized as follows. First, the WRF-Chem model, model settings and domain settings are briefly described and then in the next section, emission changes from 1985 to 2010 and accordingly $PM_{2.5}$ changes are discussed. After that, the responses of $PM_{2.5}$ to $NH_3$ and $NO_x$ emission changes are analyzed. At last, the impacts of temperature, RH increase and decrease in wind speeds on $PM_{2.5}$ are also discussed.

## 3.3 Methodology

### 3.3.1 WRF-Chem model

The online coupled WRF-Chem model is the modeling tool used in this study. The WRF-Chem model simulates emissions, transport, chemical reactions and depositions of gases and aerosols. In this study, we used a configuration that includes direct and indirect feedbacks. The gas phase mechanism used in this study is the Carbon Bond Mechanism version Z (CBM-Z), which includes 67 species and 164 reactions (Zaveri and Peters, 1999; Zaveri et al., 2008). The gas-particle portioning module used is the MOSAIC, which considers all important aerosol components, such as sulfate, nitrate, ammonium, BC, and OC (Zaveri et al., 2008). Eight size bins version of MOSAIC was used and the aerosol sizes range from 0.039μm to 10μm. The thermodynamic module in MOSAIC consists of two methods: Multicomponent Taylor Expansion Method (METM) to obtain activity coefficients in aqueous aerosols and Multicomponent Equilibrium Solver for Aerosols (MESA) to calculate the intraparticle solid-liquid phase equilibrium, which has been proven to be accurate and computationally efficient (Zaveri et al., 2008). Other chosen parameterization schemes and the model domain settings in this study are the same as Gao et al. (2015). Three nested domains with 81km, 27km, and 9km grid resolutions from outer to innermost were used Gao et al. (2015). Inputs into the model include meteorological boundary and initial conditions from NCEP FNL 1°×1° data and chemical boundary and initial conditions from MOZART model simulations (Emmons et al., 2010). The anthropogenic emission inventory used is the Multi-resolution Emission Inventory for China (MEIC) dataset (http://www.meicmodel.org/), which provides monthly CO, $NO_x$, $SO_2$, VOC, $PM_{2.5}$, BC, OC , $CO_2$ and $NH_3$ emissions by five sectors (industry, residential, transportation and agriculture) in 2010. Simulations for evaluating $SO_2$, BC and OC emission

changes were conducted using 2010 MEIC emission with $SO_2$, BC and OC emissions overwritten by Argonne National Laboratory's annual emissions for 1985, 2000 and 2010 in China (Lu et al., 2011). Biogenic emissions were estimated online using the MEGAN model (Guenther et al., 2006). The simulation was based on a winter month January (1-31 January 2010) and five days in previous month were modeled as spin-up to overcome the influences of initial conditions.

### 3.3.2 Sensitivity experiments

To quantify the influences of emission changes of $SO_2$, BC, OC, $NH_3$, and $NO_x$, and meteorology (temperature, RH and wind speeds) changes on $PM_{2.5}$ and its major species, we simulated 9 cases. They are listed and explained in Table 3.1. The changes of $PM_{2.5}$ and its major components due to perturbations in emissions and meteorology are analyzed for the NCP region. The NCP region is defined using domain 3 in Gao et al. (2015) and the statistics of changes are calculated within domain 3 for the January 2010 month.

Table 3.1. Simulation cases and descriptions

| Cases | Descriptions |
|---|---|
| CTL | Base case, all emissions are from MEIC for 2010 |
| T2 | Temperature boundary conditions and initial conditions were increased by +2K |
| RH2 | RH boundary conditions and initial conditions were increased by +2% |
| WS90 | Wind speed boundary conditions and initial conditions were reduced by 10% |
| EMI_ANL1985 | $SO_2$, OC and BC emissions are overwritten with the ANL emissions for 1985, while other emissions were kept with MEIC 2010. |
| EMI_ANL2010 | $SO_2$, OC and BC emissions are overwritten with the ANL emissions for 2010, while other emissions were kept with MEIC 2010. |
| $NH_3$-$NO_x$-1985 | Speculate $NH_3$ and $NO_x$ emission level in 1985 based on Liu et al. (2013), while other emissions were kept with MEIC 2010. |
| $NH_3$-1985 | Speculate $NH_3$ emission level in 1985 based on Liu et al. (2013), while other emissions were kept with MEIC 2010. |
| $NO_x$-1985 | Speculate $NO_x$ emission level in 1985 based on Liu et al. (2013), while other emissions were kept with MEIC 2010. |

### 3.3.3 Model Verification

The WRF-Chem model performance has been verified using multiple observations, including surface meteorological, chemical and optical data, and satellite data in Gao et al. (2015a). The model captured the variations of surface temperature, relative humidity, while wind speed was

slightly overestimated (Gao et al., 2015a), which has been reported as a common problem of current WRF-Chem model under low wind speed conditions. The Root Mean Square Error (RMSE) of temperature varies were all less than 3.2K and RMSEs of RH vary from 6.4 to 11.1%. The RMSE of wind speeds were below the proposed criteria (2m/s) at the Beijing, Tianjin and Baoding stations, but larger than the criteria at the Chengde stations. The time series of simulated surface $PM_{2.5}$, $NO_2$, and $SO_2$ showed good agreement with observations and also with simulated aerosol optical depth (AOD) (Gao et al., 2015a). The calculated Mean Fractional Bias (MFB) and Mean Fractional Error (MFE) values of $PM_{2.5}$ ranged from -21.8% to 0.4% and ranged from 26.3% to 50.7% (Gao et al., 2015a). In addition, the comparison between model results and satellite suggested that the vertical distribution of aerosol and horizontal distribution are captured well by the model (Gao et al., 2015a). Compared with observed $PM_{2.5}$ compositions, sulfate and OC were underestimated and nitrate was overestimated by the model (Gao et al., 2015a). The underestimation of sulfate may be due to underestimation of $SO_2$ gas phase oxidation, the errors in aqueous-phase chemistry, and/or missing heterogeneous sulfate formation (Gao et al., 2015a). In general, the performance of the WRF-Chem model in predicting $PM_{2.5}$ and chemical species is reasonably acceptable.

## 3.4 Results and Discussion

### 3.4.1 $PM_{2.5}$ sensitivity to $SO_2$, BC and OC emission changes

The emission changes of $SO_2$, BC and OC and resulted impacts on $PM_{2.5}$ from 1985 to 2010 were examined based on the emission inventory of $SO_2$, BC and OC for 1985 and 2010 from ANL. Figure 3.1(a-c) displays $SO_2$, BC and OC emissions for 2010 and Figure 3.1(d-f) shows

the changes of them from 1985 to 2010. Populated regions of the NCP, such as urban Beijing, urban Tianjin, and urban Shijiazhuang, exhibit large emissions of $SO_2$, BC and OC that relate to residential and power generation. From 1985 to 2010, $SO_2$ surface emissions in urban Beijing and urban Tianjin areas decreased, but markedly increased in most areas of Hebei province, especially in Tangshan, Baoding and Shijiazhuang cities. This is because the Beijing government moved many factories out to Hebei and many new iron and steel industries appeared in Hebei after 2000. In general, averaged $SO_2$ emission in the NCP increased 25.7% from 1985 to 2010, but $SO_2$ emissions in Beijing and Tianjin decreased. Unlike $SO_2$ emissions, BC emissions significantly increased in urban Beijing from 1985 to 2010. This is because residential sources are the biggest contributor to BC in winter (Li et al., 2015) and the population in urban Beijing sharply increased with rapid urbanization. However, BC emissions in south Hebei province and Tianjin city decreased from 1985 to 2010. This may be because people living in these areas changed their cooking energy from biomass to gas. From 1985 to 2010, the mean BC emissions in the NCP increased about 6.6%. Similar to BC emissions, OC emissions increased in the center of Beijing from 1985 to 2010. In addition, OC emissions increased in most areas of Hebei province. On average, OC emissions increased 26.5% from 1985 to 2010. The enhancements of $SO_2$, BC and OC emissions in the NCP are expected to result in substantial increase in $PM_{2.5}$ concentrations.

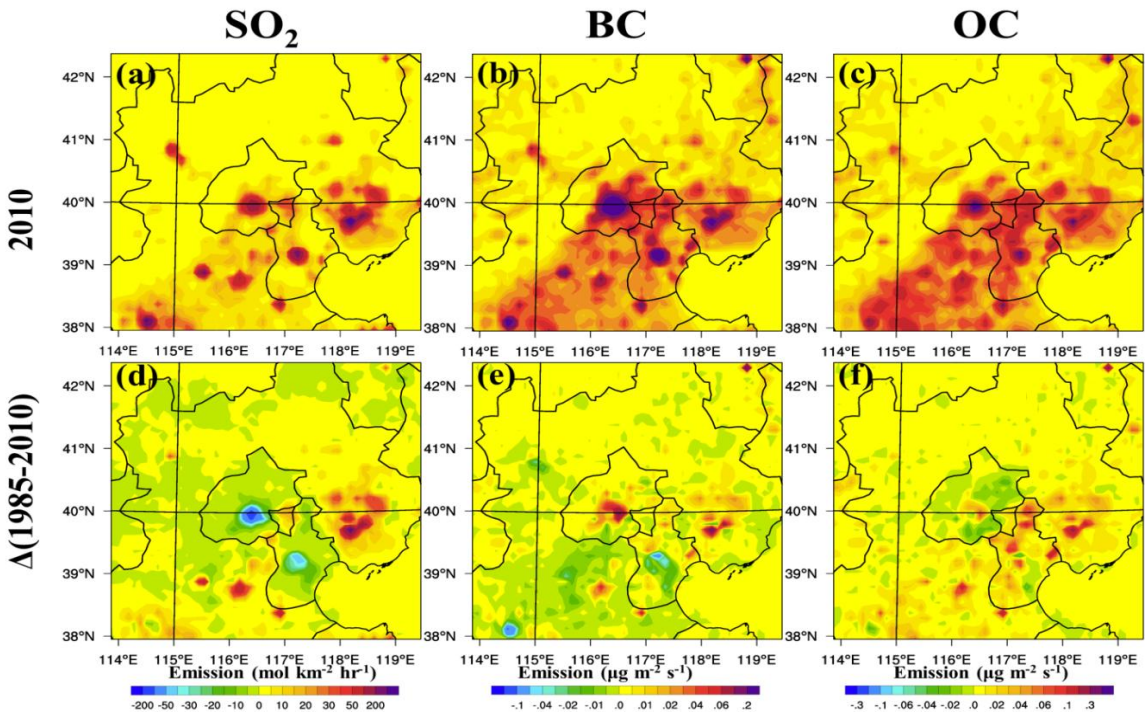


Figure 3.1. Surface SO2, BC and OC emissions for 2010 (a-c), and the changes of them from 1985 to 2010 (d-f)

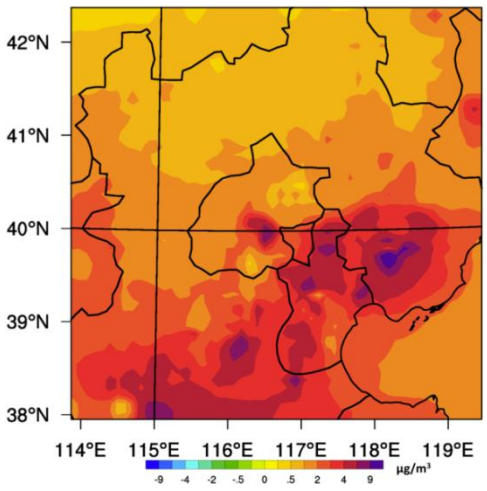


Figure 3.2. Predicted monthly mean $PM_{2.5}$ changes due to $SO_2$, BC and OC emission changes from 1985 to 2010

Figure 3.2 shows the simulated monthly mean $PM_{2.5}$ changes due to $SO_2$, BC and OC emission changes from 1985 to 2010. Predicted monthly mean $PM_{2.5}$ concentrations increase everywhere in the domain due to emission changes resulting from the rapid urbanization and industrialization processes after the implementation of Chinese economic reform in 1978. The domain mean $PM_{2.5}$ concentrations increase by 2.0μg/m$^3$ and the domain maximum increase is about 15μg/m$^3$. The most influenced regions are urban Beijing, urban Tianjin, Tangshan City and south Hebei province. Fine sulfate increases in most regions of the domain except in the urban Beijing area (Figure 3.3(d)), which is mainly caused by the substantial decrease of $SO_2$ emission from 1985 to 2010 (Figure 3.1(d)). In Figure 3.1(d), $SO_2$ emission also decreases in the urban Tianjin area, but the predicated fine sulfate increases in that area, showing that the responses of fine aerosol can be affected by emission changes in surrounding regions. The spatial distributions of fine BC and fine OC for 2010 are similar, but the magnitudes of OC concentrations are higher than BC, except in the urban Beijing area (Figure 3.3(b-c)). From 1985 to 2010, simulated fine OC increases almost over the whole domain, but fine BC decreases in some regions of Tianjin and south Hebei province (Figure 3.3(e-f)) due to the decreases in BC emissions in those areas. The increase in OC emissions in south Hebei province and Tianjin city may be related to the increasing vehicle population from 1985 to 2010. The monthly domain mean and peak fine sulfate, BC, OC and $PM_{2.5}$ for 2010 and for changes from 1985 to 2010 were computed and summarized in Table 3.2. From 1985 to 2010, sulfate increased by 30.8%, BC increased by 9.8% and OC increased by 26.8% due to 25.7% increase in $SO_2$ emissions, 6.6% increase in BC emissions and 26.5% increase in OC emissions. The nearly linear response of both BC and OC aerosols to their emissions is due to the omission of a secondary organic aerosol formation in the chosen CBMZ/MOSAIC mechanism. Thus, both were treated as primary aerosols. Our analyses

indicate that SOA contribution in this time period was small (Gao et al., 2015a). The increase in OC is more than the sum of sulfate and BC. Considering the underestimation of sulfate by the current model, the magnitudes of the sulfate enhancement due to $SO_2$ emission changes should be higher, but the enhancement fraction should be estimated more correctly. The increase of $SO_2$ emissions also causes a slight decrease in nitrate (-0.45%) and a 2.1% increase in ammonium. More free $NH_3$ reacts with enhanced $H_2SO_4$ due to increasing $SO_2$ and as a result, ammonium increases and less $HNO_3$ gas is transferred to the aerosol phase, which is consistent with the responses to increasing $SO_2$ emissions in Kharol et al. (2013).

Table 3.2. Monthly domain mean and peak BC, sulfate and $PM_{2.5}$ concentrations for 2010 and for changes from 1985 to 2010 due to BC, OC and $SO_2$ emission changes ($\mu g/m^3$)

| Years | | $SO_4^{2-}$ | BC | OC | $PM_{2.5}$ |
|---|---|---|---|---|---|
| 1985-2010 | Domain peak ($\mu g/m^3$) | 0.9 | 4.8 | 9.7 | 14.9 |
| | Domain mean ($\mu g/m^3$) | 0.3 (30.8%) | 0.3 (9.8%) | 1.4 (26.8%) | 2.0 |
| 2010 | Domain peak (µg/m3) | 3.0 | 29.6 | 25.2 | 138.9 |
| | Domain mean (µg/m3) | 1.4 | 3.6 | 6.4 | 56.4 |

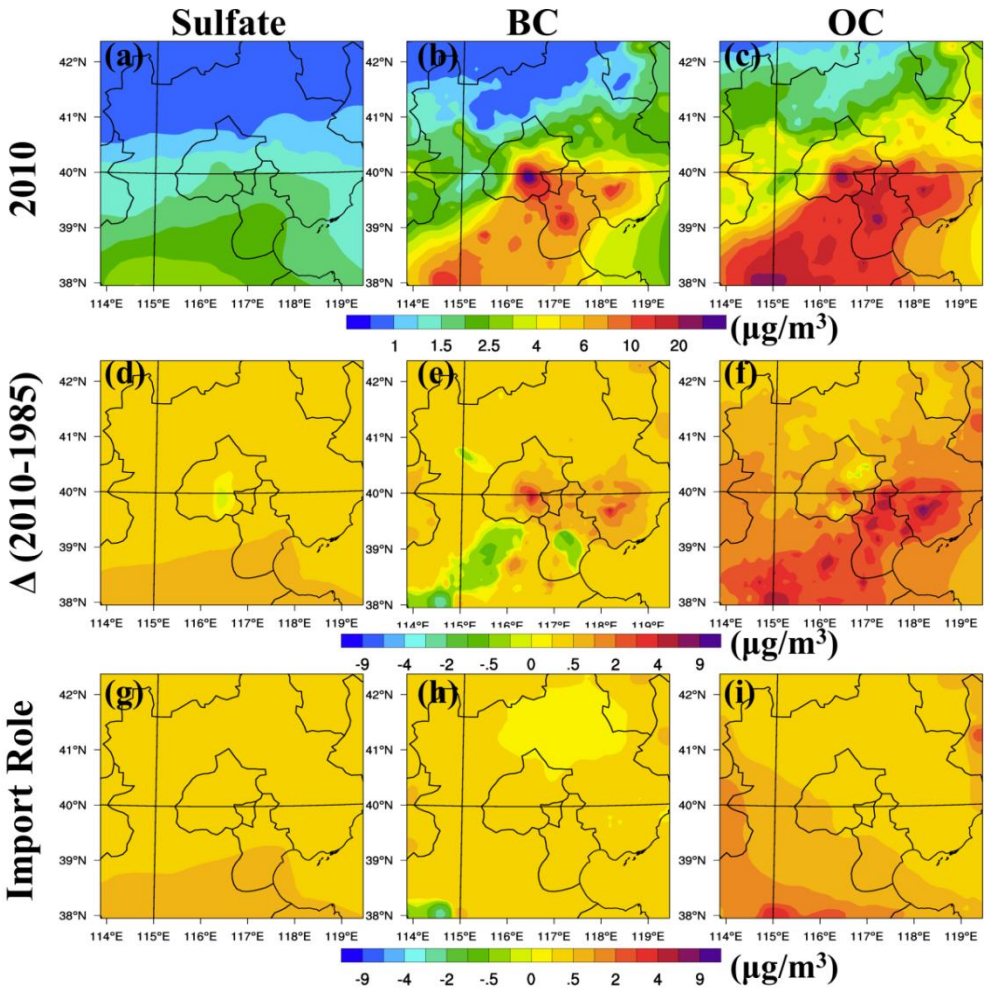


Figure 3.3. Predicted monthly mean fine sulfate, BC and OC concentrations for 2010 (a-c), the changes of them from 1985 to 2010 (d-f), and the impact of the emissions changes outside the domain (g-i)

As mentioned above, aerosol concentrations can also be affected by emission changes in surrounding areas. To explore the impact of emission changes outside the domain on aerosols in the NCP domain, we changed emissions in outer domains from 1985 to 2010 and kept emission in the innermost domain unchanged. The impact on fine sulfate, fine BC and fine OC are shown in Figure 3.3(g-i). The impact on fine sulfate shows a gradient from south to north, reflecting that

$SO_2$ and/or sulfate aerosol from south are transported into the innermost domain during this period. The magnitude of the import role is comparable to the impact of emission changes from 1985 to 2010. The impact on BC inside the innermost domain is also positive, except in the region of Shijiazhuang City. This is probably because BC emission decreases outside the innermost domain and thus less BC aerosol are imported. The domain mean of import role of OC is about 0.6μg/$m^3$, accounting for 42.9% of the total impact of emission changes from 1985 to 2010. As the emission changes of surrounding regions has significant impact on the aerosols changes in the NCP, air pollution control strategies have to be implemented in not only the NCP region, but also surrounding regions.

### 3.4.2 Sensitivity to $NH_3$ and $NO_x$ emission increases

$NH_3$ and $NO_x$ are the other two important secondary inorganic aerosol gaseous precursors in addition to $SO_2$, but we do not have detailed information about their emissions in the last two to three decades. Liu et al. (2013) provides historical trends in $NH_3$ and $NO_x$ emission over China from 1980 to 2010. From 1985 to 2010, $NH_3$ and $NO_x$ emissions over China increased about 306.6% and 121.9% respectively (Liu et al., 2013). Based on this information and available MEIC $NH_3$ and $NO_x$ emissions for 2010, we inferred $NH_3$ and $NO_x$ emissions in 1985 (other emissions were kept the same as 2010 levels. The predicted changes of $PM_{2.5}$ and major $PM_{2.5}$ inorganic species at the ground-level after a 300% increases in $NH_3$ and 120% in $NO_x$ emissions are shown in Figure 3.4 and monthly domain maximum and mean aerosol changes are summarized in Table 3.3.

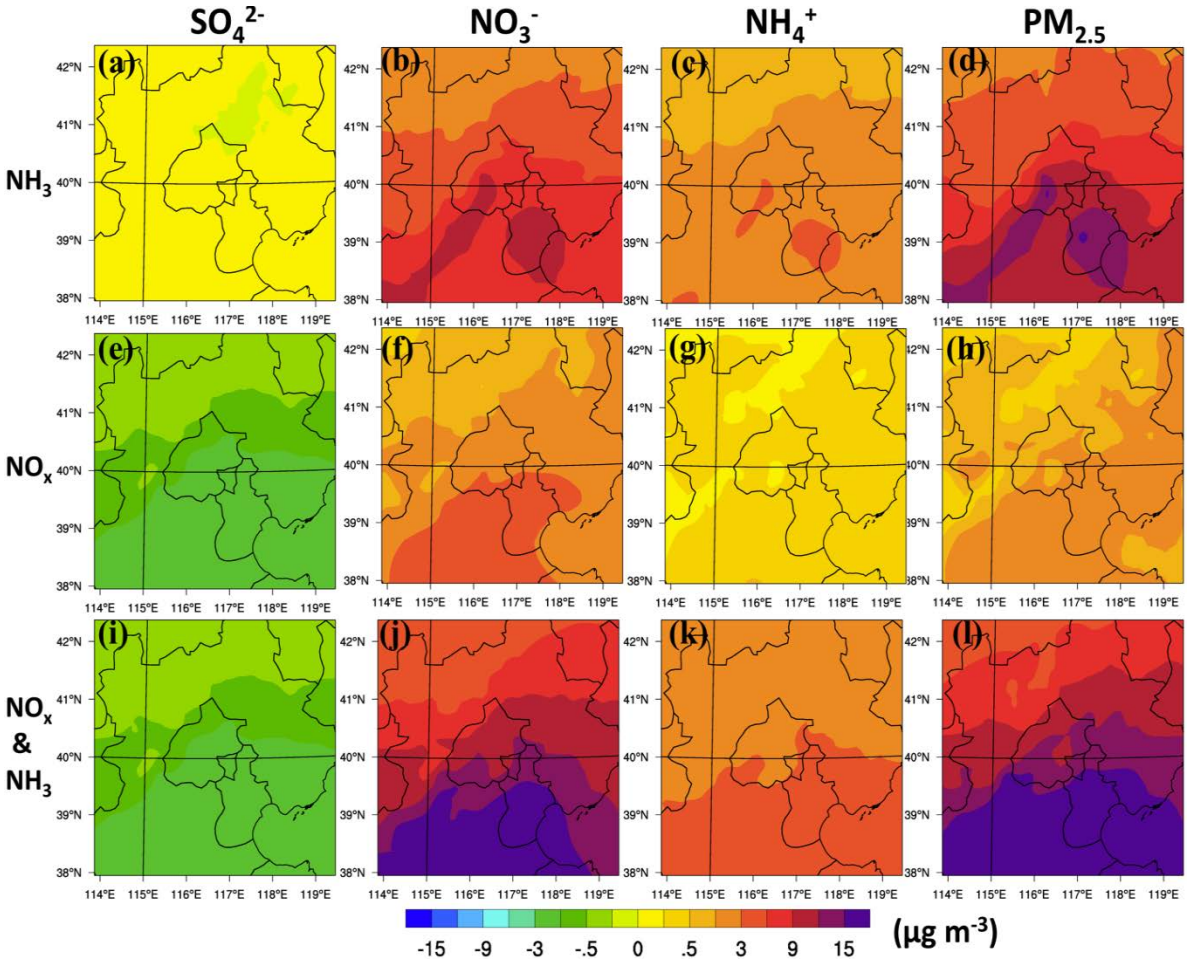


Figure 3.4. Responses of $PM_{2.5}$ and major $PM_{2.5}$ inorganic species (sulfate, nitrate, and ammonium) to $NH_3$ and $NO_x$ emission changes from 1985 to 2010

### 3.4.2.1 Increase of $NH_3$ emissions

We further explored the sensitivity of $PM_{2.5}$ to changes in $NH_3$ and $NO_x$ emission by carrying out simulation where $NH_3$ and $NO_x$ emissions varied separately. Figure 3.4(a-d) shows the spatial distributions of sulfate, nitrate, ammonium, and $PM_{2.5}$ changes due to the increase of $NH_3$ emissions. The 300% increase in $NH_3$ emissions results in significant increases in nitrate (+101.7%) and ammonium (+67.0%). The domain mean changes of sulfate due to increase in

$NH_3$ is close to zero (about 0.02μg/$m^3$), which is consistent with the results from Kharol et al. (2013).

Table 3.3. Monthly domain maximum and mean aerosol changes (μg/m3) due to $NH_3$ and $NO_x$ increases from 1985 to 2010

| | $SO4^{2-}$ | $NO^{3-}$ | $NH^{4+}$ | $PM_{2.5}$ |
|---|---|---|---|---|
| Increase $NH_3$ | 0.1 | 11.6 | 3.5 | 15.6 |
| | 0.02(0.6%) | 5.7 (101.7%) | 1.8 (67.0%) | 7.5 |
| Increase $NO_x$ | -2.66 | 4.57 | 0.5 | 3.0 |
| | -1.0 (-36.8%) | 2.0 (+35.2%) | 0.2 (7.3%) | 1.1 |
| Increase Both | -2.7 | 18.8 | 4.9 | 22.2 |
| | -1.0 (-36.4%) | 10.7 (190.5%) | 2.8 (108.2%) | 12.5 |

The monthly domain maximum and mean nitrate changes are about 11.6μg/$m^3$, and 5.7μg/$m^3$ (Table 3.3) and the maximum change occurred in urban Beijing and urban Tianjin where anthropogenic $NO_x$ emissions are very high. The significant increases of nitrate after $NH_3$ emission increase indicate that $NH_3$ limits the $NH_3NO_3$ formation in the NCP region in this period and its reduction might be useful to control winter $PM_{2.5}$ in the NCP. Megaritis et al. (2013) found that $NH_3$ reduction is effective to control $NH_3NO_3$ formation in the eastern United States and in Europe.

The monthly domain mean increase of ammonium is about 1.8μg/m$^3$ and the peak change also occurred in urban Bejing and urban Tianjin. Due to $NH_3$ emission increase, monthly domain averaged $PM_{2.5}$ increases 7.5μg/m$^3$ and the peak increase is about 15.6μg/m$^3$ in urban areas.

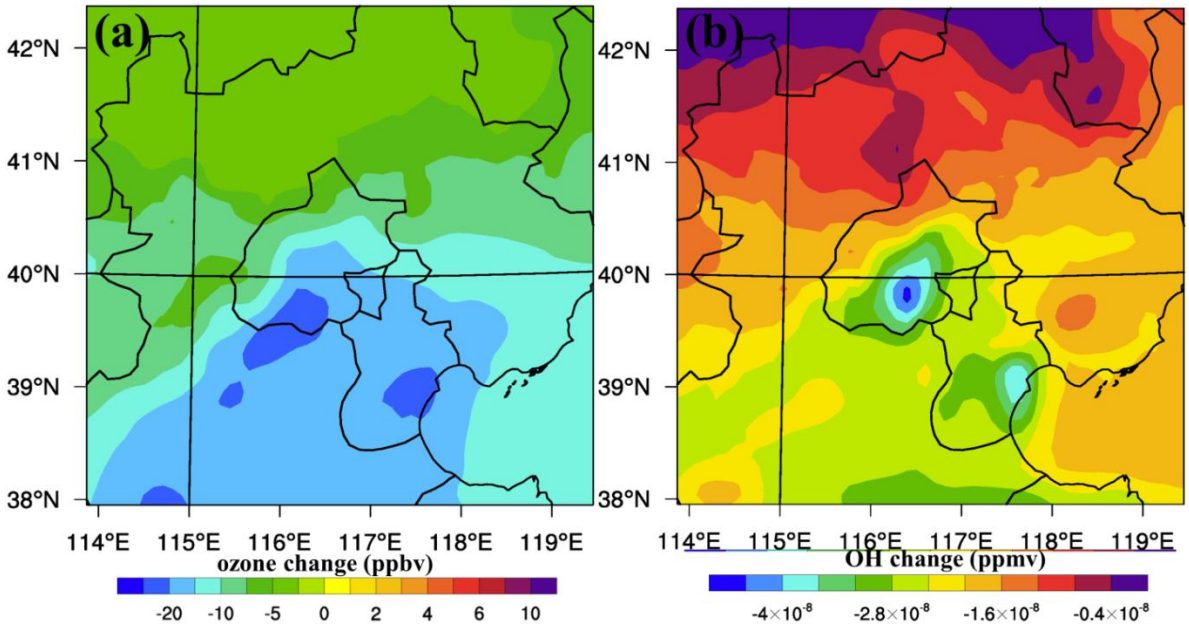


Figure 3.5. Daytime ozone (a) and OH (b) changes due to $NO_x$ emission increases

### 3.4.2.2 Increase of $NO_x$ emissions

After 120% increases in $NO_x$ emissions, domain mean surface $PM_{2.5}$ increases about 3.0μg/m$^3$, but the changes of individual $PM_{2.5}$ inorganic components vary. The increase of $NO_x$ emissions cause 1.0μg/m$^3$ (-36.8%) decrease in monthly domain mean sulfate and the domain peak sulfate reduction is about 2.7μg/m$^3$. The OH radical is critical in the sulfate formation in the regions where $SO_2$ concentrations are high and there is a competition between $NO_x$ and VOCs to react with OH (Tsimpidi et al. 2012b). When the VOCs/$NO_x$ concentration ratio is close to 5.5:1,

the OH reacts with $NO_x$ and VOCs at an equal rate (Seinfeld and Pandis, 2006). When the concentration ratio is lower than 5.5:1, the OH will primarily react with $NO_x$, and the region with this concentration ratio is called VOC-limited region. In VOC-limited region, an increase of $NO_x$ will cause a decrease of OH and ozone concentration. When the VOCs/$NO_x$ concentration ratio is higher than 5.5:1, the OH will preferentially react with VOCs, and the region with this high ratio is called $NO_x$-limited region. In the $NO_x$-limited region, an increase of $NO_x$ will increase OH and ozone concentrations. In the simulated winter month, biogenic emissions are low and $NO_x$ emissions in the NCP is very high, leading to lower VOCs to $NO_x$ ratio, and it can be considered as VOC-limited region. Fu et al. (2012) pointed out that north East Asia is VOC-limited in January and urban areas of Beijing are VOC-limited in both January and July. As a result, the 120% increase in $NO_x$ emissions result in a 21.9% decrease in daytime surface ozone concentration and 45.8% decrease in daytime surface OH concentration, which are shown in Figure 3.5. Over the entire domain, ozone and OH decrease due to $NO_x$ emission increases (Figure 3.5). Consequently, sulfate aerosol decrease over the entire domain, as shown in Figure 3.4(e). In addition, the decrease in sulfate might also be related to the changes in thermodynamics of the ammonium-sulfate-nitrate system. Although OH decreases, nitrate still rises (2.0μg/$m^3$, +35.2%) due to increase in $NO_x$ emissions, and so does ammonium (0.2μg/$m^3$, +7.3%). The net effects of $NO_x$ emission increases bring about 1.1μg/$m^3$ increase in monthly domain mean $PM_{2.5}$ concentration and the domain peak increase is about 3.0μg/$m^3$ (Table 3.3), both of which are much less than the net effects of increase in $NH_3$ emissions.

#### 3.2.2.3 Coupled increases of $NH_3$ and $NO_x$ emissions

As shown above, increasing $NH_3$ emissions significantly increases $PM_{2.5}$ concentrations in the NCP region and increasing $NO_x$ emissions also increases $PM_{2.5}$ concentrations but to a lesser extent. The effects of coupled increases of $NH_3$ and $NO_x$ emissions are shown in Figure 3.4(i-l) and the effects on sulfate, nitrate, ammonium and $PM_{2.5}$ are mostly a simple addition of the effect of increasing $NH_3$ emissions and the effect of increasing $NO_x$ emissions. Due to the coupled increases of $NH_3$ and $NO_x$ emissions, monthly domain mean $PM_{2.5}$ increases 2.5μg/m$^3$ and the peak increase is about 17.5μg/m$^3$ (Table 3.3).

### 3.4.3 Effects of temperature increases

The model used in this study is a fully online-coupled model, which simulates meteorological variables and chemical variables together. Therefore, it is impossible to increase temperature uniformly, unlike previous studies using offline models (Dawson et al., 2007; Megartis et al., 2013; Megartis et al., 2014). To examine the sensitivity of $PM_{2.5}$ to temperature increase (reflecting the winter warming trends), we increase temperature by +2°C in the initial and boundary conditions. As a result, the monthly domain mean surface temperature increases 2.0 °C, but in a non-uniform manner. The spatial distributions of monthly mean surface temperature and temperature changes are shown in Figure 3.6(a-b). The monthly mean surface temperature increases more along top left domain boundaries and less over the Bohai sea. The influence of increasing temperature on biogenic emissions is included using temperature-sensitive biogenic emission model MEGAN (Guenther et al., 2006).

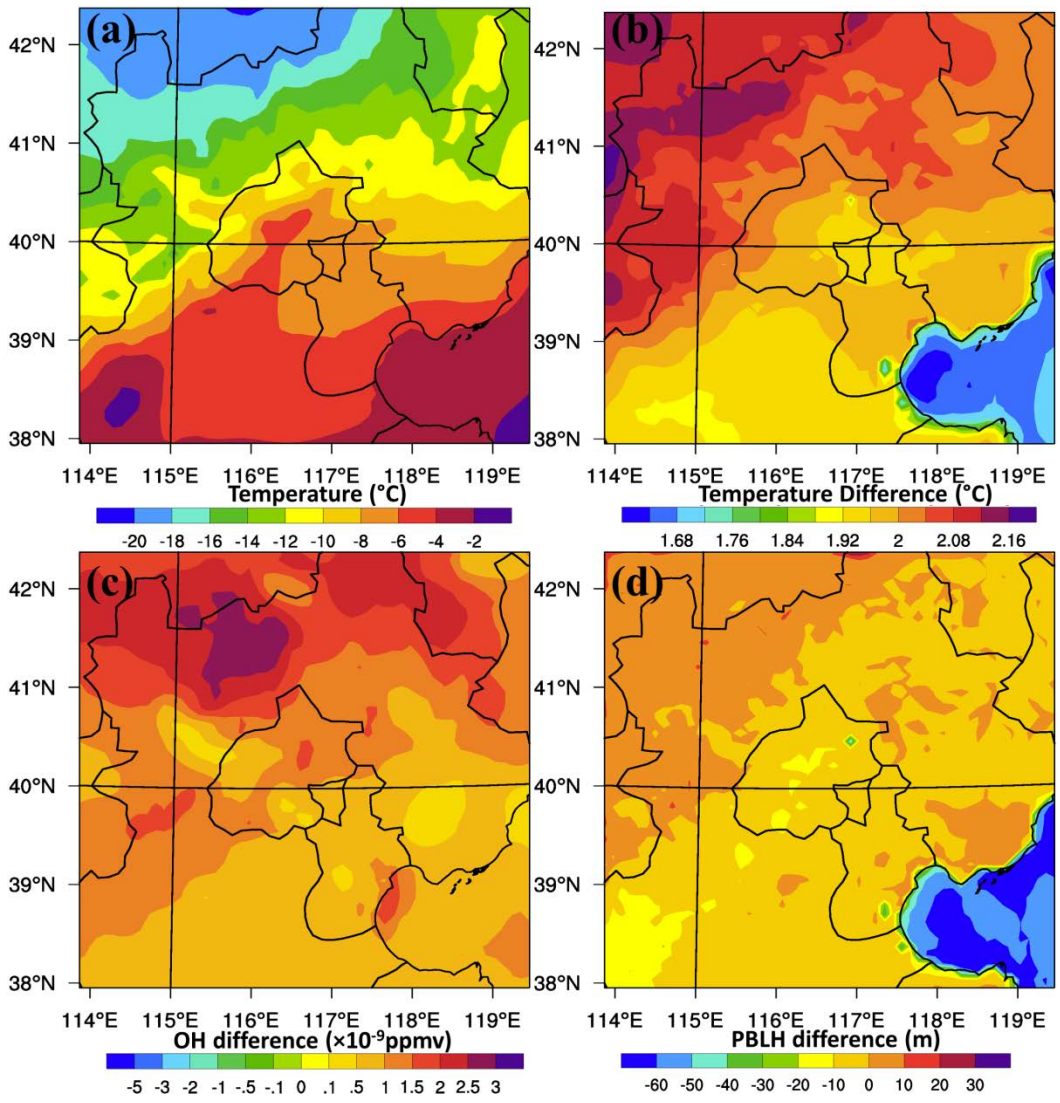


Figure 3.6. Monthly mean temperature (a) and temperature difference due to perturbation in initial and boundary conditions (b), and daily mean OH (c), mean PBLH (d) changes due to temperature increase

Due to the perturbation in temperature as mentioned above, sulfate, nitrate, ammonium and $PM_{2.5}$ are predicted to increase throughout the domain (Figure 3.7). Predicted monthly mean sulfate increase 0.1μg/m$^3$ (+9.8%), nitrate increase 0.7μg/m$^3$ (+4.8%), and ammonium increase

0.3μg/m$^3$ (+5.3%). Monthly $PM_{2.5}$ concentration increases by 2.6μg/m$^3$ on domain average, and the domain peak increase is about 6.0μg/m$^3$. The increases of sulfate, nitrate and ammonium are mostly attributed to the increasing OH radicals, as shown in Figure 3.6(c). After the temperature perturbation, daily OH increase about 6.1% on domain average, and the distributions of OH increase roughly corresponds to the distributions of temperature increase, with more increase along top left domain boundaries and less increase near the Bohai sea. It was found that higher temperature increased volatilization of ammonium nitrate and partitions it to the gas phase (Megaritis et al., 2014), but it is not significant here (ammonium nitrate decreases only in small areas close to the Bohai sea) due to the low temperature in winter. In addition, the increase of sulfate, nitrate, and ammonium could be partially due to accelerated gas-phase reaction rate at higher temperature (Dawson et al., 2007; Megaritis et al., 2014).

As shown in Figure 3.7, $PM_{2.5}$ concentration increases more than the sum of sulfate, nitrate, and ammonium increases, suggesting that primary aerosols also increase after the temperature perturbations (In the chosen CBMZ-MOSAIC mechanism, there is no secondary organic aerosol formation). On average, monthly BC concentration increases 2.4% and monthly OC concentration increases 2.5%. Since the temperature is perturbated in an online-coupled way, it can affect other physical parameter, such as wind direction, wind speed, and PBLHs, which are key factors in the diffusion of air pollutants.

Figure 3.6(d) shows that monthly PBLHs in most NCP areas decrease after the temperature perturbation, and PBLHs over the Bohai sea decrease the most, with monthly mean decrease over 60 meters. The monthly domain average PBLHs decrease about 2.2% due to increasing temperature. Besides, surface horizontal winds also change due to temperature increase, as shown in Figure 3.8. Wind speeds decrease over the whole domain (Figure 3.8(b)). Over the

Bohai sea, wind fields have larger differences compared to the changes over the NCP land. The decreases in PBLHs and surface wind speeds due to temperature perturbation directly affect the distributions and magnitudes of $PM_{2.5}$ concentrations in the NCP.

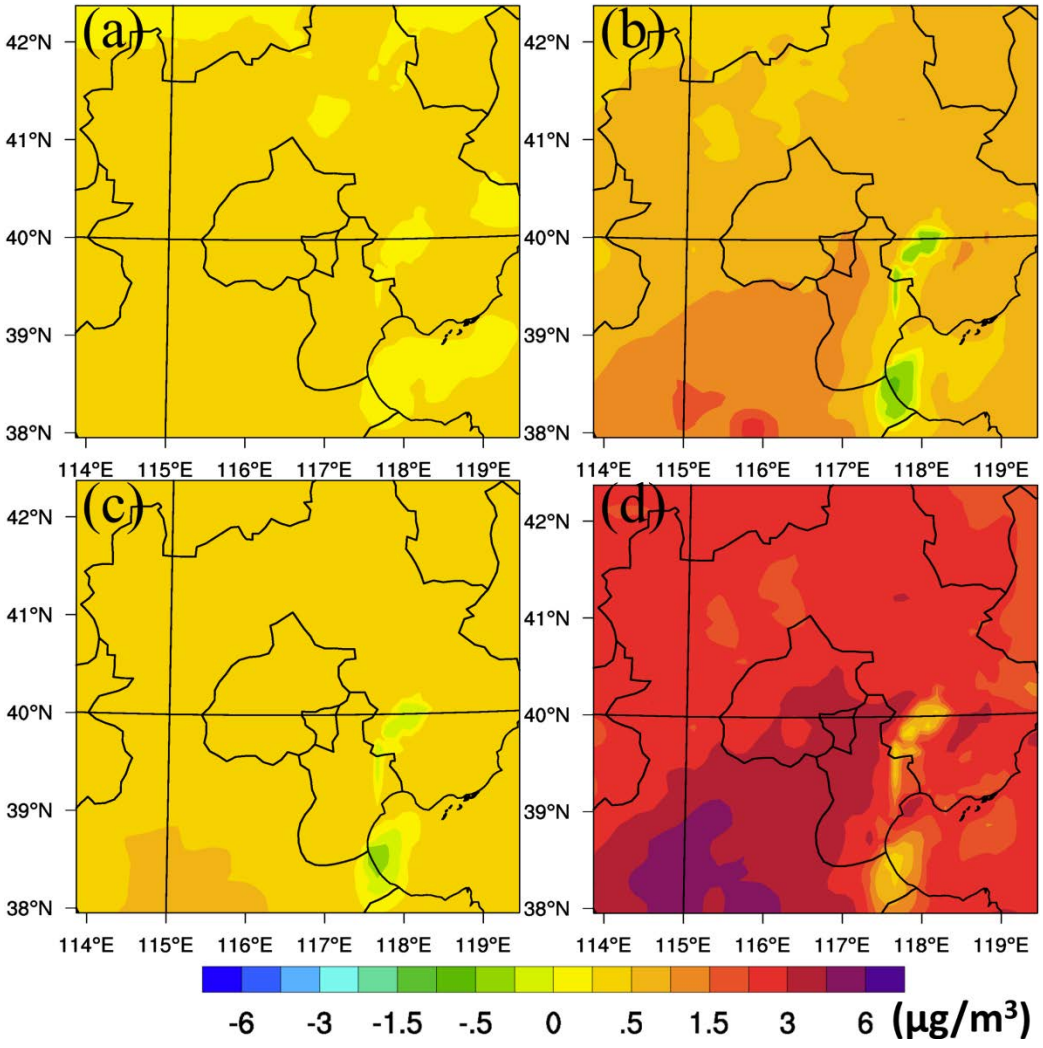


Figure 3.7. Monthly mean changes of sulfate (a), nitrate (b), ammonium (c), and $PM_{2.5}$ (d) due to temperature increase

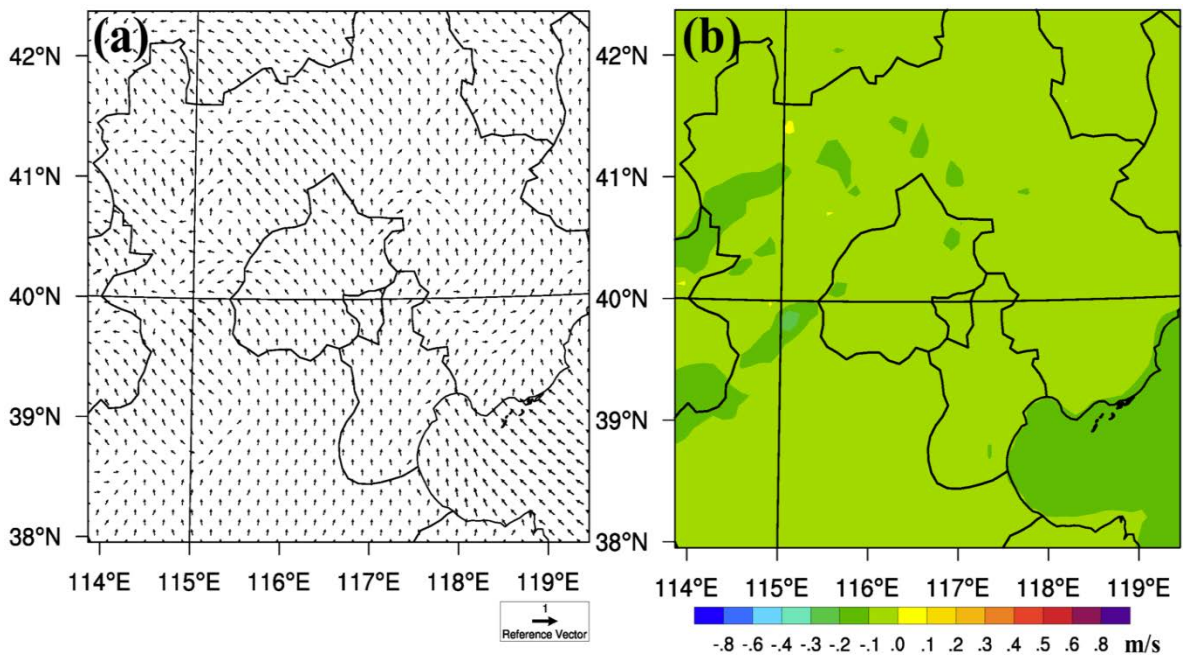


Figure 3.8. Monthly mean changes of wind fields (a) and surface horizontal wind speeds (b) due to temperature increase

### 3.4.4 Effects of RH increases

The RH was enhanced by 10% in model initial and boundary conditions, as a result, the simulated monthly mean RH increase 11.4% on domain average. We chose to increase by 10% because the variations of RH in the past several decades in the NCP are close to 10%. The monthly mean RH and the changes are shown in Figure 3.9(a-b). RH increases more in the west and northeast regions than in the middle region. Because of higher RH, dry $PM_{2.5}$ decreases 9.3μg/m$^3$ and water $PM_{2.5}$ increases about 8.1μg/m$^3$. In addition, more clouds form near the surface (5.9 times). The spatial distributions of dry $PM_{2.5}$ changes are corresponding to the changes of water $PM_{2.5}$ and clouds (Figure 3.10). The changes of sulfate, nitrate and ammonium are shown in Figure 3.11. All these species decrease due to RH increase. Previous sensitivity

studies found that increases in RH can enhance nitrate as more $HNO_3$ is shifted to the aerosol phase (Dawson et al., 2007; Megaritis et al., 2014) and other species are less sensitive to humidity changes (Dawson et al., 2007). However, the increases in RH may affect the wet deposition rate to change aerosol concentration. The decreases in $PM_{2.5}$ concentration and its species are due to wet deposition. Wet deposition is one of the major sinks of aerosols. The increase RH promotes the formation of clouds, as shown in Figure 3.10(c), and as a result, the in-cloud scavenging loss rate is enhanced.

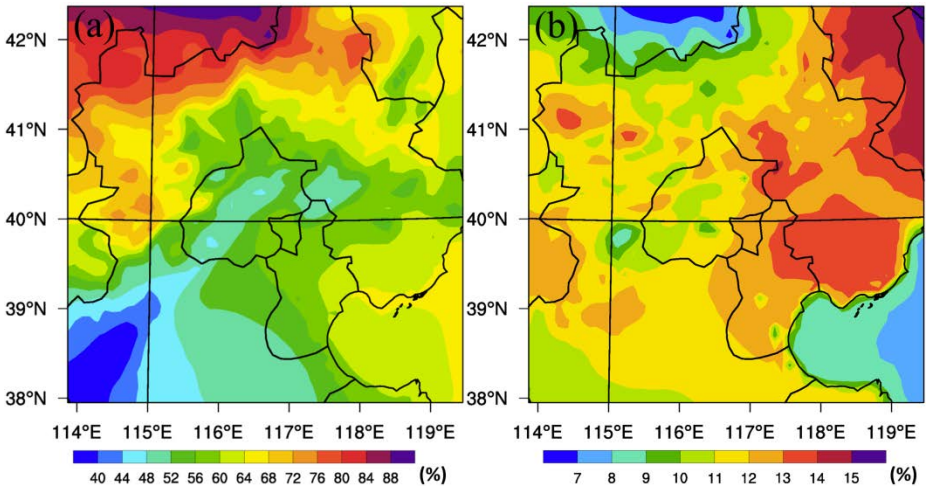


Figure 3.9. Monthly mean RH (a) and RH difference due to perturbation in RH initial and boundary conditions (b)

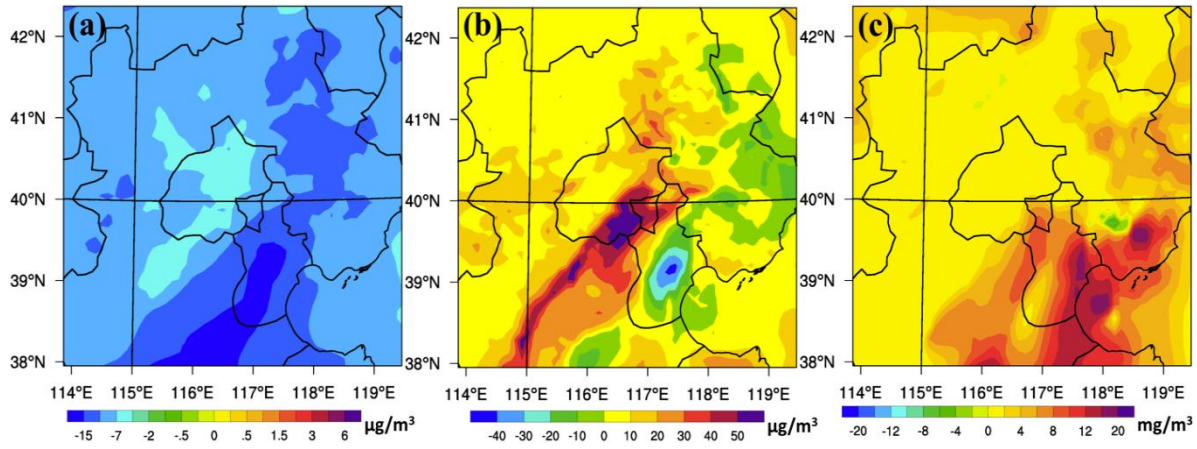


Figure 3.10. Monthly mean changes of dry $PM_{2.5}$ (a), water $PM_{2.5}$ (b), and cloud (c) due to RH increase

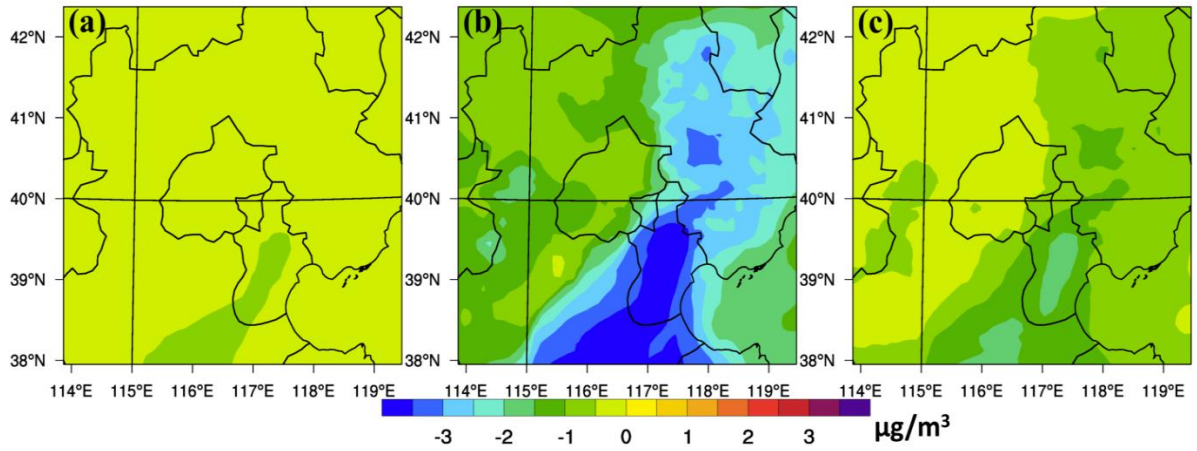


Figure 3.11. Monthly mean changes of sulfate (a), nitrate (b), and ammonium (c) due to RH increase

### 3.4.5 Effects of wind speed decreases

Simulations were also carried out when wind speeds were reduced. A 10% decrease in wind speed in initial and boundary conditions resulted in monthly mean wind speed decrease of about

0.2 m/s (5.3%). The monthly mean wind vectors of the CTL case, WS90 case and differences between them are shown in Figure 3.12. The differences are pronounced in mountainous areas (northwest areas of the domain) and relatively smaller in other areas. Figure 3.13 presents the spatial distributions of wind speeds in CTL case, and the changes of wind speeds and $PM_{2.5}$ concentrations due to perturbation of wind speeds in initial and boundary conditions. The lower wind speeds results in large areas with increased $PM_{2.5}$ due to lower dispersion rates. Monthly mean $PM_{2.5}$ is predicted to increase by 1.3% (0.7μg/$m^3$) on domain average. $PM_{2.5}$ decreases in some areas, reflecting regions with increases in wind speeds and changes in directions.

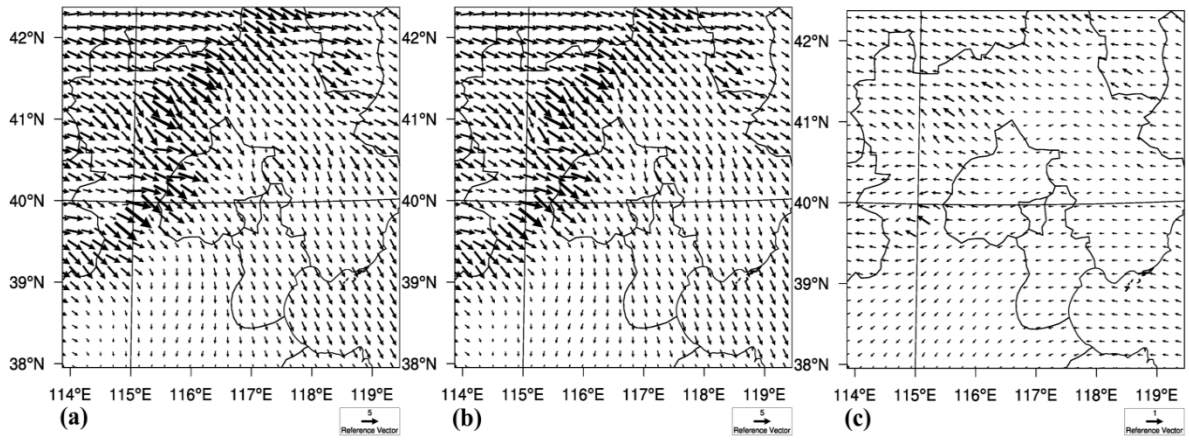


Figure 3.12. Monthly mean wind vectors of CTL case (a), WS90 case (b) and the difference between them (WS90-CTL) (c)

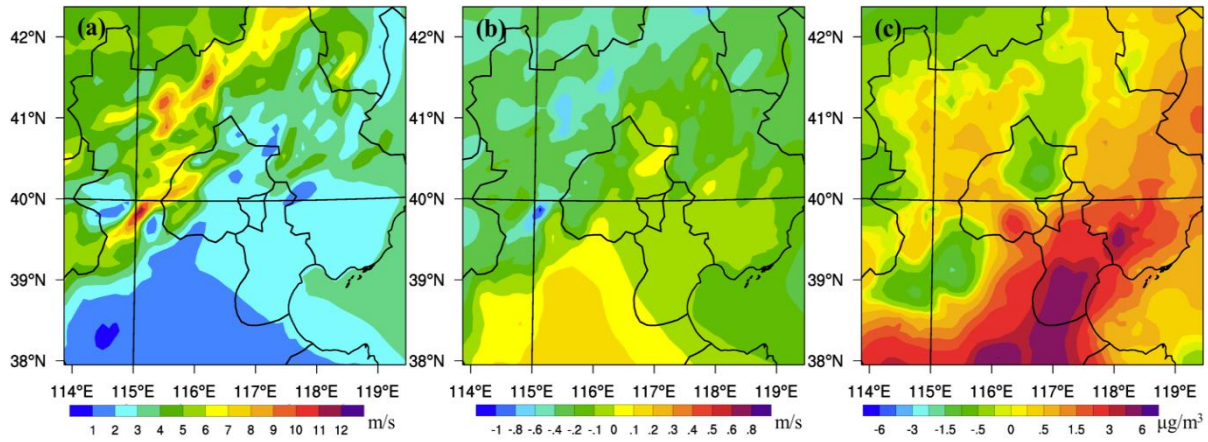


Figure 3.13. Monthly mean wind speeds of CTL case (a), changes of wind speeds (WS90-CTL) (b), and changes of $PM_{2.5}$ concentration

## 3.5 Summary

A fully online coupled meteorological and chemical transport model, WRF-Chem was used to study responses of winter $PM_{2.5}$ concentrations to changes in emissions of $SO_2$, BC, OC, $NH_3$, and $NO_x$ and to meteorology (temperature, RH, and wind speeds) changes in the NCP region, where people are suffering from severe winter haze pollution.

The detailed historical emissions of $SO_2$, BC, and OC in 1985 and 2010 from ANL were used to evaluate the impacts of changes in emissions of $SO_2$, BC, and OC. From 1985 to 2010, the 25.7% increases in $SO_2$ surface emissions lead to a 30.8% increase in surface sulfate aerosols. BC and OC emissions increased by 6.6% and 26.5%, and accordingly monthly domain mean BC and OC aerosols increased by 9.8% and 26.8%. Due to $SO_2$, BC, and OC emission changes from 1985 to 2010, the domain maximum monthly $PM_{2.5}$ changes reached 14.9µg/m$^3$, and OC accounted for more than half of this change. The 300% increases in $NH_3$ emission and 120% increases in $NO_x$ emissions were inferred from Liu et al. (2013), and the responses of winter

$PM_{2.5}$ concentrations showed that increasing $NH_3$ emissions significantly increased $PM_{2.5}$ concentrations in the NCP region. The increases in $NO_x$ emissions also increased $PM_{2.5}$ concentrations, but to a lesser extent. The increases in $NO_x$ emissions actually caused a 27.5% decrease in surface ozone concentration and 44.7% decrease in surface OH radical concentrations, because the NCP region is VOC-limited in the winter and the reduced oxidants decrease sulfate aerosol.

The sensitivities of $PM_{2.5}$ to emission changes of its precursors provide some implications for haze pollution control. Although $SO_2$ emissions in Beijing significantly decreased from 1985 to 2010 due to strict air pollution control measures, sulfate may still increase in Beijing under stable conditions. Therefore, air pollution control measures should be implemented on a regional scale, not just in megacities. The $SO_2$ emissions in China are mostly from power plants and industry, and $SO_2$ emissions have been decreasing after 2006 because of the usage of flue-gas desulfurization technology and the phase-out of some power units (Lu et al., 2011). As shown above, OC accounts for a large fraction in $PM_{2.5}$ changes. In China, the residential sector, particularly biofuel usage is the primary sources of OC. Therefore, the usage of natural gas or other clean energy should be promoted to reduce the usage of coal and biofuel. $PM_{2.5}$ is sensitive to increasing $NH_3$, indicating control of $NH_3$ emissions may be effective to control haze pollution. $NH_3$ emissions in China are mainly from agriculture sources (about 90%), including livestock, fertilizer, and agricultural soil (Huang et al., 2012). Lelieveld et al. (2015) found that agricultural emissions make the largest relative role in $PM_{2.5}$ concentration in eastern USA, Europe, Russia and East Asia. To control $NH_3$ emissions from agriculture sources, some animal feeding and animal housing strategies should be taken.

The effects of changes in winter time meteorology conditions were also studied. A 2 °C perturbation in model initial and boundary conditions lead to a 2 °C increase in domain mean surface temperature. Due to temperature increase, monthly mean sulfate increased 0.1μg/$m^3$ (+9.8%), nitrate increased 0.7μg/$m^3$ (+4.8%), and ammonium increased 0.3μg/$m^3$ (+5.3%). The predicted monthly $PM_{2.5}$ concentration increased 2.6μg/$m^3$ on domain average, and the domain peak increased by 6.0μg/$m^3$. The increases of sulfate, nitrate, and ammonium mostly resulted from increasing OH radicals and higher chemical reaction rate under enhanced temperature. The other causes of the increased $PM_{2.5}$ are the large changes in surface wind fields and PBLHs. A increase in RH promotes more clouds and water aerosols, but dry $PM_{2.5}$ decreased due to enhanced wet deposition rate. Because of the decrease in wind speeds (0.2 m/s, 5.3%), monthly mean $PM_{2.5}$ increased by 1.3% (0.7μg/$m^3$) on domain average.

Previous studies (Dawson et al., 2007; Megartis et al., 2013; Megartis et al., 2014) applied identical temperature increase to the model to investigate the effects of temperature increase, but the temperature increase in reality is not uniform, which may lead to large changes in atmospheric circulations. Recently, Chen and Wang (2015) found that haze over North China is associated with atmospheric circulation anomalies. Future climate change will potentially significantly impact fine particulate matter and thus human health, and conversely aerosol will affect meteorology. More studies are necessary to get a better understanding of the aerosol-meteorology/climate interactions.

## 3.6 References


Aksoyoglu, S., Keller, J., Barmpadimos, I., Oderbolz, D., Lanz, V. a., Prévăt, a. S.H., Baltensperger, U., 2011. Aerosol modelling in Europe with a focus on Switzerland during summer and winter episodes. Atmos. Chem. Phys. 11, 7355–7373. doi:10.5194/acp-11-7355-2011

Andreani-Aksoyoglu, S., Keller, J., Prévôt, A.S.H., Baltensperger, U., Flemming, J., 2008. Secondary aerosols in Switzerland and northern Italy: Modeling and sensitivity studies for summer 2003. J. Geophys. Res. Atmos. 113, 1–12. doi:10.1029/2007JD009053

Aw, J., 2003. Evaluating the first-order effect of intraannual temperature variability on urban air pollution. J. Geophys. Res. 108. doi:10.1029/2002JD002688

Bowman, F.M., Karamalegos, A.M., 2002. Estimated effects of composition on secondary organic aerosol mass concentrations. Environ. Sci. Technol. 36, 2701–2707.

Chen, H., Wang, H., 2015. Journal of Geophysical Research : Atmospheres. J. Geophys. Res. Atmos. 1–15. doi:10.1002/2015JD023225.Received

Cheung, H.C., Wang, T., Baumann, K., Guo, H., 2005. Influence of regional pollution outflow on the concentrations of fine particulate matter and visibility in the coastal area of southern China. Atmos. Environ. 39, 6463–6474. doi:10.1016/j.atmosenv.2005.07.033

Dawson, J.P., Adams, P.J., Pandis, S.N., 2007. Sensitivity of $PM_{2.5}$ to climate in the Eastern U.S.: a modeling case study. Atmos. Chem. Phys. Discuss. 7, 6487–6525. doi:10.5194/acpd-7-6487-2007

Dawson, J.P., Bloomer, B.J., Winner, D. a., Weaver, C.P., 2014. Understanding the meteorological drivers of U.S. particulate matter concentrations in a changing climate. Bull. Am. Meteorol. Soc. 95, 521–532. doi:10.1175/BAMS-D-12-00181.1

Emmons, L.K., Walters, S., Hess, P.G., Lamarque, J.-F., Pfister, G.G., Fillmore, D., Granier, C., Guenther, a., Kinnison, D., Laepple, T., Orlando, J., Tie, X., Tyndall, G., Wiedinmyer, C., Baughcum, S.L., Kloster, S., 2010. Description and evaluation of the Model for Ozone and Related chemical Tracers, version 4 (MOZART-4). Geosci. Model Dev. 3, 43–67. doi:10.5194/gmd-3-43-2010

Ezzati, M., Dockery, D.W., 2009. Fine-Particulate Air Pollution and Life Expectancy in the United States. N. Engl. J. Med.

Fu, J.S., Dong, X., Gao, Y., Wong, D.C., Lam, Y.F., 2012. Sensitivity and linearity analysis of ozone in East Asia: The effects of domestic emission and intercontinental transport. J. Air Waste Manage. Assoc. 62, 1102–1114. doi:10.1080/10962247.2012.699014

Gao, M., Carmichael, G.R., Wang, Y., Saide, P.E., Yu, M., Xin, J., Liu, Z., Wang, Z., 2015a. Modeling study of the 2010 regional haze event in the North China Plain. Atmos. Chem. Phys. Discuss. 15, 22781–22822. doi:10.5194/acpd-15-22781-2015

Gao, M., Guttikunda, S.K., Carmichael, G.R., Wang, Y., Liu, Z., Stanier, C.O., Saide, P.E., Yu, M., 2015b. Health impacts and economic losses assessment of the 2013 severe haze event in Beijing area. Sci. Total Environ. 511, 553–561. doi:10.1016/j.scitotenv.2015.01.005

Guenther, a., Karl, T., Harley, P., Wiedinmyer, C., Palmer, P.I., Geron, C., 2006. Estimates of global terrestrial isoprene emissions using MEGAN (Model of Emissions of Gases and Aerosols from Nature). Atmos. Chem. Phys. Discuss. 6, 107–173. doi:10.5194/acpd-6-107-2006

Heald, C.L., Henze, D.K., Horowitz, L.W., Feddema, J., Lamarque, J.F., Guenther, a., Hess, P.G., Vitt, F., Seinfeld, J.H., Godstein, a. H., Fung, I., 2008. Predicted change in global secondary organic aerosol concentrations in response to future climate, emissions, and land use change. J. Geophys. Res. Atmos. 113, 1–16. doi:10.1029/2007JD009092

Hu, Z.-Z., 2003. Long-term climate variations in China and global warming signals. J. Geophys. Res. 108, 1–13. doi:10.1029/2003JD003651

Huang, X., Song, Y., Li, M., Li, J., Huo, Q., Cai, X., Zhu, T., Hu, M., Zhang, H., 2012. A high-resolution ammonia emission inventory in China. Global Biogeochem. Cycles 26, n/a–n/a. doi:10.1029/2011GB004161

Jacob, D.J., Winner, D. a., 2009. Effect of climate change on air quality. Atmos. Environ. 43, 51–63. doi:10.1016/j.atmosenv.2008.09.051

Jiménez-Guerrero, P., Montávez, J.P., Gómez-Navarro, J.J., Jerez, S., Lorente-Plazas, R., 2012. Impacts of climate change on ground level gas-phase pollutants and aerosols in the Iberian Peninsula for the late XXI century. Atmos. Environ. 55, 483–495. doi:10.1016/j.atmosenv.2012.02.048

Kharol, S.K., Martin, R. V., Philip, S., Vogel, S., Henze, D.K., Chen, D., Wang, Y., Zhang, Q., Heald, C.L., 2013. Persistent sensitivity of Asian aerosol to emissions of nitrogen oxides. Geophys. Res. Lett. 40, 1021–1026. doi:10.1002/grl.50234

Lelieveld, J., Evans, J.S., Fnais, M., Giannadaki, D., Pozzer, A., 2015. The contribution of outdoor air pollution sources to premature mortality on a global scale. Nature. doi:10.1038/nature15371

Li, K., Liao, H., Mao, Y., Ridley, D. a., 2015. Source sector and region contributions to concentration and direct radiative forcing of black carbon in China. Atmos. Environ. doi:10.1016/j.atmosenv.2015.06.014

Liu, X., Zhang, Y., Han, W., Tang, A., Shen, J., Cui, Z., Vitousek, P., Erisman, J.W., Goulding, K., Christie, P., Fangmeier, A., Zhang, F., 2013. Enhanced nitrogen deposition over China. Nature 494, 459–62. doi:10.1038/nature11917

Lu, Z., Zhang, Q., Streets, D.G., 2011. Sulfur dioxide and primary carbonaceous aerosol emissions in China and India, 1996-2010. Atmos. Chem. Phys. 11, 9839–9864. doi:10.5194/acp-11-9839-2011

Megaritis, a G., Fountoukis, C., Charalampidis, P.E., Denier van der Gon, H. a C., Pilinis, C., Pandis, S.N., 2014. Linking climate and air quality over Europe: effects of meteorology on $PM_{2.5}$ concentrations. Atmos. Chem. Phys. Discuss. 14, 10345–10391. doi:10.5194/acpd-14-10345-2014

Megaritis, a. G., Fountoukis, C., Charalampidis, P.E., Pilinis, C., Pandis, S.N., 2013. Response of fine particulate matter concentrations to changes of emissions and temperature in Europe. Atmos. Chem. Phys. 13, 3423–3443. doi:10.5194/acp-13-3423-2013

Mu, Q., Liao, H., 2014. Simulation of the interannual variations of aerosols in China: role of variations in meteorological parameters. Atmos. Chem. Phys. Discuss. 14, 11177–11219. doi:10.5194/acpd-14-11177-2014

Pay, M.T., Jiménez-Guerrero, P., Baldasano, J.M., 2012. Assessing sensitivity regimes of secondary inorganic aerosol formation in Europe with the CALIOPE-EU modeling system. Atmos. Environ. 51, 146–164. doi:10.1016/j.atmosenv.2012.01.027

Ren, G., Ding, Y., Zhao, Z., Zheng, J., Wu, T., 2012. Recent progress in studies of climate change in China. Adv. Atmos. … 29, 958–977. doi:10.1007/s00376-012-1200-2.1.Introduction

Seinfeld, John H.; Pandis, S.N., 2012. Atmospheric chemistry and physics: from air pollution to climate change. John Wiley & Sons.

Steiner, A.L., Tonse, S., Cohen, R.C., Goldstein, A.H., Harley, R. a., 2006. Influence of future climate and emissions on regional air quality in California. J. Geophys. Res. Atmos. 111, 1–22. doi:10.1029/2005JD006935

Tagaris, E., Manomaiphiboon, K., Liao, K.J., Leung, L.R., Woo, J.H., He, S., Amar, P., Russell, A.G., 2007. Impacts of global climate change and emissions on regional ozone and fine particulate matter concentrations over the United States. J. Geophys. Res. Atmos. 112. doi:10.1029/2006JD008262

Tai, a. P.K., Mickley, L.J., Jacob, D.J., 2012. Impact of 2000-2050 climate change on fine particulate matter (PM 2.5) air quality inferred from a multi-model analysis of meteorological modes. Atmos. Chem. Phys. 12, 11329–11337. doi:10.5194/acp-12-11329-2012

Tai, a. P.K., Mickley, L.J., Jacob, D.J., Leibensperger, E.M., Zhang, L., Fisher, J. a., Pye, H.O.T., 2011. Meteorological modes of variability for fine particulate matter ($PM_{2.5}$) air quality in the United States: implications for $PM_{2.5}$ sensitivity to climate change. Atmos. Chem. Phys. Discuss. 11, 31031–31066. doi:10.5194/acpd-11-31031-2011

Tai, A.P.K., Mickley, L.J., Jacob, D.J., 2010. Correlations between fine particulate matter ($PM_{2.5}$) and meteorological variables in the United States: Implications for the sensitivity of $PM_{2.5}$ to climate change. Atmos. Environ. 44, 3976–3984. doi:10.1016/j.atmosenv.2010.06.060

Tsigaridis, K., Kanakidou, M., 2007. Secondary organic aerosol importance in the future atmosphere. Atmos. Environ. 41, 4682–4692. doi:10.1016/j.atmosenv.2007.03.045

Tsimpidi, A.P., Karydis, V. a, Pandis, S.N., 2007. Response of inorganic fine particulate matter to emission changes of sulfur dioxide and ammonia: the eastern United States as a case study. J. Air Waste Manag. Assoc. 57, 1489–1498. doi:10.3155/1047-3289.57.12.1489

Tsimpidi, A.P., Karydis, V. a, Pandis, S.N., 2008. Response of fine particulate matter to emission changes of oxides of nitrogen and anthropogenic volatile organic compounds in the eastern United States. J. Air Waste Manag. Assoc. 58, 1463–1473. doi:10.3155/1047-3289.58.11.1463

Wang, J., Wang, S., Jiang, J., Ding, A., Zheng, M., Zhao, B., Wong, D.C., Zhou, W., Zheng, G., Wang, L., Pleim, J.E., Hao, J., 2014. Impact of aerosol–meteorology interactions on fine particle pollution during China's severe haze episode in January 2013. Environ. Res. Lett. 9, 094002. doi:10.1088/1748-9326/9/9/094002

Wang, L.T., Wei, Z., Yang, J., Zhang, Y., Zhang, F.F., Su, J., Meng, C.C., Zhang, Q., 2014. The 2013 severe haze over southern Hebei, China: model evaluation, source apportionment, and policy implications. Atmos. Chem. Phys. 14, 3151–3173. doi:10.5194/acp-14-3151-2014

Zaveri, R. a., Easter, R.C., Fast, J.D., Peters, L.K., 2008. Model for Simulating Aerosol Interactions and Chemistry (MOSAIC). J. Geophys. Res. 113, D13204. doi:10.1029/2007JD008782

Zaveri, R. a., Peters, L.K., 1999. A new lumped structure photochemical mechanism for large-scale applications. J. Geophys. Res. 104, 30387. doi:10.1029/1999JD900876

Zhang, Q., Streets, D.G., He, K., Wang, Y., Richter, A., Burrows, J.P., Uno, I., Jang, C.J., Chen, D., Yao, Z., Lei, Y., 2007. NOx emission trends for China, 1995 - 2004: The view from the ground and the view from space. J. Geophys. Res. Atmos. 112, 1995–2004. doi:10.1029/2007JD008684

Zhao, X.J., Zhao, P.S., Xu, J., Meng, W., Pu, W.W., Dong, F., He, D., Shi, Q.F., 2013. Analysis of a winter regional haze event and its formation mechanism in the North China Plain. Atmos. Chem. Phys. 13, 5685–5696. doi:10.5194/acp-13-5685-2013

Zheng, B., Zhang, Q., Zhang, Y., He, K.B., Wang, K., Zheng, G.J., Duan, F.K., Ma, Y.L., Kimoto, T., 2014. Heterogeneous chemistry: a mechanism missing in current models to explain secondary inorganic aerosol formation during the January 2013 haze episode in North China. Atmos. Chem. Phys. Discuss. 14, 16731–16776. doi:10.5194/acpd-14-16731-2014

# CHAPTER 4: HEALTH IMPACTS AND ECONOMIC LOSSES ASSESSMENT OF THE 2013 SEVERE HAZE EVENT IN BEIJING AREA[41]

## 4.1 Abstract

Haze is a serious air pollution problem in China, especially in Beijing and surrounding areas, affecting visibility, public health and regional climate. In this study, the Weather Research and Forecasting-Chemistry (WRF-Chem) model was used to simulate $PM_{2.5}$ concentrations during the 2013 severe haze event in Beijing, and health impacts and health-related economic losses were calculated based on model results. Compared with surface monitoring data, the model results reflected pollution concentrations accurately (correlation coefficients between simulated and measured $PM_{2.5}$ were 0.7, 0.4, 0.5 and 0.6 in Beijing, Tianjin, Xianghe and Xinglong stations, respectively). Health impacts assessments show that the $PM_{2.5}$ concentrations in January might cause 690 (95% Confidence Interval (CI): (490, 890)) premature deaths, 45350 (95% CI: (21640, 57860)) acute bronchitis and 23720 (95% CI: (17090, 29710)) asthma cases in Beijing area. Results of the economic losses assessments suggest that the haze in January 2013 might lead to 253.8 (95% CI: (170.2, 331.2)) million US$ losses, accounting for 0.08% (95% CI: (0.05%, 0.1%)) of the total 2013 annual Gross Domestic Product (GDP) of Beijing.

## 4.2 Introduction

Air pollution is a severe public health problem associated with industrialization and urbanization. The World Health Organization (WHO) Global Burden of Disease (GBD) project links over 3.2 million premature deaths worldwide in 2010 to ambient particulate matter (PM)

[41] This work has been published as Gao et al. (2015).

pollution; furthermore, ambient PM pollution ranked 4$^{th}$ in health risk factors in East Asia in 2010 (Lim et al., 2012). Previous epidemiological studies have revealed robust associations between PM pollution and health effects (Dockery and Pope, 1994; Seaton et al., 1995) and recent studies provide strong evidence for the causal relationships between long and short term exposure to $PM_{2.5}$ and cardiovascular effects, mortality and likely causal relationships between long and short term exposure to $PM_{2.5}$ and respiratory effects (Burnett et al., 2014; U.S. Environmental Protection Agency, 2012). The evidence providing causal determination between $PM_{10-2.5}$ (aerodynamic diameter $\geq$ 2.5 μm but $\leq$ 10 μm), mortality and morbidity is not as strong as that for proving $PM_{2.5}$'s health impacts (U.S. Environmental Protection Agency, 2012). $PM_{2.5}$ may seriously affect human health because it is able to penetrate deeper into the lungs with small size, and various chemicals are absorbed on its surface (Pope and Dockery, 2006).

In January 2013, a severe and long-lasting haze episode occurred over eastern and northern China. According to the monitoring data by the Chinese Academy of Sciences (CAS), downtown Beijing's daily mean $PM_{2.5}$ concentrations exceeded 75 μg/m$^3$ (the Grade II daily $PM_{2.5}$ standard in China) for 70% days in January (He et al., 2014; Wang et al., 2013). As the political and cultural center of China, Beijing's air quality influences a large populace and is often prominently featured in global news and media channels. Extreme high population density increases the population weighted effects of air pollutants when air pollution events occur. To provide the basis for air pollution control, human exposures to air pollutants and health-related economic losses are needed to be quantified.

Most previous studies used monitoring data to estimate human exposures to PM (An et al., 2013; Hou et al., 2012; Zhang et al., 2008). While individual monitors have low measurement uncertainty, they do not provide or provide less information on spatial variability of PM;

furthermore, monitors may not be operated continuously in time or may suffer from missing data due to mechanical and quality assurance failures. Air quality models provide an alternative method of establishing population exposure to outdoor PM, with the benefit of complete spatial and temporal coverage. For example, Marlier et al. (2012) includes the results from GEOS-Chem model to quantify health effects from fire emissions in Southeast Asia; The chemical transport model ATMoS was used to quantify health impacts of particulate pollution in Delhi (Guttikunda and Goel, 2013) and Hyderabad, India (Guttikunda and Kopakka, 2013). These studies have been based on annual average air pollution, but there are far fewer studies that focus on the evaluation of acute air pollution episodes, which have well documented impacts on mortality. Historical examples (summarized by Henschel et al., 2012) include 60 deaths in the Meuse Valley of France in 1930 (Godlee, 1991), 18 deaths in the small town of Donora, Pennsylvania in 1952 (Godlee, 1991), and 4000-12000 excess deaths in London in 1952 (Godlee, 1991; Bell and Davis, 2001). In addition, time-series analysis shows that short-term increase in hospital admission rates is related to $PM_{2.5}$, especially for heart failure hospitalization, which increased 1.28% for every 10 $\mu g/m^3$ increase in daily mean $PM_{2.5}$ concentrations (Dominici et al., 2006).

In this paper, we aim to quantify the burden of $PM_{2.5}$ during the 2013 severe haze on both mortality and morbidity in Beijing area. Health-related economic losses are also calculated and the findings of this study can provide scientific basis for implementation of air pollution control strategies.

## 4.3 Methodology and Data

Our integrated assessments include three steps: (1) define the study region and simulate $PM_{2.5}$ concentrations; (2) estimate human exposure and health impacts, including both mortality

and morbidity; and (3) quantify the economic losses of those impacts. These three steps are described in detail here.

### 4.3.1 WRF-Chem settings and defining the study region

The 2013 haze event simulation was performed with WRF-Chem model. The model considers the interactions between meteorology and chemistry. Domain settings (definitions of simulation regions) in this study are the same as those of Jing-Jin-Ji modeled area of Yu et al. (2012). Three domains with two-way nesting were employed (Figure 4.1) and grid resolutions are 81km × 81km, 27km × 27km and 9km × 9km from outer to inner domains. Beijing was set to be the center of the innermost domain. Gas-phase chemical mechanism CBMZ (Zaveri and Peters, 1999) coupled to the 8-bin sectional MOSAIC model with aqueous chemistry (Zaveri et al., 2008) was used. We used monthly 2010 Multi-resolution Emission Inventory for China (MEIC) (http://www.meicmodel.org/) as model anthropogenic emissions inputs. Spatial resolution of this emission inventory is 0.25×0.25 degree. Biogenic emissions were predicted hourly by the MEGAN algorithm (Guenther et al., 2006). Meteorological and chemical initial and boundary conditions were obtained from National Centers for Environmental Prediction (NCEP) Final Analysis and MOZART-4 (Model for Ozone and Related chemical Tracers, version 4) forecasts (Emmons et al., 2010), respectively. The study period is January 2013 and the last five days of December, 2012 were simulated as spin-up time to overcome the impacts of initial conditions. The study region is defined with the black rectangle (between 115.5°E and 117.54°E longitude and 39.42°N and 41.12°N latitude) shown in Figure 4.1. Simulated $PM_{2.5}$ concentrations from the innermost domain were interpolated to the study region and the interpolated $PM_{2.5}$ concentrations were used to estimate human exposures and health impacts.

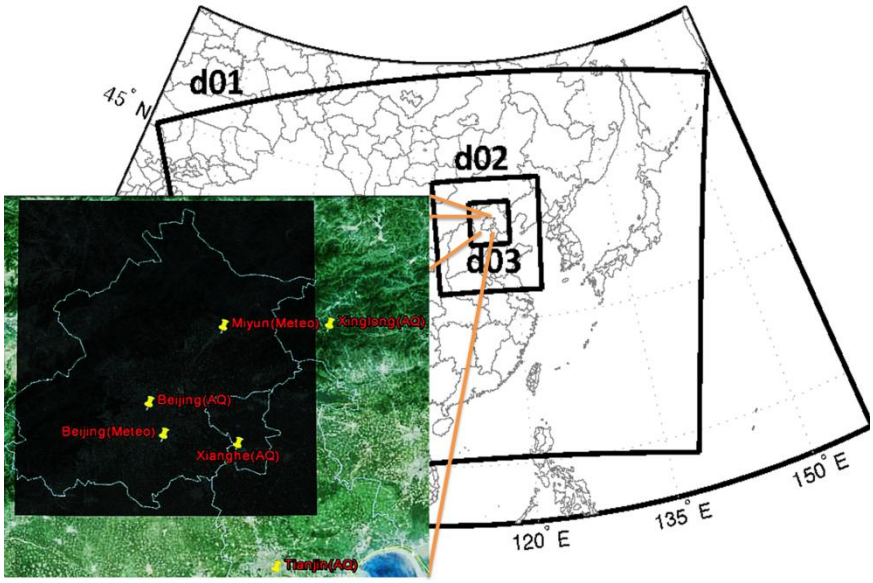


Figure 4.1. WRF-Chem domain settings, study region and geographic locations of meteorological and air quality measurements

### 4.3.2 Estimating human exposures and health impacts

Cases of mortality and morbidity can be calculated using the Poisson regression model, shown as follows (Guttikunda and Kopakka, 2013):

$$\Delta E = \sum_{i=1}^{\#grids} \Delta POP * IR * \left(1 - \frac{1}{e^{(\beta * \Delta C)}}\right) \qquad (5.1)$$

$\Delta E$ Number of estimated cases of mortality and morbidity

$\Delta C$ The incremental concentration (use WHO 24-hour mean $PM_{2.5}$ guideline as reference)

$\Delta POP$ The population exposed to the incremental concentration $\Delta C$ in grid i

$IR$ Incidence rate of the mortality and morbidity end points

$\beta$ The concentration-response function, defined as the change in number cases per unit change in concentration per capita

Simulated daily mean $PM_{2.5}$ concentrations were used to estimate exposure level using function (1). In the calculation, WHO 24-hour mean $PM_{2.5}$ guideline value (25μg/m$^3$) was used as reference to obtain the incremental concentration. The gridded population data we used are from the Gridded Population of the World (GPW) future estimates for 2015 dataset. The resolution of this dataset is 2.5 arc-minute for each grid. According to the results of the sixth population census (http://data.stats.gov.cn), 8.6% residents are between 0 and 14 years old and 8.7% residents are above 65 years old. For children, adults and old people, concentration-response functions are different. Concentration-response function and incidence rate are important in health impacts evaluation and they have variations for different countries and regions.

In this study, $\beta$ values and IRs were cited from published findings. Some studies using $PM_{10}$ for exposure assessment were also included and the following conversion relation was used: $PM_{2.5} = PM_{10} \times 0.6$ (Kan et al., 2004; Teng et al., 1999). The short-term $\beta$ values and daily IRs are summarized in Table 4.1. The $\beta$ values represent the increase in daily mortality and morbidity cases corresponding to a 10 μg/m$^3$ increase of $PM_{2.5}$ concentration. Chen et al. (2011) estimated the short-term association between $PM_{2.5}$ and daily mortality in Beijing using time-series method. For $PM_{2.5}$'s acute effects on respiratory and cardiovascular hospital admission, the $\beta$ values were collected from the meta-analysis results in China (Aunan and Pan, 2004). Xu et al. (1995) investigated the association of air pollution with daily outpatient visits in Beijing and Jin et al. (2000) provided the relation between air pollution and new occurrence of chronic bronchitis in Benxi, China using statistical regression model. The $\beta$ value for asthma was also obtained using meta-analysis method by Xie et al. (2009). Mortality and hospitalization IRs were cited from BMBPH (2013) Due to the limited data available, other IRs were cited from

Zhang et al. (2007). These IRs were converted from annually to daily with the assumption that the cases took place equally in each day (Xie et al., 2014).

Table 4.1. β values and daily IRs

| Health endpoints | β values (per 10 μg/m$^3$, 95% CI) (%) | References | IRs (‰) | References |
|---|---|---|---|---|
| Mortality | 0.53(0.37,0.69) | Chen et al. (2011) | 0.022377 | BMBPH,2012 |
| Respiratory hospital admission | 2(1.33,2.67) | Aunan et al. (2004); Zhang et al. (2007) | 0.051925 | BMBPH,2012 |
| Cardiovascular hospital | 1.17(0.5,1.83) | Aunan et al. (2004); Zhang et al. (2007) | 0.093509 | BMBPH,2012 |
| Outpatient visits-internal medicine (15+) | 0.57(0.32,0.82) | Xu et al. (1995); Zhang et al. (2007) | 2.92083 | Zhang et al.(2007) |
| Outpatient visits-pediatrics (0-14) | 0.65(0.23,1.07) | Xu et al. (1995); Zhang et al. (2007) | 0.811925 | Zhang et al.(2007) |
| Acute Bronchitis | 9.17(3.15,15.18) | Jing et al. (2000); Zhang et al. (2007) | 0.140377 | Zhang et al.(2007) |
| Asthma | 2.1(1.45,2.74) | Xie et al. (2009) | 0.215982 | Zhang et al.(2007) |

### 4.3.3 Economic valuation of the health impacts

We further evaluated the economic losses of the health impacts associated with the high $PM_{2.5}$ concentrations during haze. Here we used the unit economic losses of related health endpoints for Beijing area borrowed from Huang and Zhang (2013), listed in Table 4.2. The unit economic cost of mortality was assessed using Value of a Statistical Life (VSL) method, which indicates how much people would be willing to pay (WTP) for a reduction of death. For the case that some morbidity endpoints cannot be valued from WTP literatures, the Cost of Illness (COI) method was used. COI considers both health expenditures and loss of labor productivity. It is shown as below (Huang and Zhang, 2013):

$$C_i = (C_{pi} + GDP_p * T_{Li}) * \Delta E_i \quad (5.2)$$

Where:

$C_i$ Total economic cost for end point i

$C_{pi}$ Health expenditures for end point i

$GDP_p$ Daily GDP per capita

$T_{Li}$ Loss of labor time due to end point i

$\Delta E_i$ Health impacts of end point i

Table 4.2. Unit losses for various health endpoints in Beijing (per case, US$) (Huang and Zhang, 2013)

| Endpoints | Mortality | Acute Bronchitis | Asthma | Clinic Visit | Hospitalized |
|---|---|---|---|---|---|
| Cost per case (US$) | 273513.36 | 407.03 | 299.61 | 83.86 | 2761.04 |

## 4.4 Model Evaluation

In this section, surface meteorological and air quality measurements are used to evaluate model performance. Figure 4.2 shows the time series of simulated and observed daily mean temperature, relative humidity (RH) and wind speed at Beijing and Miyun stations. The geographic locations of these two stations are marked in Figure 4.1. The meteorological measurements were collected from the surface stations of the Chinese National Meteorological Center (http://cdc.cma.gov.cn/home.do). Local-scale meteorology is an important driver of regional air pollution (Pearce et al., 2011), so the accuracy of simulated meteorological variables is critical to the performance of air quality modeling. Simulated temperature, relative humidity and wind speed capture the main features and variations as observed at both Beijing and Miyun

stations, although small underestimation of temperature (~ -3 °C) and overestimation of wind speed exist at Beijing station. Mean bias (MB), mean error (ME) and root mean square error (RMSE) are calculated for temperature, relative humidity and wind speed at the above mentioned two stations and these evaluation metrics are summarized in Table 4.3. Emery et al. (2001) proposed that good model performance would be classified as temperature bias smaller than 0.5 degree, wind speed RMSE smaller than 2 m/s, and wind speed bias smaller than 0.5 m/s. In general, the model performs better at Miyun station than at Beijing station.

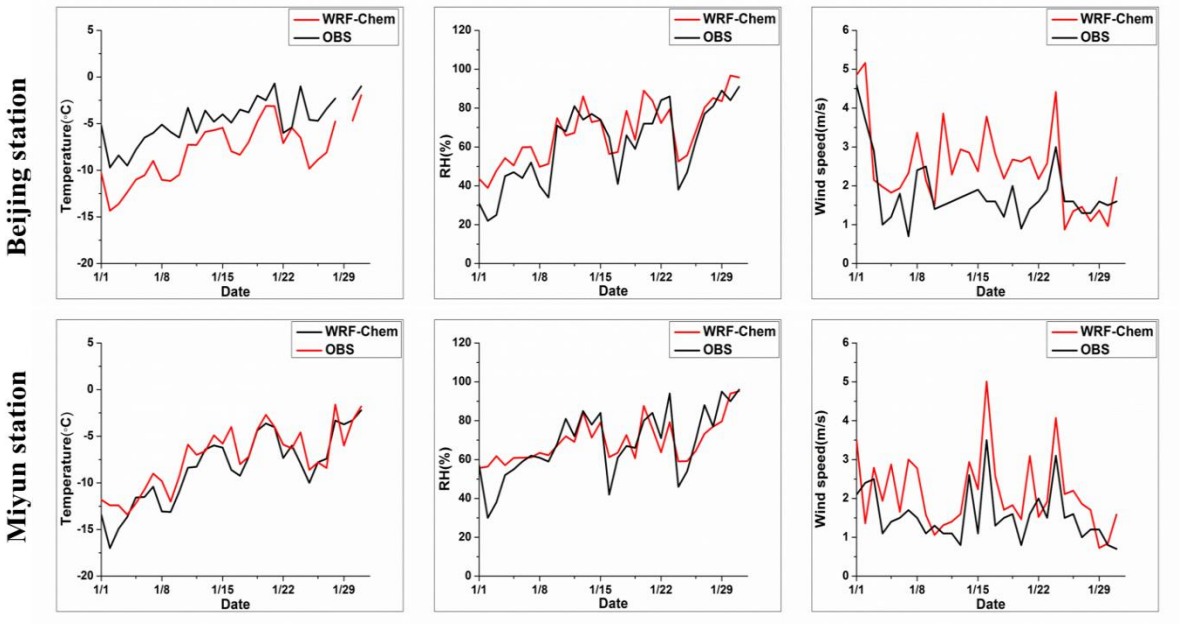


Figure 4.2. Observed (black lines) and simulated (red lines) daily meteorological variables at Beijing and Miyun stations

Table 4.3. Performance statistics for meteorological predictions at Beijing and Miyun stations

| | Bejing | | | Miyun | | |
|---|---|---|---|---|---|---|
| | MB | ME | RMSE | MB | ME | RMSE |
| Temperature (°C) | -3.2 | 3.2 | 3.6 | -1.1 | 1.4 | 1.8 |
| RH (%) | 6.3 | 9.7 | 11.1 | 0.9 | 7.3 | 9.9 |
| Wind Speed (m/s) | 0.7 | 0.9 | 1.0 | 0.6 | 0.7 | 0.9 |

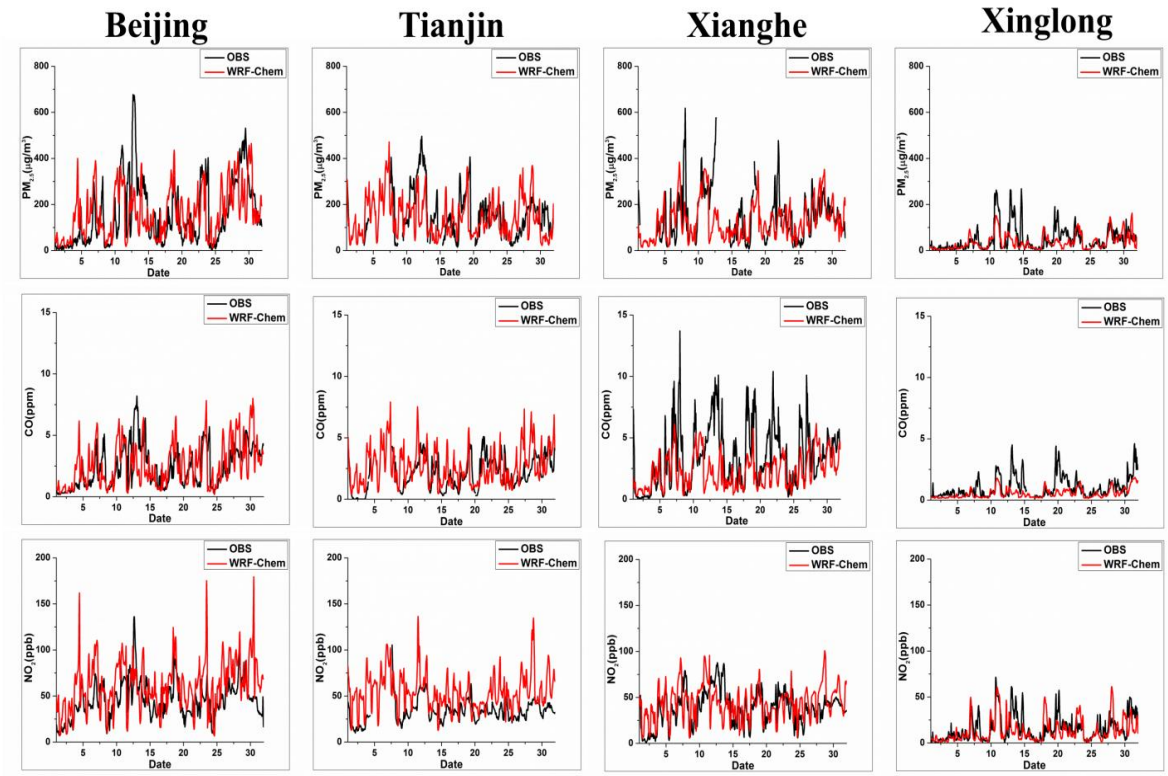


Figure 4.3. Observed (black lines) and simulated (red lines) hourly $PM_{2.5}$, CO and $NO_2$ at Beijing, Tianjin, Xianghe and Xinglong stations

The simulated hourly $PM_{2.5}$, CO and $NO_2$ were compared with air quality measurements at Beijing, Tianjin, Xianghe, and Xinglong stations in the CARE-China network. The geographic locations of these four stations are marked in Figure 4.1. As shown in Figure 4.3, the WRF-Chem model generally captured the hourly variation of $PM_{2.5}$, CO and $NO_2$ at these four stations. Underestimations of CO exist at Xianghe and Xinglong stations compared to measured concentrations. This might be caused by large uncertainties in emission inventories. On January 13, there is also an underestimation of $PM_{2.5}$. The underestimations of air pollutants may be caused by the overestimation of wind speeds (e.g. Figure 4.2). Since this paper focuses on the health impacts assessment of $PM_{2.5}$ using numerical modeling results, the accuracy of modeling $PM_{2.5}$ plays a crucial role in the assessment. MB, ME, correlation coefficients R, the normalized mean bias (NMB), the normalized mean error (NME), the mean fractional bias (MFB), and the mean fractional error (MFE) were calculated versus 24-h observations for simulated and measured $PM_{2.5}$ at four stations. The MB values for $PM_{2.5}$ at Beijing, Tianjin, Xianghe and Xinglong are 2.4, -13.7, -13.9 and -12.8, respectively (Table 4.4). Boylan et al. (2006) proposed that MFB should be within ±60% and MFE should be below 75% for a satisfactory model performance. For our results, MFB values are within 22% and MFE values are below 50%, indicating that our model results are good and reasonably represent the real pollution states. As shown in Table 4.4, $PM_{2.5}$ is slightly overestimated at Beijing station and underestimated at other three stations. Large uncertainties in aerosol emissions and lack of some secondary aerosol formation mechanisms in WRF-Chem are the two main reasons for the overestimation and underestimation. During haze events, secondary aerosols play an important role (Sun et al., 2014), which has not been well represented in WRF-Chem model.

Table 4.4. Performance statistics for $PM_{2.5}$ at four stations

| Stations | Obs. Mean ($\mu g/m^3$) | Mod. Mean ($\mu g/m^3$) | R | MB ($\mu g/m^3$) | ME ($\mu g/m^3$) | MNB (%) | MNE (%) | NMB (%) | NME (%) | MFB (%) | MFE (%) |
|---|---|---|---|---|---|---|---|---|---|---|---|
| Beijing | 158.5 | 160.9 | 0.7 | 2.4 | 70.8 | 40.7 | 64.2 | 1.5 | 44.0 | 19.2 | 48.9 |
| Tianjin | 158.2 | 144.5 | 0.4 | -13.7 | 64.4 | 17.4 | 53.7 | -8.7 | 44.6 | 2.6 | 44.8 |
| Xianghe | 152.5 | 138.6 | 0.5 | -13.9 | 55.6 | 13.7 | 43.0 | -9.1 | 40.1 | 1.0 | 39.7 |
| Xinglong | 50.8 | 38.0 | 0.6 | -12.8 | 20.6 | -8.9 | 39.1 | -25.2 | 54.3 | -21.7 | 44.1 |

## 4.5 Results and Discussion

### 4.5.1 Causing factors of this event

#### 4.5.1.1 Weather system

As shown in Figure 4.3, $PM_{2.5}$ in Beijing reached peak value ($677\mu g/m^3$) at 17:00 on January 12th. Figure 4.4 shows the surface weather analysis on that day (0000 UTC). The figure is provided by the Korea Meteorological Administration (KMA), and Beijing city is denoted with a red arrow in the figure. There were two weak high pressure systems, one in the western direction and another one in the southern direction of Beijing. Pressure gradient force was very small, and wind speeds were weak around the Beijing area, which is unfavorable to the dispersion of air pollutants.

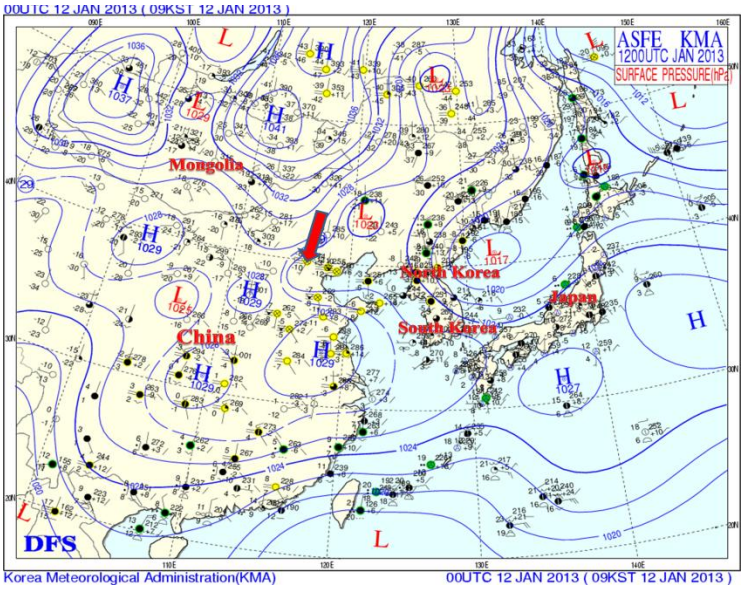


Figure 4.4. Weather maps at 0000 UTC on January 12th, 2013

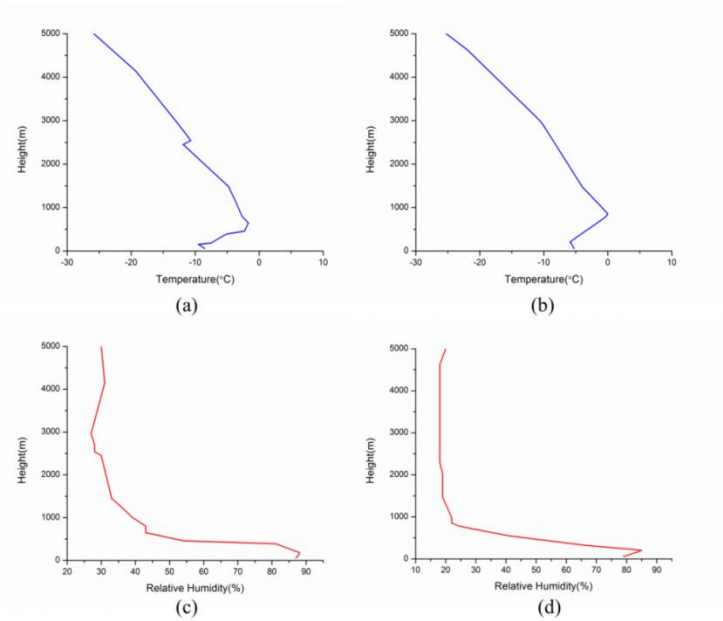


Figure 4.5. Observed vertical profile of (a) temperature at 0800 (0000 UTC) (b) temperature at 2000(1200 UTC) (c) relative humidity at 0800 (0000 UTC) (d) relative humidity at 2000 (1200UTC) on January 12$^{th}$ in Beijing

#### 4.5.1.2 Boundary layer

Figure 4.5 shows observed vertical temperature and relative humidity profiles at 0000 UTC and 1200 UTC on January 12th, 2013. These atmospheric sounding data are retrieved from the NCAR Earth observing laboratory (http://weather.uwyo.edu/upperair/sounding.html). Obvious strong temperature inversions are apparent up to heights of 500 and 1000 meters (Figure 4.5). The temperature inversions are 10°C and 5°C, indicating extreme stable vertical conditions near surface. Figures 4.5(c) and 4.5(d) show that relative humidity near surface on January 12th was above 80%. Sun et al (2006) pointed out that high RH can accelerate the formation of secondary species, such as sulfate and nitrate. The stable boundary layer and high RH near surface aggravate the pollution. In addition, Zheng et al. (2014) pointed out that regional transport played a significant role in this haze event.

### 4.5.2 Simulated $PM_{2.5}$ concentrations

The simulated monthly averaged $PM_{2.5}$ concentrations are displayed in Figure 4.6 and daily averaged $PM_{2.5}$ concentrations are shown in Figure 4.7. In the center of Beijing city, monthly averaged $PM_{2.5}$ is above 170μg/$m^3$ and the pollution level for the north part of Beijing is lower than it in the south part. Rural areas are located in the north of Beijing and economically active areas are in the south of Beijing. As shown in Figure 4.7, there are five small haze episodes in January, from 3 to 7, from 9 to 13, from 17 to 19, from 21 to 23 and from 25 to 31. High PM concentrations happen around urban area and extend to all southern regions.

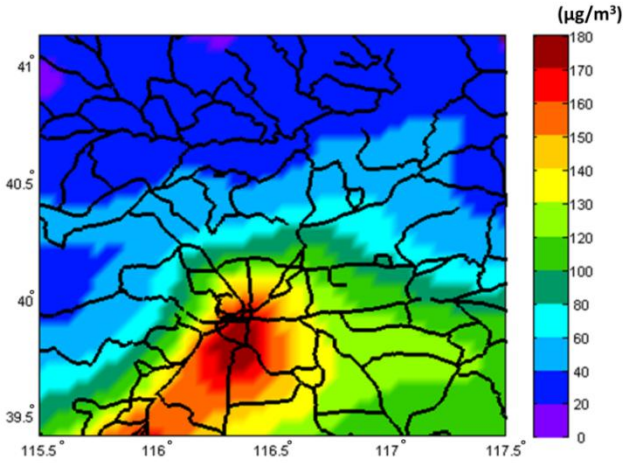


Figure 4.6. Horizontal distribution of monthly averaged $PM_{2.5}$ (x axis means longitude and y axis means latitude)

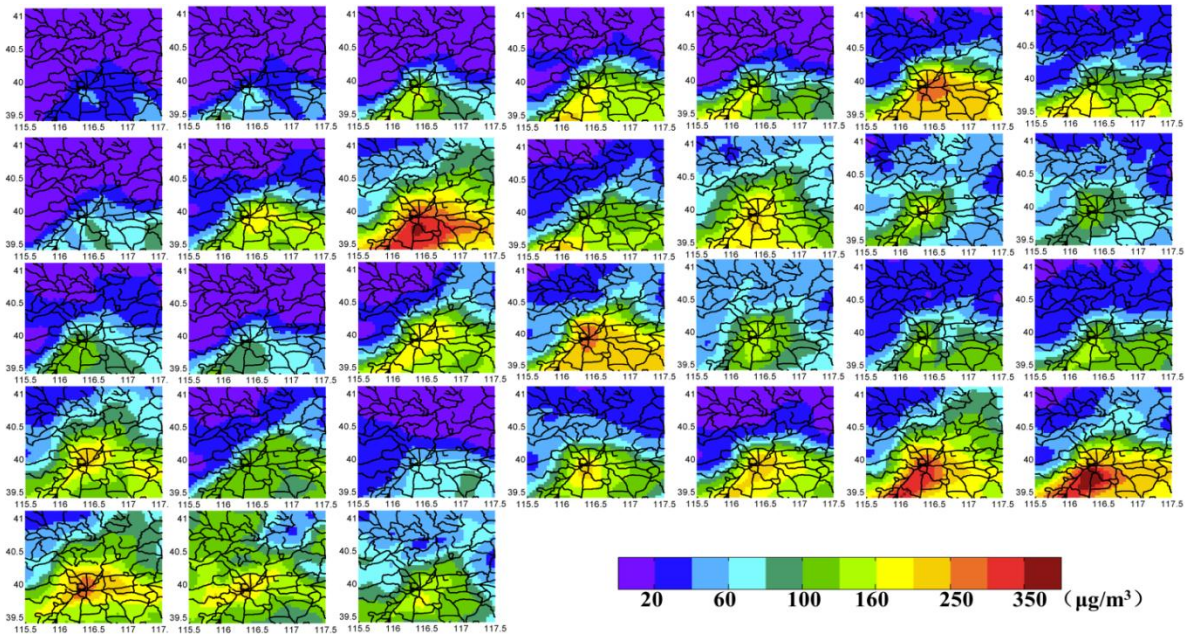


Figure 4.7. Horizontal distribution of daily (from January 1 to January 31) averaged $PM_{2.5}$ (x axis means longitude and y axis means latitude)

### 4.5.3 Mortality and morbidity losses

Daily health impacts of $PM_{2.5}$ were calculated using equation (1) for the Beijing area specified in Figure 4.1 by the black area. Total mortality during haze in Beijing in January was estimated to be 690, with the 95% confidence interval from 490 to 890. The total morbidities in January are summarized in Table 4.5. For comparison, Xie et al. (2014) estimated 201 deaths during period from 10 to 15 January, 2013. Li et al. (2013) estimated 725 premature deaths for the 2013 January haze in Beijing and Zhang et al. (2013) calculated 2725 premature deaths for 12 cities in NCP area from 10 to 31 January, 2013. These three studies used station measurements to represent pollution levels in the city. But pollution has high variation from urban to rural areas. That people live in urban and rural areas are exposed to different pollution levels should be considered in air pollution exposure studies. For this study, monitoring data from four sites were used to validate the model results. As shown in Table 4.4, model performs well compared with observations but with lower mean at Tianjin, Xianghe and Xinglong stations. The simulated fields provide more detailed information regarding concentration gradients and thus our estimates may be more realistic.

Table 4.5. Health impacts estimates for January

| Mortality | Hospitalized for Respiratory Disease | Hospitalized for Cardiovascular Disease | Clinic Visit (age 0-14) | Clinic Visit (age above 15) | Acute Bronchitis | Asthma |
|---|---|---|---|---|---|---|
| 690 (95% CI: (490,890)) | 5470(95% CI: (3800,6990)) | 6080 (95% CI: (2720,9190)) | 2610 (95% CI: (950,4180)) | 88160 (95% CI: (50360,124660)) | 45350 (95% CI: (21640,57860)) | 23720 (95% CI: (17090,29710)) |

### 4.5.4 Economic losses

Using the unit economic losses of various health endpoints, we calculated the economic losses for the haze in January. The total GDP of Beijing was 317,302.36 million US$ in 2013 (http://data.stats.gov.cn) and the total economic losses for this haze event in January is estimated at 253.8 (95% CI: (170.2, 331.2)) million US$, accounting for 0.08% (95% CI: (0.05%, 0.1%)) of the total annual GDP of Beijing. Detailed economic losses of each health endpoint are listed in Table 4.6. The calculations of confidence intervals in Table 4.6 only consider the uncertainties of β values. For all economic losses, economic losses due to deaths account for about 74.3% of the total losses. For economic losses of morbidity, the losses of hospitalization and acute bronchitis are dominant.

Table 4.6. Economic loss estimates

| Health Endpoints | Economic cost (million US$) |
|---|---|
| Mortality | 188.7 (134, 243.4) |
| Hospitalization | 31.9 (18,44.5) |
| Clinic Visits | 7.6 (4.3, 10.8) |
| Acute Bronchitis | 18.5 (8.8, 23.6) |
| Asthma | 7.1 (5.1, 8.9) |
| Total | 253.8 (170.2, 331.2) |

### 4.5.5 Uncertainty Discussion

Evaluating health impacts and economic loss of air pollution is becoming critical since it can analyze the cost-benefits of air pollution control measures. Previous studies assume that the

whole population was exposed to the average concentration levels recorded in monitoring stations (Kan et al., 2004). In this study, WRF-Chem was used to overcome this unreasonable assumption. However, using simulated $PM_{2.5}$ to approximate human exposure also has uncertainties. As mentioned in the model evaluation section, WRF-Chem overestimated $PM_{2.5}$ concentration in Beijing station slightly, and underestimated in other three stations. It's difficult to quantify how uncertainties of WRF-Chem affect the results in this study since data from only one monitoring station in Beijing area are available. For the available Beijing station, slightly overestimated $PM_{2.5}$ could lead overestimations of health impacts and economic losses. The sensitivity of health impacts and economic losses to $PM_{2.5}$ concentrations are calculated and summarized in Table 4.7. Estimated premature deaths increase 70 (about 10% increase) and estimated economic losses increase 25.7 million US$ (about 10% increase) when simulated $PM_{2.5}$ concentrations increase 10 $\mu g/m^3$. More studies are needed to reduce uncertainties in air quality modeling.

Table 4.7. Sensitivity of health impacts and economic losses to 10 $\mu g/m^3$ increase of $PM_{2.5}$ concentrations (mean and 95% CI)

| Deaths | Total economic losses (million US$) |
|---|---|
| 70 (50, 90) | 25.7 (17.5, 33.1) |

In the calculation of health impacts, it is crucial to choose the reference concentration. In this study, we used the WHO 24-hour mean $PM_{2.5}$ guideline 25 $\mu g/m^3$ as the reference concentration with the assumption that there are no health impacts under this threshold. At present, there is no scientific basis to set a threshold to evaluate health impacts, but the threshold is commonly used

in health impacts evaluation studies. For example, Guttikunda and Goel (2013) set 10μg/m$^3$ as the threshold value for the impact analysis. In addition, we explored the sensitivity of estimated premature deaths and total economic losses to different threshold assumptions. As shown in Table 4.8, the assumed threshold could significantly affect the estimations.

Concentration-response function is another important factor in health impacts assessment studies. In this study, most concentration-response functions used are from meta-analyses, which can avoid errors from individual study. Apart from this, 95% CI is included to represent the uncertainties caused by concentration-response functions. Burnett et al. (2014) considered nonlinear relation between $PM_{2.5}$ exposure and excess mortality relative risk, but it is ignored in this study, which could lead to overestimations of damages at high $PM_{2.5}$ levels. For health endpoints selection, only those endpoints that could be quantified are chosen, leading to an underestimation of the impacts. Furthermore, only acute effects are assessed in this study, while air pollution also has chronic effects on public health. Based upon above mentioned uncertainties, our assessments are very conservative.

Table 4.8. Sensitivity analysis of $PM_{2.5}$ –related deaths and total economic losses using different thresholds

| Thresholds | Death number | Total economic losses (million US$) |
|---|---|---|
| 0 μg/m$^3$ | 880 (620, 1130) | 322.5 (215.6, 418. 7) |
| 25 μg/m$^3$ | 690 (490, 890) | 253.8 (170.2, 331.2) |
| 75 μg/m$^3$ | 380 (270, 490) | 141 (94.2, 184.8) |

## 4.6 Summary

During the 2013 January haze event in Beijing, $PM_{2.5}$ concentrations were extremely high, with maximum hourly concentration about 650 $\mu g/m^3$ and the high PM concentrations persisted for a long time. As mentioned above, ambient particulate pollution is one of the top 5 risk factors of deaths in East Asia (Lim et al., 2012) and there have been many examples in history that air pollution events caused extensive premature deaths and diseases. Summarizing methods of evaluating heath impacts and economic losses, we established an approach to assess health impacts and economic losses of the 2013 January severe haze event in Beijing, using simulated $PM_{2.5}$ concentrations, which were verified with both meteorology and air quality measurements, dose-response functions from epidemiology studies in Beijing area, and gridded population data. The results show that the $PM_{2.5}$ pollution levels in January might cause 690 (95% CI: (490, 890)) premature deaths and 253.8 (95% CI: (170.2, 331.2)) million US$ economic losses. We only evaluated the health impacts of $PM_{2.5}$ and the impacts of other air pollutants, like ozone, CO, are not included. Considering many aspects, including model uncertainty, reference concentration selection, our assessments are conservative. The results imply the severity of haze event from both health and economic loss perspectives.

## 4.7 References

An, X., Hou, Q., Li, N., Zhai, S., 2013. Assessment of human exposure level to PM10 in China. Atmospheric Environment 70, 376–386. doi:10.1016/j.atmosenv.2013.01.017

Aunan, K., Pan, X.-C., 2004. Exposure-response functions for health effects of ambient air pollution applicable for China -- a meta-analysis. The Science of the total environment 329, 3–16. doi:10.1016/j.scitotenv.2004.03.008

Beijing Municipal Bureau of Public Health (BMBPH), 2013. Beijing Health Yearbook. Beijing Science and Technology Press, Beijing (in Chinese).

Bell, M.L., Davis, D.L., 2001. Reassessment of the Lethal London Fog of 1952 : Novel Indicators of Acute and Chronic Consequences of Acute Exposure to Air Pollution. Environmental Health Perspectives 109, 389–394.

Boylan, J.W., Russell, A.G., 2006. PM and light extinction model performance metrics, goals, and criteria for three-dimensional air quality models. Atmospheric Environment 40, 4946–4959. doi:10.1016/j.atmosenv.2005.09.087

Burnett, R.T., Iii, C.A.P., Ezzati, M., Olives, C., Lim, S.S., Mehta, S., 2014. An Integrated Risk Function for Estimating the Global Burden of Disease Attributable to Ambient Fine Particulate Matter Exposure. Environmental health perspectives 3, 397–404.

Chen, R., Li, Y., Ma, Y., Pan, G., Zeng, G., Xu, Xiaohui, Chen, B., Kan, H., 2011. Coarse particles and mortality in three Chinese cities: the China Air Pollution and Health Effects Study (CAPES). The Science of the total environment 409, 4934–8. doi:10.1016/j.scitotenv.2011.08.058

Dockery, D.W.;Pope III, C.A., 1994. Acute respiratory effects of particulate air pollution. Annual Review Public Health.

Dominici, F., Peng, R.D., Bell, M.L., Pham, L., McDermott, A., Zeger, S.L., Samet, J.M., 2006. Fine particulate air pollution and hospital admission for cardiovascular and respiratory diseases. Jama 295, 1127–34. doi:10.1001/jama.295.10.1127

Emery, Chris;Tai, Edward;Yarwood, G., 2001. Enhanced Meteorological Modeling and Performance Evaluation for Two Texas Ozone Episodes, in: Prepared for the Texas Natural Resource Conservation Commission. ENVIRON International Corporation, Novato, CA.

Emmons, L.K., Walters, S., Hess, P.G., Lamarque, J.-F., Pfister, G.G., Fillmore, D., Granier, C., Guenther, a., Kinnison, D., Laepple, T., Orlando, J., Tie, X., Tyndall, G., Wiedinmyer, C., Baughcum, S.L., Kloster, S., 2010. Description and evaluation of the Model for Ozone and Related chemical Tracers, version 4 (MOZART-4). Geoscientific Model Development 3, 43–67. doi:10.5194/gmd-3-43-2010

Gao, M., Guttikunda, S.K., Carmichael, G.R., Wang, Y., Liu, Z., Stanier, C.O., Saide, P.E., Yu, M., 2015. Health impacts and economic losses assessment of the 2013 severe haze event in Beijing area. Sci. Total Environ. 511, 553–561. doi:10.1016/j.scitotenv.2015.01.005

Godlee, F., 1991. Health and the Environment Air pollution : II-road traffic and modem industry. BMJ 303, 1539–1543.

Guenther, a., Karl, T., Harley, P., Wiedinmyer, C., Palmer, P.I., Geron, C., 2006. Estimates of global terrestrial isoprene emissions using MEGAN (Model of Emissions of Gases and Aerosols from Nature). Atmospheric Chemistry and Physics Discussions 6, 107–173. doi:10.5194/acpd-6-107-2006

Guttikunda, S.K., Goel, R., 2013. Health impacts of particulate pollution in a megacity—Delhi, India. Environmental Development 6, 8–20. doi:10.1016/j.envdev.2012.12.002

Guttikunda, S.K., Kopakka, R. V., 2013. Source emissions and health impacts of urban air pollution in Hyderabad, India. Air Quality, Atmosphere & Health. doi:10.1007/s11869-013-0221-z

He, H., Wang, Yuesi, Chu, B., Ji, Dongsheng, Tang, Guiqian, Liu, C., Zhang, H., Hao, J., 2014. Mineral dust and NOx promote the conversion of SO2 to sulfate in heavy pollution days. Scientific reports 1–5. doi:10.1038/srep04172

Henschel, S., Atkinson, R., Zeka, A., Le Tertre, A., Analitis, A., Katsouyanni, K., Chanel, O., Pascal, M., Forsberg, B., Medina, S., Goodman, P.G., 2012. Air pollution interventions and their impact on public health. International journal of public health 57, 757–68. doi:10.1007/s00038-012-0369-6

Hou, Q., An, X., Wang, Yu, Tao, Y., Sun, Z., 2012. An assessment of China's PM10-related health economic losses in 2009. The Science of the total environment 435-436, 61–5. doi:10.1016/j.scitotenv.2012.06.094

Huang, D.;Zhang, S., 2013. Health benefit evaluation for $PM_{2.5}$ pollution control in Beijing-Tianjin-Hebei region of China.pdf. China Environmental Science 33, 166~174 (in Chinese)..

Jing, Libin; Qin, Yi; Xu, Zhaoyi; Ren, Chixia; Wang; Shufan; Ren, Ling; Li, Jinping; Sha, Fei; Chen, B., 2000. Relationship between air pollution and acute and chronic respiratory diseases in Benxi. Journal of Environment and Health 17, 268–270 (in Chinese)..

Kan, H., Chen, B., 2004. Particulate air pollution in urban areas of Shanghai, China: health-based economic assessment. The Science of the total environment 322, 71–9. doi:10.1016/j.scitotenv.2003.09.010

Li, Tiantian; Du, Yanjun; Xue, Wenbo; Xu, Dongqun; Wang, J., 2013. Assessment of haze-related human health risks for four Chinese cities during extreme haze in January 2013. Natl Med J China 93, 2699~2702 (in Chinese)..

Lim, S.S., Vos, T., Flaxman, A.D., Danaei, G., Shibuya, K., et al., 2012. A comparative risk assessment of burden of disease and injury attributable to 67 risk factors and risk factor clusters in 21 regions, 1990-2010: a systematic analysis for the Global Burden of Disease Study 2010. Lancet 380, 2224–60. doi:10.1016/S0140-6736(12)61766-8

Marlier, M.E., DeFries, R.S., Voulgarakis, A., Kinney, P.L., Randerson, J.T., Shindell, D.T., Chen, Y., Faluvegi, G., 2012. El Niño and health risks from landscape fire emissions in southeast Asia. Nature Climate Change 3, 131–136. doi:10.1038/nclimate1658

Pearce, J.L., Beringer, J., Nicholls, N., Hyndman, R.J., Tapper, N.J., 2011. Quantifying the influence of local meteorology on air quality using generalized additive models. Atmospheric Environment 45, 1328–1336. doi:10.1016/j.atmosenv.2010.11.051

Pope, C.A., Dockery, Douglas W., 2006. Health Effects of Fine Particulate Air Pollution: Lines that Connect. Journal of the Air & Waste Management Association 56, 709–742. doi:10.1080/10473289.2006.10464485

Seaton, a, MacNee, W., Donaldson, K., Godden, D., 1995. Particulate air pollution and acute health effects. Lancet 345, 176–8.

Sun, Yele, Zhuang, G., Tang, a A., Wang, Ying, An, Z., 2006. Chemical characteristics of $PM_{2.5}$ and PM10 in haze-fog episodes in Beijing. Environmental science & technology 40, 3148–55.

Sun, Yele; Jiang, Qi; Wang, Zifa; Fu, Pingqing; Li, Jie; Yang, Ting; Yin, Y., 2014. Investigation of the sources and evolution processes of severe haze pollution in Beijing in January 2013. Journal of Geophysical Research : Atmospheres 1–19. doi:10.1002/2014JD021641.Received

Teng, Enjiang;Hu, Wei;Wu, Guoping; Wei, F., 1999. The composing characteristics of elements in coarse and fine particle in air of the four cities in China. China Environmental Science 19, 238–242 (in Chinese)..

U.S. Environmental Protection Agency, 2012. Provisional Assessment of Recent Studies on Health Effects of Particulate Matter Exposure.

Wang, YueSi, Yao, L., Wang, L., Liu, Z., Ji, DongSheng, Tang, GuiQian, Zhang, J., Sun, Yang, Hu, B., Xin, J., 2013. Mechanism for the formation of the January 2013 heavy haze pollution episode over central and eastern China. Science China Earth Sciences 57, 14–25. doi:10.1007/s11430-013-4773-4

Xie, Peng; Liu, Xiaoyun; Liu, Zhaorong; Li, Tiantian; Bai, Y., 2009. Exposure-response functions for health effects of ambient particulate matter pollution applicable for China. China 29, 1034–1040 (in Chinese)..

Xie, Yuanbo; Chen, Juan; Li, W., 2014. An assessment of $PM_{2.5}$ related health risks and impaired values of Beijing residents in a consecutive high-level exposure during heavy haze days. Environmental Science 35, 1–8 (in Chinese)..

Xu, X, Dockery, D W, Christiani, D.C., Li, B., Huang, H., 1995. Association of air pollution with hospital outpatient visits in Beijing. Archives of environmental health 50, 214–20. doi:10.1080/00039896.1995.9940390

Yu, M., Carmichael, G.R., Zhu, T., Cheng, Y., 2012. Sensitivity of predicted pollutant levels to urbanization in China. Atmospheric Environment 60, 544–554. doi:10.1016/j.atmosenv.2012.06.075

Zaveri, R. a., Easter, R.C., Fast, J.D., Peters, L.K., 2008. Model for Simulating Aerosol Interactions and Chemistry (MOSAIC). Journal of Geophysical Research 113, D13204. doi:10.1029/2007JD008782

Zaveri, R. a., Peters, L.K., 1999. A new lumped structure photochemical mechanism for large-scale applications. Journal of Geophysical Research 104, 30387. doi:10.1029/1999JD900876

Zhang, M., Song, Y., Cai, X., 2007. A health-based assessment of particulate air pollution in urban areas of Beijing in 2000-2004. The Science of the total environment 376, 100–8. doi:10.1016/j.scitotenv.2007.01.085

Zhang, M., Song, Y., Cai, X., Zhou, J., 2008. Economic assessment of the health effects related to particulate matter pollution in 111 Chinese cities by using economic burden of disease analysis. Journal of Environmental Management 88, 947–54. doi:10.1016/j.jenvman.2007.04.019

Zhang, Yanshen; Ma, Guoxia; Yu, Fang; Cao, D., 2013. Health damage assessment due to $PM_{2.5}$ exposure during haze pollution events in Bejing-Tianjin-Hebei region in January 2013. Natl Med J China 93, 2707~2710 (in Chinese).

Zheng, G.J., Duan, F.K., Ma, Y.L., Cheng, Y., Zheng, B., Zhang, Q., Huang, T., Kimoto, T., Chang, D., Su, H., Pöschl, U., Cheng, Y.F., He, K.B., 2014. Exploring the severe winter haze in Beijing. Atmospheric Chemistry and Physics Discussions 14, 17907–17942. doi:10.5194/acpd-14-17907-2014

# CHAPTER 5: IMPROVING MODELING OF SULFATE AEROSOLS DURING THE JANUARY 2013 HAZE EPISODE IN NORTH CHINA[51]

## 5.1 Abstract

The online WRF-Chem model was implemented to reproduce the 2013 January haze event in North China. Compared to observations, temperature and relative humidity (RH) are simulated well (mean biases are -0.2K and 2.7%, respectively), but wind speeds are overestimated (mean bias is 0.5m/s). At the Beijing site, peak $PM_{2.5}$ concentration is not captured by the model and comparisons between simulated and observed $PM_{2.5}$ species show that sulfate is largely underestimated, which may result from uncertainty in $SO_2$ emission and missing heterogeneous sulfate formation in current model. To investigate the sensitivity of sulfate formation to $SO_2$ emission and heterogeneous chemistry, three parallel experiments were conducted and results suggest that heterogeneous chemistry is more important in sulfate formation. With included heterogeneous formation, model results agree better with observations. Domain mean sulfate concentrations increase 8.8μg/m$^3$ after including heterogeneous sulfate formation. Although the enhanced $SO_2$ to sulfate conversion in the HetS case reduces $SO_2$ concentrations, it is still largely overestimated by the model, suggesting the overestimations of $SO_2$ concentrations in the NCP are mostly due to errors in $SO_2$ emission inventory.

## 5.2 Introduction

Frequent haze pollution in China has drawn great attention due to its adverse impacts on visibility, public health and climate (M. Gao et al., 2015; R. J. Huang et al., 2014). In January

[51] This work is under preparation to be submitted.

2013, a persistent unprecedented severe haze episode occurred in central and eastern China. During this episode, highest instantaneous $PM_{2.5}$ concentration reached 1000 ug $m^{-3}$ in some highly polluted areas of Beijing (J. K. Zhang et al., 2014). This month is considered as the haziest month in the past 60 years in Beijing (Y. Gao et al., 2015; L. T. Wang et al., 2014). Many field experiments and modeling studies have been conducted to investigate the formation mechanism of this event and high emissions of primary air pollutants, stagnant weather condition, regional pollution transport, and fast gas-to-particle conversion are considered as the main causes (Sun et al., 2014; Wang et al., 2014a; Wang et al., 2014b; J. K. Zhang et al., 2014; B. Zheng et al., 2015; G. J. Zheng et al., 2015). In the past three decades, NCP has experienced rapid urbanization and industrialization processes, causing high atmospheric pollutant emissions. In January 2013, a weak East Asian winter monsoon existed over eastern China, inhibiting convection and bringing in more water vapor (R. H. Zhang et al., 2014). Under the stagnant and wet environment, primary gaseous pollutants transformed into aerosols quickly, which is considered as the internal cause of the growth of $PM_{2.5}$ (Wang et al., 2014a). The percentage of sulfate in $PM_{2.5}$ increases from 13% in normal days to 25% in haze days (Quan et al., 2014). However, photochemical activity in haze days may be lower than it in normal days, indicating that heterogeneous inorganic aerosol formation may be important in the 2013 winter haze episode (Quan et al., 2014), which also agrees with the conclusion from He et al. (2014) that sulfate formation is a main reason for fine particle growth, and that mineral dust promotes fast conversion of sulfur dioxide ($SO_2$) to sulfate in haze days.

This haze episode with extremely high $PM_{2.5}$ concentrations provides an opportunity to evaluate the extent that added chemical pathways can improve current air quality models. In this study, we apply the WRF-Chem model to reproduce the 2013 January haze episode. It is found

that sulfate is largely underestimated by the WRF-Chem model when applied in Europe, which could be caused by the underestimation of the $SO_2$ gas phase oxidation rate (Tuccella et al., 2012), uncertainty in $SO_2$ emission, and some missing formation mechanisms in current models, including heterogeneous chemistry. This modeling study is designed to evaluate how WRF-Chem performs on simulating the 2013 January haze episode and to investigate the impacts of $SO_2$ emission and heterogeneous chemistry on the formation of sulfate aerosols.

## 5.3 Model and Observations

### 5.3.1 Model Configurations

This study uses WRF-Chem version 3.5.1, with two nested domains, covering China and most parts of East Asia. Horizontal resolutions are 81km and 27km from outer to inner domains and 27 vertical layers are used. The meteorological initial and lateral boundary conditions are from the European Center for Medium-Range Weather Forecasts (ECMWF)'s Operational Model Analysis dataset. Chemical boundary and initial conditions are obtained from global Model for Ozone and Related Chemical Tracers (MOZART-4) (Emmons et al., 2010). Anthropogenic emissions and biogenic emissions are the same as the descriptions in Chapter 2. The model configuration options used are the same as those in Chapter 2. The aerosol model used is the 8-bin sectional MOSAIC (Zaveri et al., 2008) model. MOSAIC treats all important aerosol species, including sulfate, nitrate, ammonium, OC, BC, sodium, chloride and other inorganics (OIN). OIN species mainly consist of minerals and trace metals.

Three parallel experiments, summarized in Table 5.1, were conducted in order to study the impacts of different factors on sulfate formation. Each experiment was run from 12:00 UTC on the 30 December 2012 to 00:00 UTC on 2 February 2013, covering the whole January haze month. Initial conditions were updated daily with a 12-hour spin-up time.

Table 5.1. Explanations of all simulations in this study

| Simulation Name | Description |
|---|---|
| CTRL | Standard simulation |
| 2SE | $SO_2$ emissions are doubled from the standard simulation |
| HetS | Heterogeneous sulfate formation is added into WRF-Chem |

### 5.3.2 Observations

Model results are compared to meteorological and chemical observations to evaluate model performance. The meteorological observations are from the China Meteorological Data Sharing Service System (http://cdc.cma.gov.cn/home.do). In this study, 25 stations in North China, including Beijing, Tianjin, Baoding, are used. The locations of each station are denoted in black in Figure 5.1. The meteorological measurements used in this study also include sounding data provided by the National Center for Atmospheric Research Earth Observing Laboratory (http://weather.uwyo.edu/upperair/sounding.html). The location of sounding measurements used in this study is denoted in blue in Figure 5.1. Surface chemical observations, including hourly $PM_{2.5}$, $SO_2$, $NO_x$, are from the CARE-China network (Wang et al., 2014a). The locations of the four stations (Beijing, Tianjin, Xianghe, and Xinglong) analyzed are shown in red in Figure 5.1.

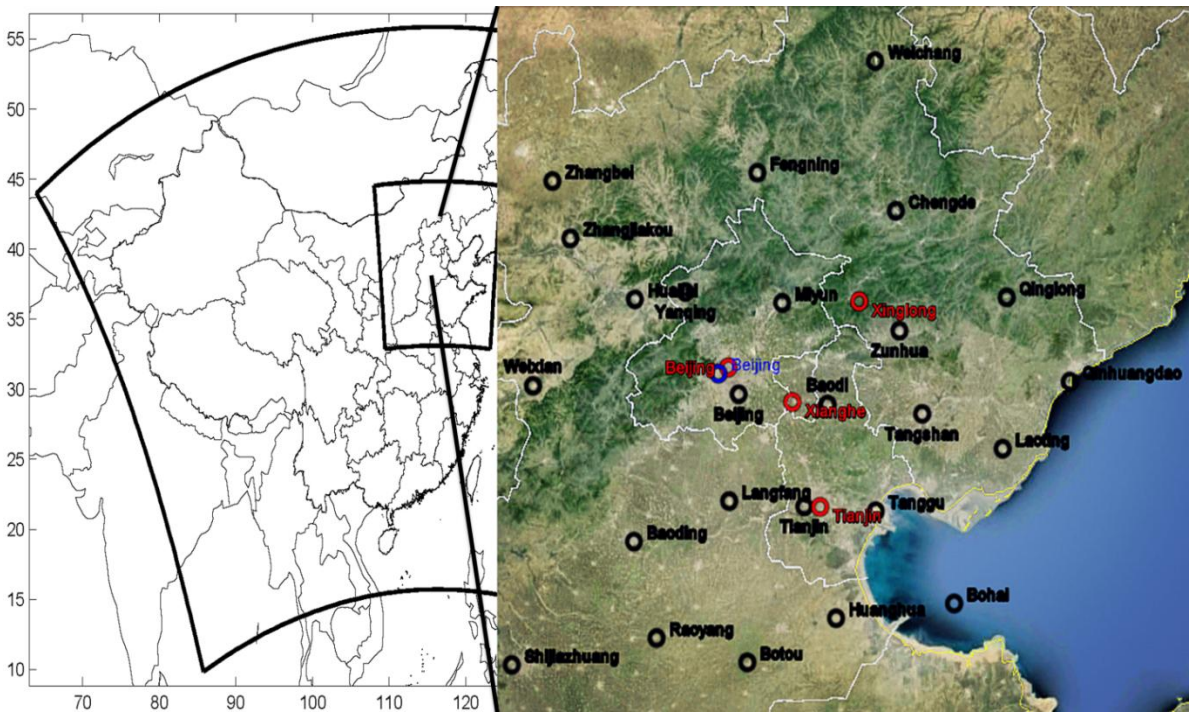


Figure 5.1. Domain settings and locations of observation sites

## 5.4 Results

### 5.4.1 Model Evaluation

In this section, we compare the model simulations of surface temperature, relative humidity (RH), wind speed, surface $PM_{2.5}$, $SO_2$, $NO_x$ concentrations and chemical composition of $PM_{2.5}$ in the CTRL experiment to observations from 1 to 31 January 2013. Statistical metrics, including correlation coefficient (R), Mean Bias (MB), Mean Error (ME), Root Mean Square Error (RMSE), Mean Fractional Bias (MFB), and Mean Fractional Error (MFE), are calculated to evaluate model performance.

Meteorology plays a critical role in the transport, diffusion, and chemical formation of aerosols. Whisker plots of simulated and observed daily mean temperature, RH, and wind speed are shown in Figure 5.2. Solid dots represent values averaged over 25 stations. The performance statistics are listed in Table 5.2. Generally, the temporal variations of temperature, RH, and wind speeds are captured well by the model. The simulated ranges of temperature, RH, and wind speeds over 25 stations are also consistent with measurements. The model reproduces temperature with a correlation coefficient (R) of 0.99 and a small negative mean bias of -0.2 K. RH is also simulated reasonably well by the model with a R of 0.99 and a small positive mean bias of 2.7%. The simulation of wind speed is not as good as those of temperature and RH. Generally, wind speeds are overestimated by the model with a positive mean bias of 0.5 m/s, and a R of 0.96. Other studies also report that wind speeds are typically overestimated by the WRF-Chem model under low wind conditions (Tuccella et al., 2012; Zhang et al., 2010). The errors in wind speeds may be related to model resolution, which affects the ability to resolve topography.

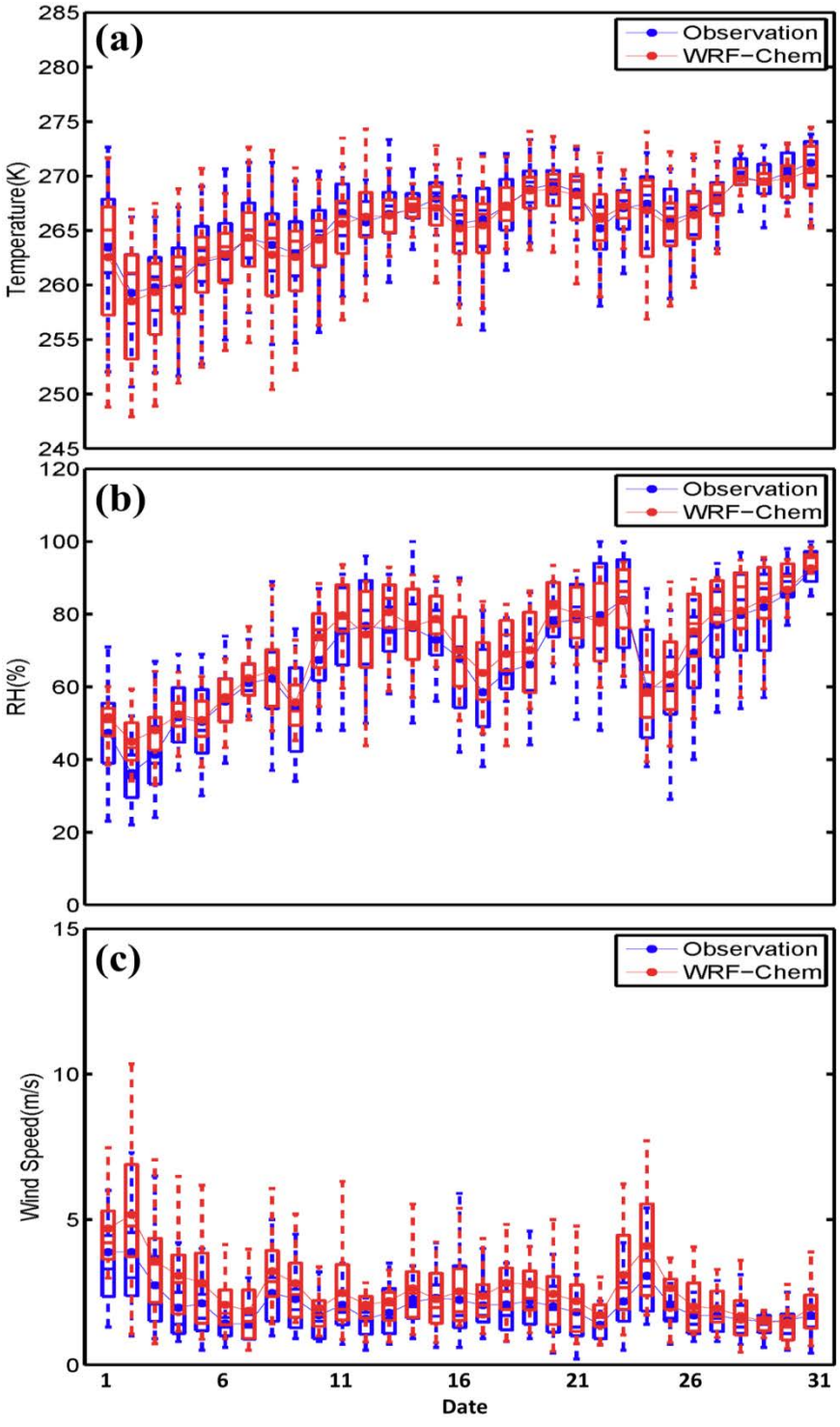


Figure 5.2. Whisker plots of simulated (red) and observed (black) daily mean 2m temperature, 2m RH and 10m wind speed; solid dots denote values averaged over 25 stations

Table 5.2. Performance statistics of meteorological and chemical variables

| Variable | Stations | Mean Obs | Mean Model | R | MB | ME | RMSE | MFB (%) | MFE (%) |
|---|---|---|---|---|---|---|---|---|---|
| Temperature (K) | 25 | 265.9 | 265.6 | 0.99 | -0.2 | 0.0 | 0.5 | -0.1 | 0.2 |
| RH (%) | 25 | 67.3 | 70.0 | 0.99 | 2.7 | 3.1 | 3.8 | 4.4 | 5.0 |
| Wind Speed (m/s) | 25 | 2.1 | 2.6 | 0.96 | 0.5 | 0.5 | 0.6 | 20.5 | 20.8 |
| $PM_{2.5}$ ($\mu g/m^3$) | 3 | 118.5 | 161.8 | 0.83 | 43.3 | 47.8 | 65.7 | 35.9 | 38.9 |
| $NO_x$ (ppbv) | 3 | 68.0 | 99.7 | 0.82 | 31.7 | 32.1 | 38.4 | 43.1 | 43.4 |
| $SO_2$ (ppbv) | 3 | 21.7 | 43.2 | 0.69 | 21.6 | 21.6 | 24.0 | 66.8 | 66.8 |
| CO (ppmv) | 3 | 2.3 | 2.3 | 0.82 | 0.0 | 0.5 | 0.6 | 3.6 | 22.0 |

The meteorological simulations are also validated against atmospheric sounding measurements, shown in Figure 5.3. The solid dots are mean vertical profiles observed and simulated at 00 and 12 UTC over January 2013. At both 00UTC and 12UTC, near surface temperature is overestimated, and near surface RH is underestimated. This is opposite to the previous comparisons shown in Figure 5.2 and Table 5.2 because this is calculated for one station in Beijing and the previous comparisons are based on values averaged over 25 stations. At higher layers, simulated temperature agrees well with observation but large discrepancies exist between simulated and observed RH, which is consistent with the results from Misenis and Zhang (2010) and Zhang et al. (2010). Misenis and Zhang (2010) reported that vertical profiles of RH are sensitive to adopted land surface model and PBL options. Wind speeds are overestimated near the surface, confirming the overestimation of surface winds shown in Figure 5.2, but are underestimated at higher levels. At 12UTC, simulated wind direction agrees well with sounding measurements, but large deviations occur at 00UTC.

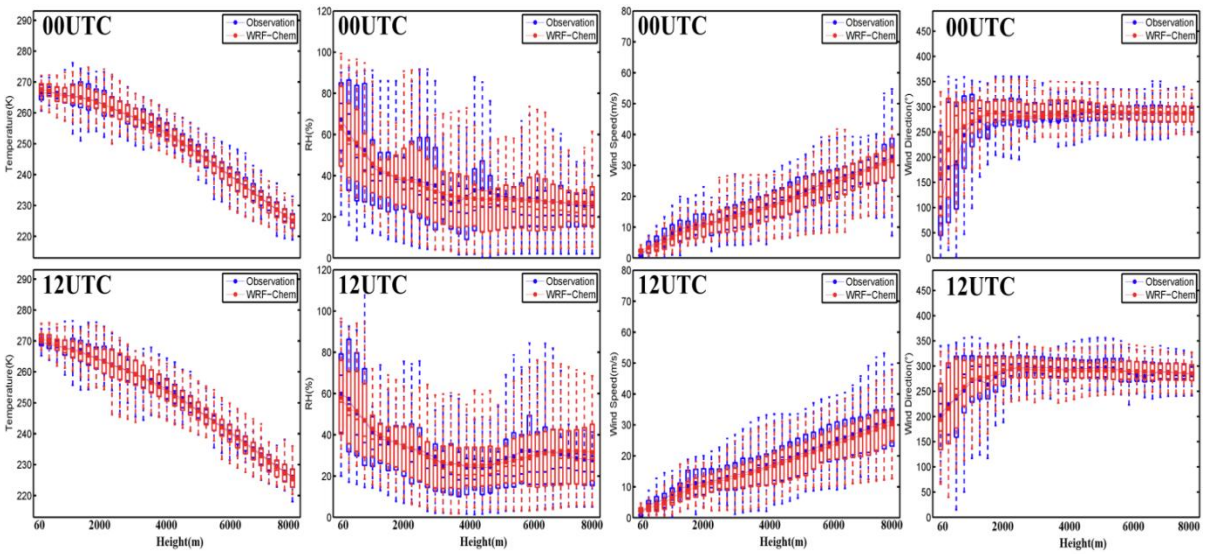


Figure 5.3. Whisker plots of observed (blue) meteorological variables vertical profiles with WRF-Chem simulations (red), averaged in Beijing for January

The errors in simulated wind speeds and wind directions affect the transport and diffusion of air pollutants and the errors in simulated temperature and RH affect the chemical reaction rates and aerosol formations. Figure 5.4 presents the temporal variations of simulated and measured hourly surface $PM_{2.5}$, CO, $SO_2$, and $NO_x$ concentrations in the Beijing, Xianghe and Xinglong stations. The model reproduces the variations of these pollutants over the month nicely, except $SO_2$. The performance statistics for averaged concentrations over three sites are summarized in Table 5.2. Generally, $PM_{2.5}$ concentrations are overestimated with a MB of 43.3μg/$m^3$, but the peak value on January 13 was not captured by the model. The calculated MFB for $PM_{2.5}$ is 35.9%, which is slightly higher than the good performance criteria (MFB should be less than or equal to ±30%) proposed by Boylan et al. (2006). However, the calculated MFE value of 38.9% for $PM_{2.5}$ is within the proposed criteria +50% (Boylan et al., 2006). The model accurately predicts CO concentrations, with a low MB of about 0.0ppbv, and a low MFB value of 3.6%.

The correlation coefficients between simulation and observation are higher than 0.8 for $PM_{2.5}$, CO and $NO_x$, but less than 0.7 for $SO_2$. Besides, the MFB and MFE values for $SO_2$ are higher than other three variables. $SO_2$ is systemically overestimated at Beijing and Xianghe. This suggests that the emieeions may be overestimated and/or rates of conversions to sulfate are underestimated. At Xinglong, model shows better predictions of $SO_2$. This is because Xinglong is a rural site, located in the Yanshan Mountains, and it was outside the hazy region during the month. $NO_x$ is overestimated by the WRF-Chem model with a mean bias of 31.7ppbv (Table 5.2). In the last several days of the month, simulated $PM_{2.5}$, CO, and $NO_x$ are significantly higher than observations and show similar variations, which may be due to the errors in simulated meteorology fields.

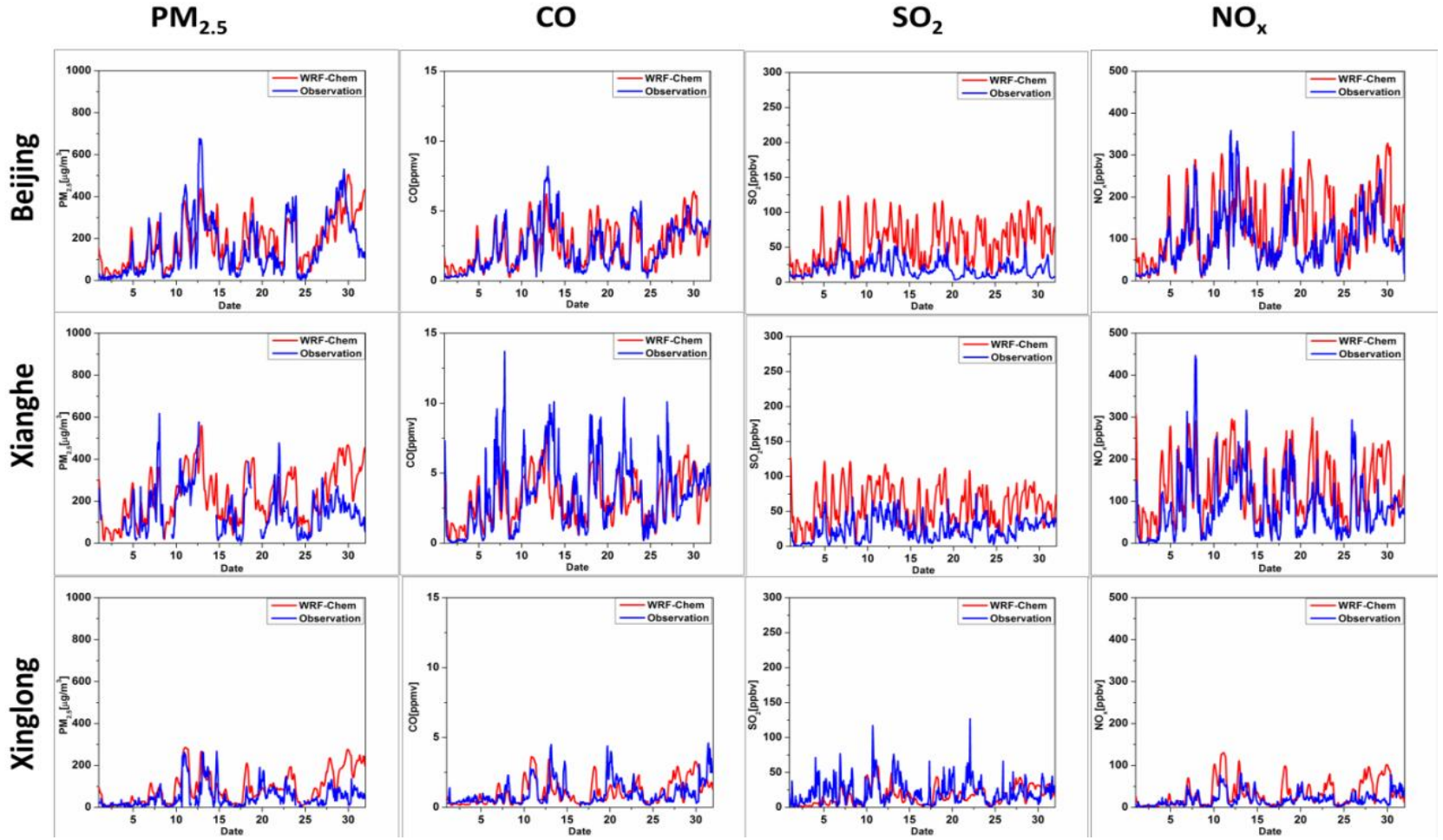


Figure 5.4. Time series of simulated and measured hourly $NO_x$ concentrations at Beijing, Tianjin, Xianghe, and Xinglong

Figure 5.5 shows the temporal variations of observed (left) and simulated (right) main $PM_{2.5}$ chemical species (sulfate, nitrate, ammonium, elemental carbon, and organic carbon) mass concentrations at Beijing from 25 to 30 January. Although the total $PM_{2.5}$ was accurately predicted during this period (Figure 5.4), the sum of these five components was underestimated. OC and sulfate are largely underestimated and nitrate is slightly overestimated by the model. The underestimation of OC could be caused by the large uncertainty of OC emission inventory and missing secondary organic aerosol formation in the selected CBMZ-MOSAIC coupled mechanism used in this study. The overestimation of nitrate is probably caused by the underestimation of sulfate because less consumed ammonium favors the formation of ammonium nitrate (Tuccella et al., 2012). The errors in simulated sulfate could be caused by uncertainties in $SO_2$ emission, and/or too low $SO_2$ to sulfate conversion rates. It is meaningful to know how these factors affect the sulfate formations during haze, because sulfate formation is a main cause of fine particle growth (He et al., 2014), which is considered to be the internal cause of the 2013 haze event (Wang et al., 2014a). The observations show sulfate grew from a few $\mu g/m^3$ before the event to over $100\mu g/m^3$ at the event peak.

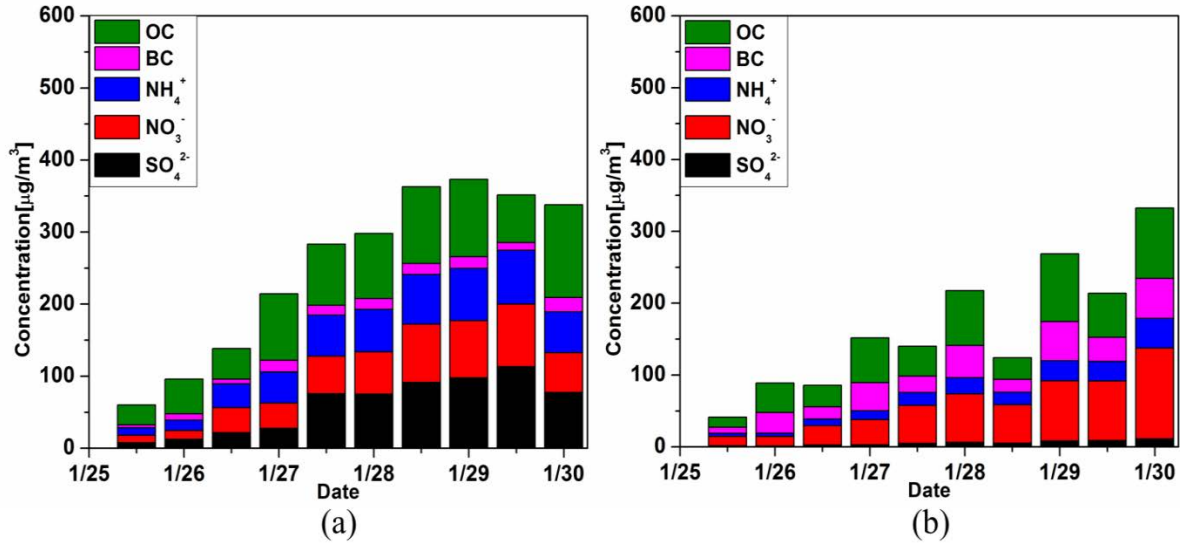


Figure 5.5. Temporal variations of observed (left) and simulated (right) $PM_{2.5}$ chemical species concentration at Beijing from 25 to 30 January

### 5.4.2 Sensitivity Tests

In the above section, it is found that sulfate is largely underestimated by the model, and thus nitrate concentration is affected. In this section, we would like to discuss the impacts of above mentioned three factors, namely $SO_2$ emission and sulfate formation, on sulfate in $PM_{2.5}$ and other $PM_{2.5}$ chemical species. In the 2SE experiment, we double the $SO_2$ anthropogenic emission. In the HetS experiment, we incorporate a heterogeneous sulfate formation chemistry into WRF-Chem.

#### 5.4.2.1 Description of the incorporation of heterogeneous chemistry

We have used KPP protocol (Damian et al., 2002) to extend the CBMZ-MOSAIC mechanism to simulate heterogeneous chemistry on the OIN surface. Many studies have

proposed the heterogeneous chemistry on mineral dust (Song et al., 2007; Usher et al., 2002), fine particles (Ding and Zhu, 2003), and sea-salt particles (Sievering et al., 1991). The heterogeneous chemistry mechanism is still not fully understood. In this study, we parameterize heterogeneous chemistry only on OIN (where mineral dust and trace metals are included). The uptake of $SO_2$ on the OIN surface is thought to be irreversible (Kumar et al., 2014; Wang et al., 2012; Zhang and Carmichael, 1999). The rate coefficient $k_g$ for losses of $SO_2$ due to heterogeneous uptake is determined by the following equations (Heikes and Thompson, 1983; Kumar et al., 2014):

$$k_g = \sum_{i=1}^{3} \frac{4\pi r_i \; D_g V \; N_i}{1 + K_n[\chi + \frac{4(1-\gamma)}{3\gamma}]} \tag{5.1}$$

where $i$ represents the used eight OIN bins, $r_i$ (cm) represents the effective radius of each OIN bin, and $D_g$ ($cm^2 s^{-1}$) represents gas diffusion coefficient. $V$ denotes the ventilation coefficient and $N_i$(# $cm^{-3}$) is the number density of OIN aerosols. $K_n$ is the dimensionless Knudsen number, $\chi$ represents correction factor and $\gamma$ (uptake coefficient) is the most important parameter. $D_g$ is calculated using the equation (3.2) (Kumar et al., 2014)

$$D_g = \frac{5}{16\rho_a A d_g^2}\sqrt{\left(\frac{m_a + m_g}{m_a}\right)\frac{RTm_a}{2\pi}} \tag{5.2}$$

where $\rho_a$ ($gcm^{-3}$) represents the atmosphere mass density, $A$ is the Avogadro number, $R$ is gas constant and $T$ (K) denotes the absolute temperature. $d_g$ (cm) represents the collision diameter. $m_a$ and $m_g$ denote air and gas molecular weights, respectively. $\chi$ is determined by

equation (3.3) and results in mass concentration in WRF-Chem are converted into number concentration using equation (3.4)

$$\chi = \frac{(\frac{4}{3} K_n + 0.71)}{K_n + 1} \tag{5.3}$$

$$N_i = \frac{M_i \rho_a}{(\frac{4}{3}\pi r_i^3)\rho_p} \tag{5.4}$$

where $M_i$ represents the mass mixing ratio and $\rho_p$ is the mass density of dust (Kumar et al., 2014).

$\gamma$ is the most important parameter in heterogeneous chemistry calculation, but large uncertainties exist in $\gamma$ values. The magnitudes of $\gamma$ may vary several orders, depending on surface properties, aerosol compositions, temperature, RH and other conditions (Wang et al., 2012; B. Zheng et al., 2015). The high dependence of $\gamma$ on RH has been reported in previous laboratory studies, but it is ignored or poorly treated in previous modeling studies (Song et al., 2007; Kumar et al., 2014). Dentener et al. (1996) set $\gamma$ value of $SO_2$ to $3\times10^{-4}$ when RH is lower than 50%, and to 0.1 when RH is greater than 50%. Song et al. (2001) set $\gamma$ value of $SO_2$ to 0.05 when RH is greater than 50%, and to 0.005 when RH is lower than 50%. Zheng et al. (2014a) assumed $\gamma$ is the low limit when RH is lower than 50%, and is increased linearly to high limit with the increase of RH to maximum RH values.

In this study, the heterogeneous $SO_2$ reaction incorporated is shown in the below equation (Wang et al., 2012; Kumar et al., 2014):

$$SO_2 + \text{OIN} \rightarrow SO_4^{2-} \tag{5.5}$$

The $\gamma$ value is determined based on the work of Kumar et al. (2014). The dependence of $\gamma$ values of $SO_2$ on RH is treated based on Preszler Prince et al. (2007), where data for $SO_2$ loss is measured under various RH values.

#### 5.4.2.2 Sensitivity Results

Observed and simulated mean inorganic aerosol concentrations and fractions from 25 to 30 January 2013 are listed in Table 5.3. Compared to the CTRL run, sulfate in the 2SE case increase by 88.7%, but it is still largely underestimated by the model. Observed sulfate aerosols account for about 23.9% in the major fine aerosol components, while simulated sulfate aerosols account for 5.3%, and 10.0% for the CTRL and 2SE cases, respectively. For the HetS experiment, sulfate fraction is significantly improved with a fraction of 18.8%. In some days, nitrate is overestimated by the model (shown in Figure 5.5), and this overestimation can be reduced with enhanced sulfate aerosols. Mean nitrate decreases from 55.5 to 53.9μg/m$^3$ when sulfate increase from 5.3 to 40.0μg/m$^3$ from the CTRL run to the HetS run.

Table 5.3. Observed and simulated mean major fine aerosol species concentrations (μg/m$^3$) and fractions from 25 to 30 January

| | $SO4^{2-}$ | $NO^{3-}$ | $NH4^{+}$ | BC | OC | Total |
|---|---|---|---|---|---|---|
| Observation | 60.1 (23.9%) | 50.5 (20.0%) | 49.0 (19.5%) | 12.6 (5.0%) | 79.4 (31.6%) | 251.6 |
| CTRL | 5.3 (3.2%) | 55.5 (33.4%) | 18.5 (11.1%) | 32.3 (19.4%) | 54.8 (32.9%) | 166.4 |
| 2SE | 10.0 (5.8%) | 55.7 (32.2%) | 20.3 (11.7%) | 32.3 (18.6%) | 54.9 (31.7%) | 173.2 |
| HetS | 40.0 (18.8%) | 53.9 (25.4%) | 31.0 (14.6%) | 32.4 (15.3%) | 55.0 (25.9%) | 212.3 |

Figure 5.6 shows the mean fractions of main $PM_{2.5}$ chemical species for the observations and the sensitivity experiments. Fractions for the 2SE case only slightly change from the fractions for the CTRL experiment. Compared to observations, the fractions in the HetS experiment are better, with enhanced sulfate fraction and reduced nitrate fraction. However, OC is still underestimated. The errors could easily be accounted for in the emissions, which are thought to have large errors. In addition, it has been suggested the SOA can be produced in low temperature winter time condition (R. J. Huang et al., 2014). This should be considered in future modeling studies. With more sulfate aerosols in the HetS case, ammonium increases about 68.0% because more ammonia is consumed to form $NH_4SO_4$.

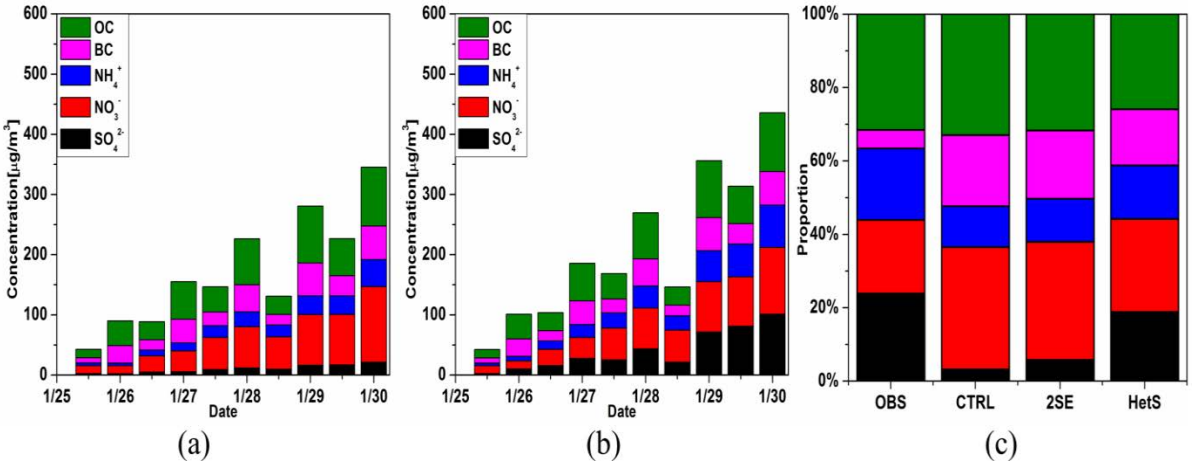


Figure 5.6. mass concentrations of $PM_{2.5}$ chemical species in the CTRL (a) case, the HetS case (b) and mean mass fractions of $PM_{2.5}$ chemical species for observation and the sensitivity simulations (c)

Figure 5.7 shows the spatial distribution of monthly mean sulfate concentration for CTRL experiment and increased sulfate concentrations for sensitivity perturbations. Domain mean sulfate concentrations increase 3.1 and 8.8μg/m3 by doubling $SO_2$ emission and incorporating heterogeneous sulfate formation, respectively. These results indicate that the sulfate formation is more sensitive to heterogeneous chemistry. Figure 5.8 shows the temporal variations of observed $SO_2$ concentrations and simulated $SO_2$ concentrations in the CTRL and HetS cases. Although the enhanced $SO_2$ to sulfate conversion in the HetS case reduces $SO_2$ concentrations, it is still largely overestimated by the model, suggesting the overestimations of $SO_2$ concentrations in the NCP are mostly due to errors in $SO_2$ emission inventory. The underestimation of sulfate is mainly attributed to low $SO_2$ to sulfate conversion rate.

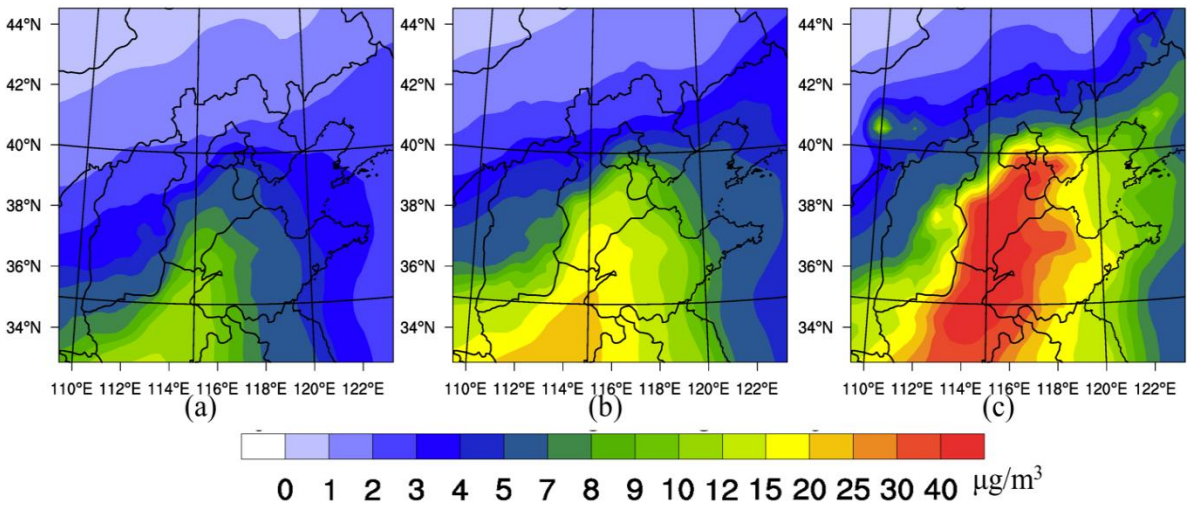


Figure 5.7. Spatial distribution of monthly mean sulfate concentration for CTRL experiment (a) and increased sulfate concentration caused by 2SE (b), and HetS (c)

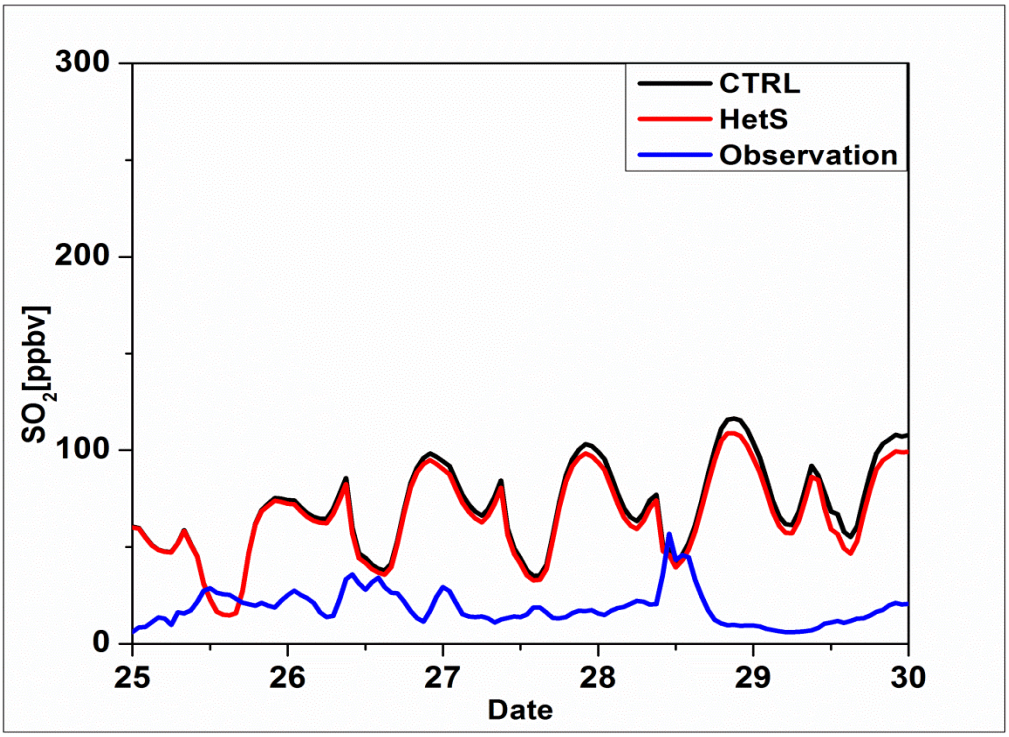


Figure 5.8. Time series of observed $SO_2$ concentration and simulations in the CTRL and HetS cases in Beijing

## 5.5 Summary

The online coupled WRF-Chem model was used to reproduce the 2013 January severe haze event over the North China Plain and evaluated using meteorological and chemical measurements. Temperature and RH are simulated well by the WRF-Chem model, but the extremely low wind speeds during haze are overestimated, which has also been reported in many previous studies.

Simulated hourly $PM_{2.5}$, CO, $SO_2$, and $NO_x$ concentrations were compared to observations at three stations. Simulated $SO_2$ concentrations were higher than observations at Beijing and Xiang stations, but consistent with observation at Xinglong. This may be because Xinglong was out of the pollution region and uncertainties of $SO_2$ emissions in Xinglong are lower than in urban areas. The temporal variations of observed $PM_{2.5}$ chemical compositions suggest that the increase in sulfate from non-haze to haze days is one of the critical causes of this haze event. However, the sulfate concentrations were largely underestimated by the model, which might be due to missing heterogeneous sulfate formation in current model.

We propose the uptake of $SO_2$ on aerosols is an important sulfate formation pathway. The uptake coefficient was treated as RH dependent and the values were from previous laboratory works. Three parallel experiments were conducted to investigate the sensitivity of sulfate formation to $SO_2$ emission and heterogeneous chemistry. The results show that doubling $SO_2$ emission does not significantly enhance sulfate concentrations, but incorporating heterogeneous sulfate formation does, suggesting missing chemical formation of sulfate is likely to be the cause of the underestimation of sulfate. Domain mean sulfate concentrations increase 8.8μg/$m^3$ after including heterogeneous sulfate formation, and the temporal variations of simulated sulfate in

Beijing were consistent with observations after including heterogeneous sulfate formation pathway.

We expected that the overestimations of $SO_2$ concentrations at Beijing and Xianghe were due to the underestimation of sulfate. However, $SO_2$ concentrations in the HetS case are still much higher than observations. Thus, we conclude that the overestimations of $SO_2$ concentrations in the NCP are mostly due to errors in $SO_2$ emission inventory and the underestimation of sulfate is mainly attributed to low $SO_2$ to sulfate conversion rate.

## 5.6 References


Boylan, J.W., Russell, A.G., 2006. PM and light extinction model performance metrics, goals, and criteria for three-dimensional air quality models. Atmos. Environ. 40, 4946–4959. doi:10.1016/j.atmosenv.2005.09.087

Damian, V., Sandu, A., Damian, M., 2002. The kinetic preprocessor KPP-a software environment for solving chemical kinetics. Comput. Chem. … 26, 1567–1579.

Dentener, F.J., Carmichael, G.R., Zhang, Y., Lelieveld, J., Crutzen, P.J., 1996. Role of mineral aerosol as a reactive surface in the global troposphere. J. Geophys. Res. 101.

Ding, Jie; Zhu, T., 2003. Heterogeneous reactions on the surface of fine particles in the atmosphere. Chinese Sci. Bull. 48, 2267. doi:10.1360/03wb0046

Gao, M., Guttikunda, S.K., Carmichael, G.R., Wang, Y., Liu, Z., Stanier, C.O., Saide, P.E., Yu, M., 2015. Health impacts and economic losses assessment of the 2013 severe haze event in Beijing area. Sci. Total Environ. 511, 553–561. doi:10.1016/j.scitotenv.2015.01.005

Gao, Y., Zhang, M., Liu, Z., Wang, L., Wang, P., Xia, X., Tao, M., Zhu, L., 2015. Modeling the feedback between aerosol and meteorological variables in the atmospheric boundary layer during a severe fog–haze event over the North China Plain. Atmos. Chem. Phys. 15, 4279–4295. doi:10.5194/acp-15-4279-2015

He, H., Wang, Y., Ma, Q., Ma, J., Chu, B., Ji, D., Tang, G., Liu, C., Zhang, H., Hao, J., 2014. Mineral dust and NOx promote the conversion of SO2 to sulfate in heavy pollution days. Sci. Rep. 4, 4172. doi:10.1038/srep04172

Heikes, Brian G;Thompson, A.M., 1983. Effects of heterogeenous processes on NO3, HONO, and HNO3 chemistry in the troposphere. J. Geophys. Res. 88.

Huang, R.-J., Zhang, Y., Bozzetti, C., Ho, K.-F., Cao, J.-J., Han, Y., Daellenbach, K.R., Slowik, J.G., Platt, S.M., Canonaco, F., Zotter, P., Wolf, R., Pieber, S.M., Bruns, E. a., Crippa, M., Ciarelli, G., Piazzalunga, A., Schwikowski, M., Abbaszade, G., Schnelle-Kreis, J., Zimmermann, R., An, Z., Szidat, S., Baltensperger, U., Haddad, I. El, Prévôt, A.S.H., 2014. High secondary aerosol contribution to particulate pollution during haze events in China. Nature. doi:10.1038/nature13774

Kumar, R., Barth, M.C., Madronich, S., Naja, M., Carmichael, G.R., Pfister, G.G., Knote, C., Brasseur, G.P., Ojha, N., Sarangi, T., 2014. Effects of dust aerosols on tropospheric chemistry during a typical pre-monsoon season dust storm in northern India. Atmos. Chem. Phys. 14, 6813–6834. doi:10.5194/acp-14-6813-2014

Misenis, C., Zhang, Y., 2010. An examination of sensitivity of WRF/Chem predictions to physical parameterizations, horizontal grid spacing, and nesting options. Atmos. Res. 97, 315–334. doi:10.1016/j.atmosres.2010.04.005

Preszler Prince, A., Kleiber, P., Grassian, V.H., Young, M. a, 2007. Heterogeneous interactions of calcite aerosol with sulfur dioxide and sulfur dioxide-nitric acid mixtures. Phys. Chem. Chem. Phys. 9, 3432–3439. doi:10.1039/b703296j

Quan, J., Tie, X., Zhang, Q., Liu, Q., Li, X., Gao, Y., Zhao, D., 2014. Characteristics of heavy aerosol pollution during the 2012–2013 winter in Beijing, China. Atmos. Environ. 88, 83–89. doi:10.1016/j.atmosenv.2014.01.058

Sievering, H.; Boatman, J.; Galloway, J.; Keene, W.; Kim, Y.; Luria, M.; Ray, J., 1991. Heterogeneous sulfur conversion in sea-salt aerosol particles: the role of aerosol water content and size distribution. Atmos. Environ. 25.

Song, C.H., Kim, C.M., Lee, Y.J., Carmichael, G.R., Lee, B.K., Lee, D.S., 2007. An evaluation of reaction probabilities of sulfate and nitrate precursors onto East Asian dust particles. J. Geophys. Res. 112, D18206. doi:10.1029/2006JD008092

Sun, Yele; Jiang, Qi; Wang, Zifa; Fu, Pingqing; Li, Jie; Yang, Ting; Yin, Y., 2014. Investigation of the sources and evolution processes of severe haze pollution in Beijing in January 2013. J. Geophys. Res. Atmos. 119, 4380–4398. doi:10.1002/2014JD021641.Received

Tuccella, P., Curci, G., Visconti, G., Bessagnet, B., Menut, L., Park, R.J., 2012. Modeling of gas and aerosol with WRF/Chem over Europe: Evaluation and sensitivity study. J. Geophys. Res. 117, D03303. doi:10.1029/2011JD016302

Usher, C.R., 2002. A laboratory study of the heterogeneous uptake and oxidation of sulfur dioxide on mineral dust particles. J. Geophys. Res. 107. doi:10.1029/2002JD002051

Wang, K., Zhang, Y., Nenes, a., Fountoukis, C., 2012. Implementation of dust emission and chemistry into the Community Multiscale Air Quality modeling system and initial application to an Asian dust storm episode. Atmos. Chem. Phys. 12, 10209–10237. doi:10.5194/acp-12-10209-2012

Wang, L., Zhang, Y., Wang, K., Zheng, B., Zhang, Q., Wei, W., 2014. Application of Weather Research and Forecasting Model with Chemistry (WRF/Chem) over northern China: Sensitivity study, comparative evaluation, and policy implications. Atmos. Environ. doi:10.1016/j.atmosenv.2014.12.052

Wang, Y., Yao, L., Wang, L., Liu, Z., Ji, D., Tang, G., Zhang, J., Sun, Y., Hu, B., Xin, J., 2014. Mechanism for the formation of the January 2013 heavy haze pollution episode over central and eastern China. Sci. China Earth Sci. 57, 14–25. doi:10.1007/s11430-013-4773-4

Wang, Y., Zhang, Q., Jiang, J., Zhou, W., Wang, B., He, K., Duan, F., Zhang, Q., Philip, S., Xie, Y., 2014. Enhanced sulfate formation during China's severe winter haze episode in January 2013 missing from current models. J. Geophys. Res. Atmos. 425–440. doi:10.1002/2013JD021426.Received

Zaveri, R. a., Easter, R.C., Fast, J.D., Peters, L.K., 2008. Model for Simulating Aerosol Interactions and Chemistry (MOSAIC). J. Geophys. Res. 113, D13204. doi:10.1029/2007JD008782

Zhang, J.K., Sun, Y., Liu, Z.R., Ji, D.S., Hu, B., Liu, Q., Wang, Y.S., 2014. Characterization of submicron aerosols during a month of serious pollution in Beijing, 2013. Atmos. Chem. Phys. 14, 2887–2903. doi:10.5194/acp-14-2887-2014

Zhang, R., Li, Q., Zhang, R., 2014. Meteorological conditions for the persistent severe fog and haze event over eastern China in January 2013. Sci. China Earth Sci. 57, 26–35. doi:10.1007/s11430-013-4774-3

Zhang, Y., Wen, X.-Y., Jang, C.J., 2010. Simulating chemistry–aerosol–cloud–radiation–climate feedbacks over the continental U.S. using the online-coupled Weather Research Forecasting Model with chemistry (WRF/Chem). Atmos. Environ. 44, 3568–3582. doi:10.1016/j.atmosenv.2010.05.056

Zhang, Yang; Carmichael, G.R., 1999. The Role of Mineral Aerosol in Tropospheric Chemistry in East Asia—A Model Study. J. Clim. Appl. Meteorol. 38, 353–367.

Zheng, B., Zhang, Q., Zhang, Y., He, K.B., Wang, K., Zheng, G.J., Duan, F.K., Ma, Y.L., Kimoto, T., 2015. Heterogeneous chemistry: a mechanism missing in current models to explain secondary inorganic aerosol formation during the January 2013 haze episode in North China. Atmos. Chem. Phys. Discuss. 14, 16731–16776. doi:10.5194/acpd-14-16731-2014

Zheng, G.J., Duan, F.K., Su, H., Ma, Y.L., Cheng, Y., Zheng, B., Zhang, Q., Huang, T., Kimoto, T., Chang, D., Pöschl, U., Cheng, Y.F., He, K.B., 2015. Exploring the severe winter haze in Beijing: the impact of synoptic weather, regional transport and heterogeneous reactions. Atmos. Chem. Phys. 15, 2969–2983. doi:10.5194/acp-15-2969-2015

# CHAPTER 6 CONSTRANTS OF SURFACE $PM_{2.5}$ PREDICTIONS USING 3DVAR ASSIMILATION: A POTENIAL OPPORTUNITY FOR BETTER RADIATIVE FORCING ESTIMATES[61]

## 6.1 Abstract

Large uncertainties exist in anthropogenic aerosol radiative forcing estimates in polluted China due to discrepancies between simulated aerosol and observations. In this study, the 3DVAR GSI DA system coupled with the fully online coupled WRF-Chem model is shown to improve the $PM_{2.5}$ predicts during a severe haze event by assimilating surface $PM_{2.5}$ measurements. The correlation coefficients between observations and model results are improved from 0.67 to 0.94. The enhanced $PM_{2.5}$ concentrations due to DA have significant effects on anthropogenic aerosol radiative forcing. We estimate the daytime monthly mean anthropogenic aerosol radiative forcing to be -29.9W/$m^2$ at the surface, 27.0W/$m^2$ inside the atmosphere, and -2.9W/$m^2$ at the top of the atmosphere using the constrained model simulations. Due to DA, the domain mean changes of daytime forcing at the surface, inside the atmosphere and at the TOA are -3.0, 2.8, and -0.2W/$m^2$, respectively.

## 6.2 Introduction

Large aerosol loadings in the North China Palin (NCP) adversely influence visibility, human health (Gao et al., 2015) and climate radiative forcing (Gao et al., 2014). Although there have been great advances in predicting aerosols, it is still challenging due to poor model parameterization, missing aerosol formation mechanisms, and large uncertainties in emission

[61] This work is under preparation to be submitted.

inventory (Carmichael et al., 2008). As a result, large discrepancies can exist between model and observations, and these discrepancies lead to large uncertainties in estimates of above-mentioned effects.

Data assimilation (DA) is a powerful technique to combine model results and observations to reduce uncertainties (Niu et al., 2008; Schwartz et al., 2012). There are various DA algorithms, including nudging, optimal interpolation, 3-dimensional variation (3DVAR), 4-dimensional variation (4DVAR) and ensemble Kalman filter (EnKF). DA has been widely used in meteorology for more than three decades, but its application in air quality modeling is a relatively recent study area (Pagowski et al., 2010; Tombette et al., 2009). A 4DVAR data assimilation was developed by Elbern et al. (Elbern et al., 1997, 2000; Elbern and Schmidt, 1999, 2001) and applied to improve $SO_2$ and ozone predictions. 4DVAR was also used to assimilate many trace gases, including ozone, NO, $NO_2$, $HNO_3$, and the improved initial conditions significantly reduce the dissimilarities between model and measurements (Chai et al., 2006, 2007). Besides tracer gases, aerosol measurements or Aerosol Optical Depth (AOD) from multiple platforms have been assimilated to improve model predictions using various methods, including optimal interpolation (Adhikary et al., 2008; Chung et al., 2010), 3DVAR (Chen et al., 2014; Jiang et al., 2013; Liu et al., 2011; Niu et al., 2008; Pagowski et al., 2010; Schwartz et al., 2012), and EnKF (Lin et al., 2008; Pagowski and Grell, 2012; Schutgens et al., 2010). However, aerosol data assimilation studies in China, particularly $PM_{2.5}$ data assimilation, are still limited due to lack of chemical observations. In addition, $PM_{2.5}$ is complicated to be treated in DA since it has various species and it will be computational expensive to assimilate it. With the improvements of computational resources and increasing presences of chemical observations, this study area can be further investigated.

In this study, we extended the 3DVAR Grid-point Statistical Interpolation (GSI) system for the Weather Research and Forecasting model coupled with Chemistry (WRF-Chem) to its use with the commonly used MOSAIC aerosol model, and applied it to evaluate the impacts of assimilating surface $PM_{2.5}$ concentrations on model predictions and anthropogenic aerosol radiative forcing during a severe haze event in the North China Plain.

## 6.3 Modeling and DA systems

### 6.3.1 WRF-Chem model configurations

We simulated $PM_{2.5}$ concentrations using the WRF-Chem model version 3.5.1. We used two nested domains with 80×56 and 48×48 grids and the resolution of the innermost domain is 27km (Figure 6.1). Other domain settings and model inputs (meteorological and chemical initial and boundary conditions, anthropogenic and biogenic emissions) are the same as Gao et al. (2015).

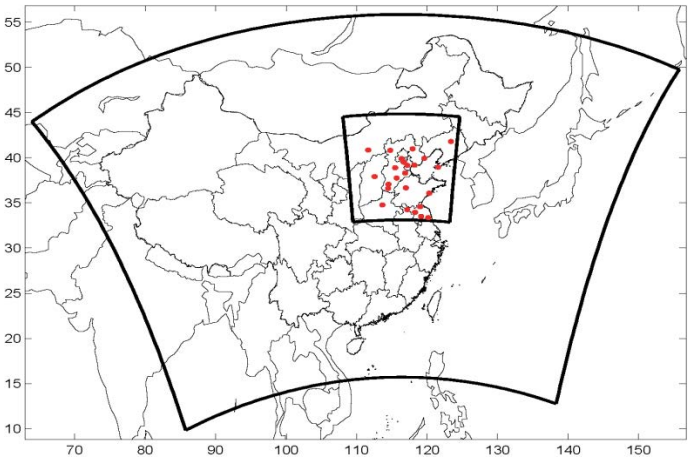


Figure 6.1. The model domain and the locations of measurement sites

### 6.3.2 GSI 3DVAR DA system

The GSI 3DVAR DA system is flexible, and can be run efficiently on many parallel computing platforms. It provides an analysis by minimizing a cost function as shown below:

$$J(x) = (x - x_b)^T B^{-1}(x - x_b) + (y - H(x))^T R^{-1}(y - H(x))$$

In this equation, x is a vector of analysis, $x_b$ denotes the forecast or background vector, y is an observation vector, B represents the background error covariance matrix, and R represents the observation error covariance matrix. Measurement and representativeness errors are combined by each element of the matrix. H is observation operator to transform model grid point values to observed quantities. The analysis variables in GSI can be unbalanced velocity potential, unbalanced part of temperature, unbalanced part of surface pressure and pseudo-relative humidity. For each analysis variable, background error covariance statistics (BECs) is required by 3DVAR data assimilation technique. In this study, the total mass per size bin instead of each $PM_{2.5}$ component, is used as control variable, which efficiently reduces the computational complexity (Saide et al., 2013). The standard deviations and vertical as well as horizontal length scales are calculated using the NMC (National Meteorological Center) method (Parrish & Derber, 1992). This method commonly uses 24- and 48-h forecasts or 12- and 24-h forecasts to compute statistics, but we use NCEP Final Analysis and ECMWF reanalysis data to calculate the statistics because this way is much computational cheaper (Saide et al., 2013).

The observation operator interpolates the aerosol analysis to the observation location and vertical extrapolation is not performed in this study. Hourly surface $PM_{2.5}$ concentrations are from the Ministry of Environmental Protection (MEP) of China stations (locations are shown in red in Figure 6.1) and observations within 1 hour window of the analysis were assimilated. The observation errors contain two parts: measurement errors and representativeness errors. The

measurement error is computed using $e_o = 1.5 + 0.0075 * Obs$, where Obs means observation values. The representativeness errors depend on the locations of the measurement sites, and are defined following Elbern et al. (2007).

### 6.3.3 Experimental Design

Two parallel experiments were designed to examine the influences of assimilating surface $PM_{2.5}$ on forecasting aerosols. One control case (CTL, also called NODA) was employed without data assimilation, and the other one (called DA) was performed via assimilating surface $PM_{2.5}$ concentrations. The experiments were conducted using same domain settings (shown in Figure 6.1) and model settings. The influences of $PM_{2.5}$ DA was first tested by performing a 24 hour test run, which initiated on 1 January, 2013 00:00 UTC and the results will be shown in section 6.4.1. Based on the results, the DA was then conducted by assimilating surface $PM_{2.5}$ every three hours from 1 January, 2013 00:00 UTC to 31 January, 2013 21:00 UTC. The analyses that were assimilated were valid at 00:00 UTC, 03:00 UTC, 06:00 UTC, 09:00 UTC, 12:00 UTC, 15:00 UTC, 18:00 UTC, and 21:00 UTC. There was no meteorological data assimilation performed in this study.

## 6.4 Results

### 6.4.1 Verification of 24 hour $PM_{2.5}$ Forecasts

The model $PM_{2.5}$ forecasts with and without DA were verified against surface $PM_{2.5}$ measurements. The simulated and observed $PM_{2.5}$ concentrations averaged over all sites

(locations are shown in Figure 6.1) are shown in Figure 6.2(a), and the $PM_{2.5}$ concentrations were overestimated by the model (NODA). The DA case shows better agreements with observations, particularly in the first several hours, indicating the improvements of $PM_{2.5}$ forecasts via data assimilation. However, the impacts of DA die out quickly and $PM_{2.5}$ forecasts with and without DA become very close after 18 hours. The improvements and decreasing impacts of better initial conditions can also be found in the calculated correlation coefficients between model and observations (Figure 6.2(b)), and calculated root mean square errors (RMSE) (Figure 6.2(c)). The correlation coefficient between model and observations increases from 0.38 to 0.81 at the first forecast hour after assimilating $PM_{2.5}$, but the impacts on correlation become insignificant after about 3 hours (Figure 6.2(b)). The RMSE values drops from 89.35μg/$m^3$ to 43.29μg/$m^3$ at the first forecast hour due to DA, and the impacts of DA on RMSE are almost gone after 19 hours (Figure 6.2(c)). The difference of RMSE of NODA case and DA case shows sharply decreases in the first three forecast hours, and then decrease slowly before becoming close to zero (Figure 6.2(c)). Since the improvements due to DA are great within three hours and die out after a long time, we decided to assimilate surface $PM_{2.5}$ concentrations every 3 hours.

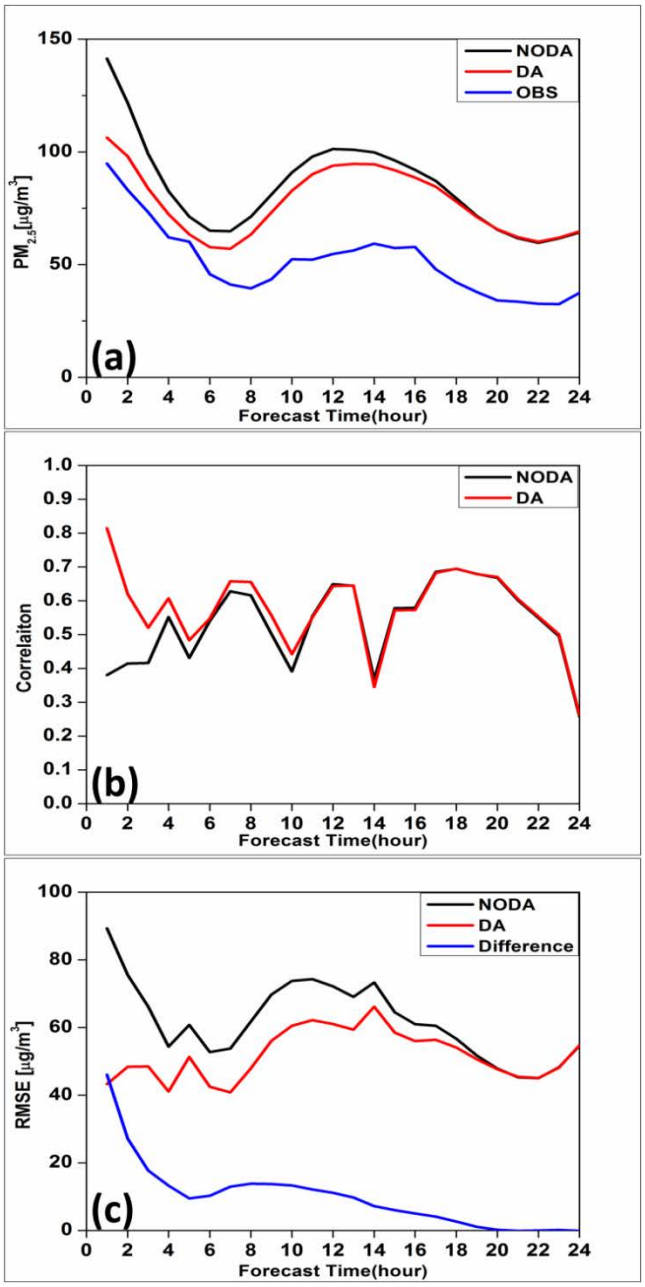


Figure 6.2. Mean $PM_{2.5}$ concentrations (a), correlation coefficients (b), and RMSE as a function of forecast hour for all sites shown in Figure 6.1

### 6.4.2 Impacts on $PM_{2.5}$ Initial Conditions

The $PM_{2.5}$ concentrations at all 00:00UTC, 06:00UTC, 12:00UTC and 18:00UTC over the whole month were plotted against observations and shown in Figure 6.3. After DA, the slope is closer to 1, indicating DA improves the initial fields effectively. The spatial distributions of averaged surface $PM_{2.5}$ differences (DA minus CTL) at 00:00UTC, 06:00UTC, 12:00UTC and 18:00UTC are displayed in Figure 6.4. Generally, the patterns are similar at four moments. At 00:00UTC, the differences in most NCP regions are positive and are negative in southwest domain areas, indicating the DA increases simulated $PM_{2.5}$ in most NCP regions and decreases simulated $PM_{2.5}$ in southwest domain areas. At 06:00UTC, DA increases simulated $PM_{2.5}$ at a higher level, with more than 80μg/$m^3$ enhancement in southern Hebei province. This plot also implies that the errors in emission vary in both time and space since the differences that shown in Figure 6.4 have variations over time and space.

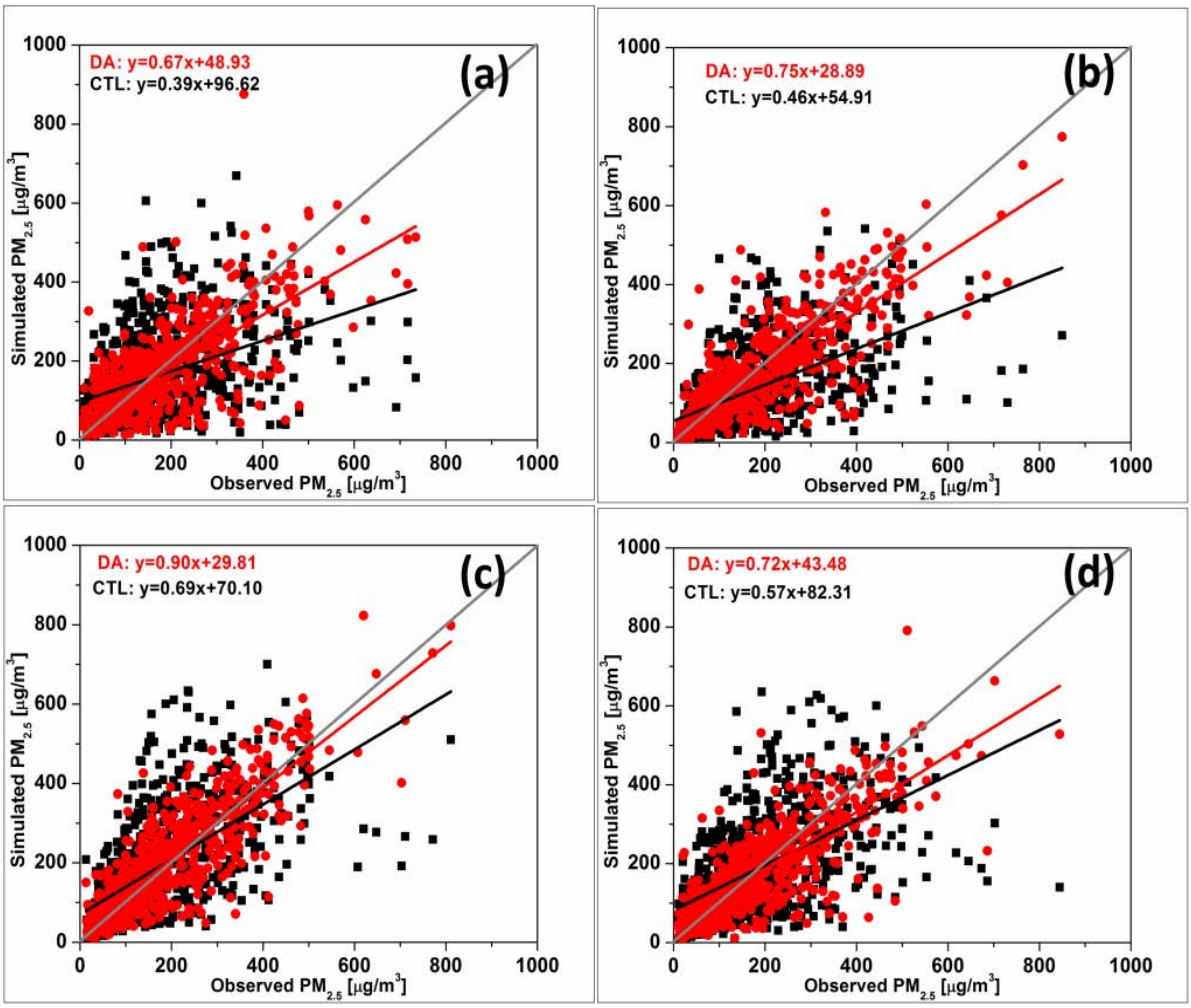


Figure 6.3. Scatter plots of simulated (CTL and DA cases) and observed $PM_{2.5}$ concentrations at all (a) 00:00, (b) 06:00, (c) 12:00 and (d) 18:00 UTC

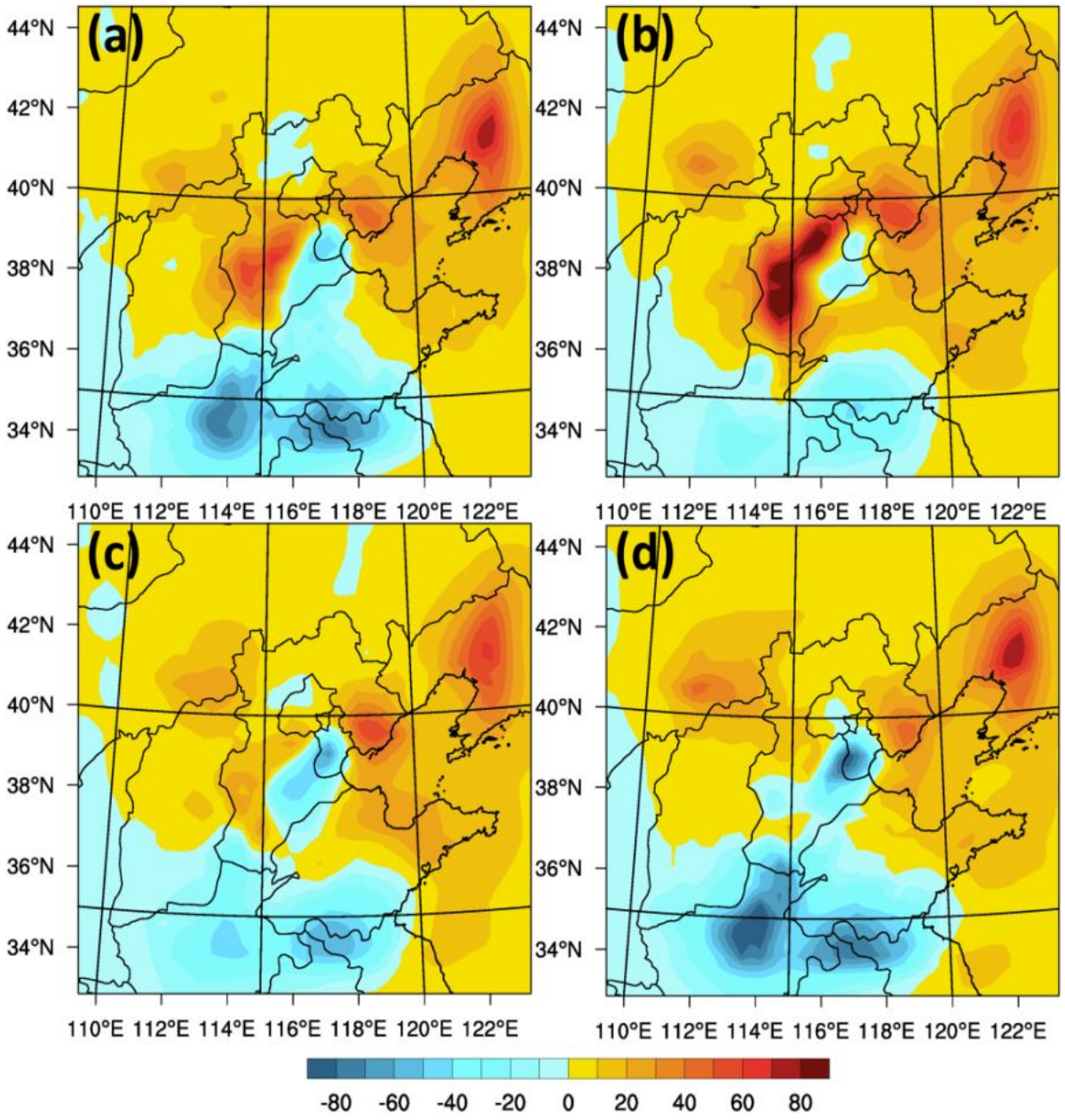


Figure 6.4. Averaged surface $PM_{2.5}$ differences (DA minus CTL) at all (a) 00:00, (b) 06:00, (c) 12:00 and (d) 18:00 UTC

### 6.4.3 Performance of $PM_{2.5}$ DA

Figure 6.5(a) shows observed and simulated $PM_{2.5}$ averaged over all measurement sites. The NODA case significantly underestimates $PM_{2.5}$ concentrations in the 12-14 January haze episode and overestimates $PM_{2.5}$ at the end of January. These underestimations and overestimations are corrected well by assimilating surface $PM_{2.5}$ every 3 hours. The correlation between simulated and observed $PM_{2.5}$ averaged over all stations improves from 0.67 to 0.94 (Table 6.1) after assimilating surface $PM_{2.5}$ concentrations. Other metrics, including mean bias (MB), mean error (ME), mean fractional bias (MFB), mean fractional error (MFE) and RMSE, are also calculated to quantify for changes after DA. Due to DA, RMSE are reduced from 38.0μg/$m^3$ to 20.5μg/$m^3$, and MFE decreases from 22% to 10% (Table 6.1).

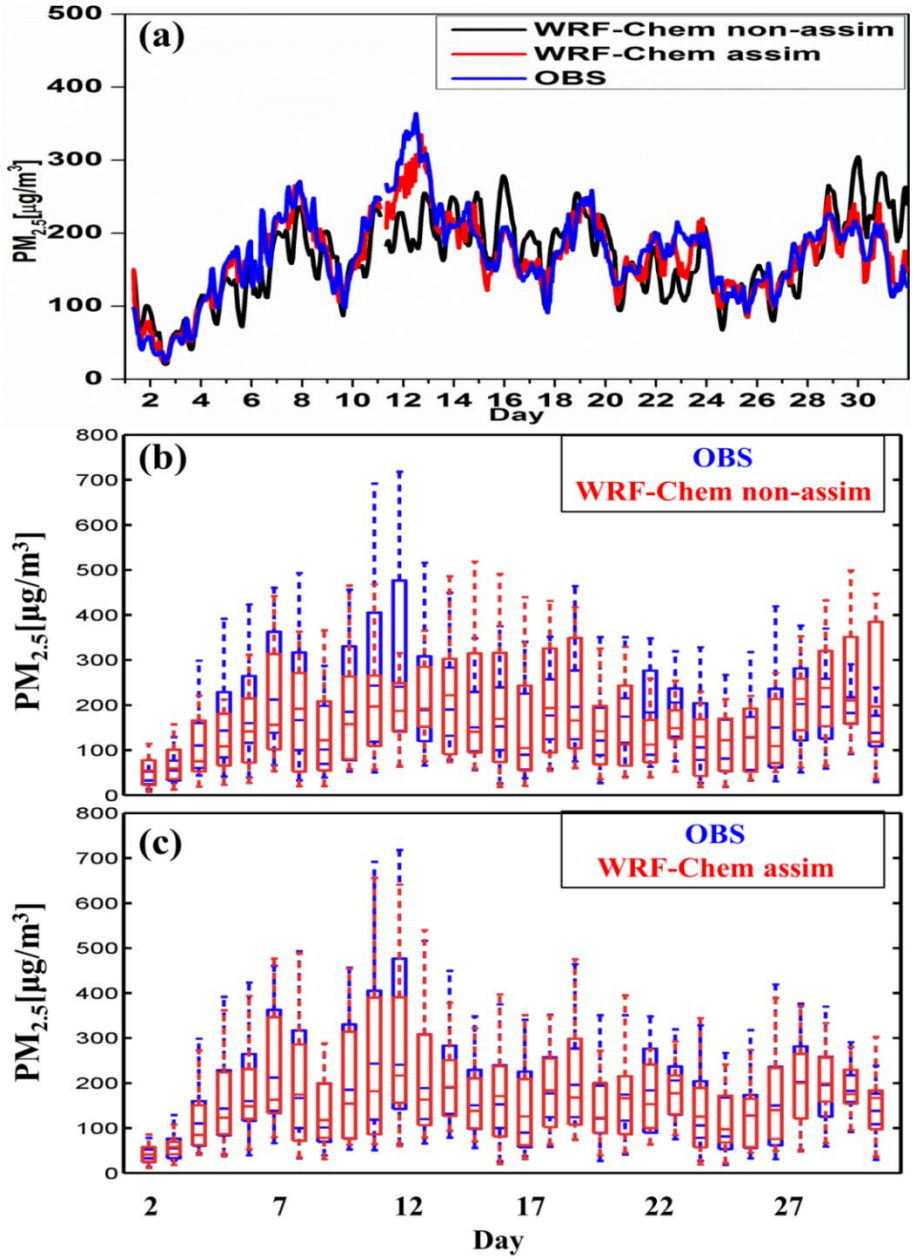


Figure 6.5. Observed and simulated (DA and NODA) hourly $PM_{2.5}$ concentrations averaged over all measurement sites (a), and whisker plot for observed daily mean $PM_{2.5}$ concentration and simulation in NODA case (b) and DA case (c)

Figure 6.5(b) displays the whisker plot of observed daily mean $PM_{2.5}$ concentrations and simulations in the NODA case. From January 9 to January 13, $PM_{2.5}$ concentrations are largely underestimated by the model. From January 28 to January 31, $PM_{2.5}$ concentrations are overestimated by the model. The model performance during these two episodes has been substantially improved by assimilating surface $PM_{2.5}$ measurements, as shown in Figure 6.5(c). After assimilating surface $PM_{2.5}$ measurements, median and maximum values show lower differences with observations.

The performance of DA has also been tested using three non-assimilated station and the comparisons are shown in Figure 6.6. In the Beijing IAP and Xianghe stations, the underestimation and overestimation of $PM_{2.5}$ during the above-mentioned two episodes have been improved. The correlation coefficients between simulation and observation have been improved from 0.73 to 0.86, and from 0.53 to 0.64 in the Beijing IAP and Xianghe stations, respectively. However, in the Xinglong station, DA does not improve the simulation according to the comparison with observations. This is mainly because Xinglong station is far away from the assimilated stations (Figure 3.1 and Figure 6.1) and thus DA has slight effects on the simulation.

Figure 6.7 shows the simulated monthly mean surface $PM_{2.5}$ concentrations in NODA case (a), in DA case (b), and the differences between them (c). In the NODA case, monthly mean surface $PM_{2.5}$ concentrations in most east China areas are above 200μg/m$^3$. Due to DA, the maximum positive changes (more than 80μg/m$^3$) occur in Liaoning province and the maximum negative changes happen in north Jiangsu province. In general, assimilating surface $PM_{2.5}$ observations increases $PM_{2.5}$ concentrations in the NCP, except in Tianjin. In south Hebei province, monthly mean $PM_{2.5}$ concentrations increase more than 40μg/m$^3$.

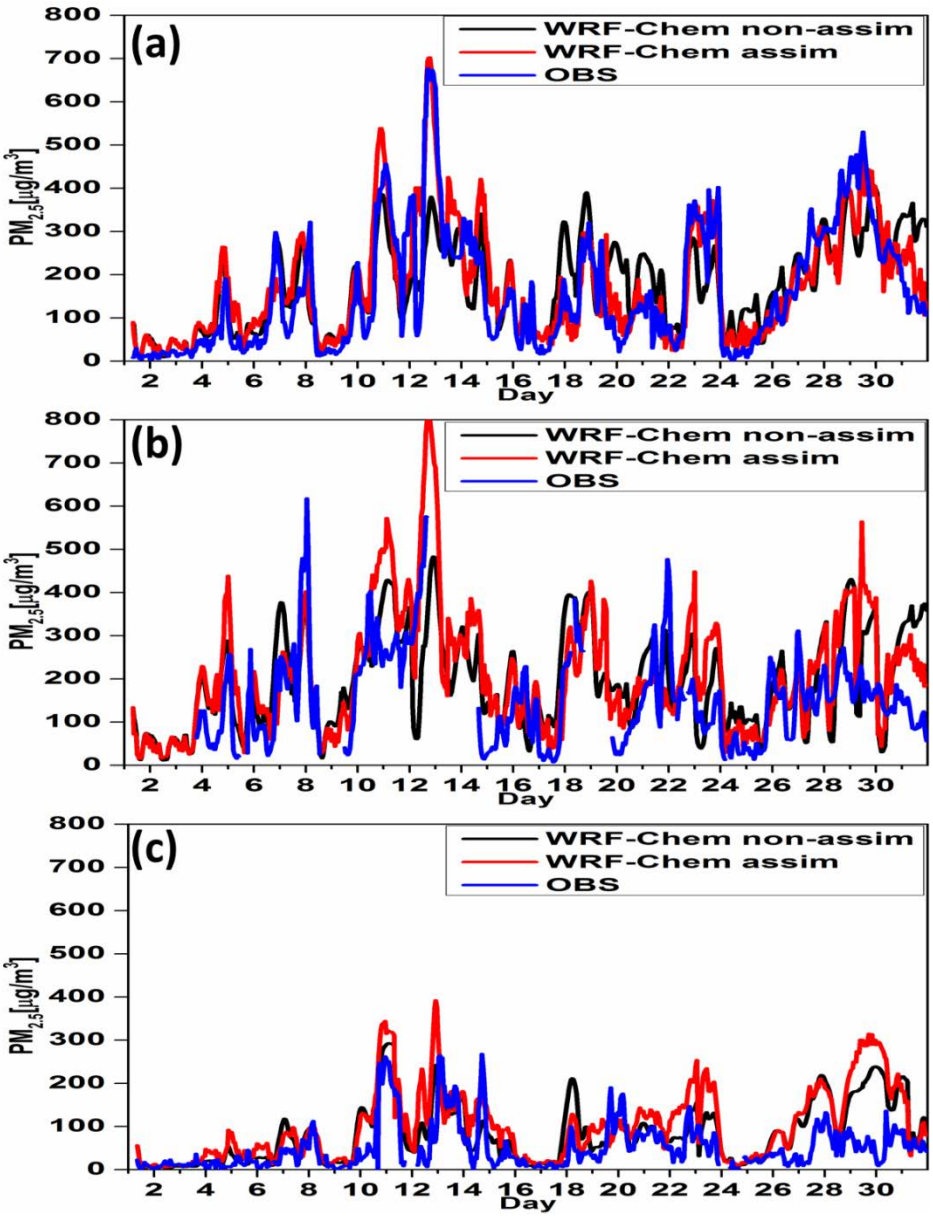


Figure 6.6. Comparisons between simulated and observed hourly $PM_{2.5}$ concentrations at three non-assimilated sites: Beijing IAP station (a), Xianghe (b), and Xinglong (c)

Table 6.1. Statistics for simulated $PM_{2.5}$ with and without DA compared against observations

| | MB ($\mu g/m^3$) | ME ($\mu g/m^3$) | MFB | MFE | RMSE ($\mu g/m^3$) | R |
|---|---|---|---|---|---|---|
| noDA | -6.1 | 37.0 | -3.0% | 20% | 38.0 | 0.67 |
| DA | -3.8 | 14.9 | -1.0% | 10% | 20.5 | 0.94 |

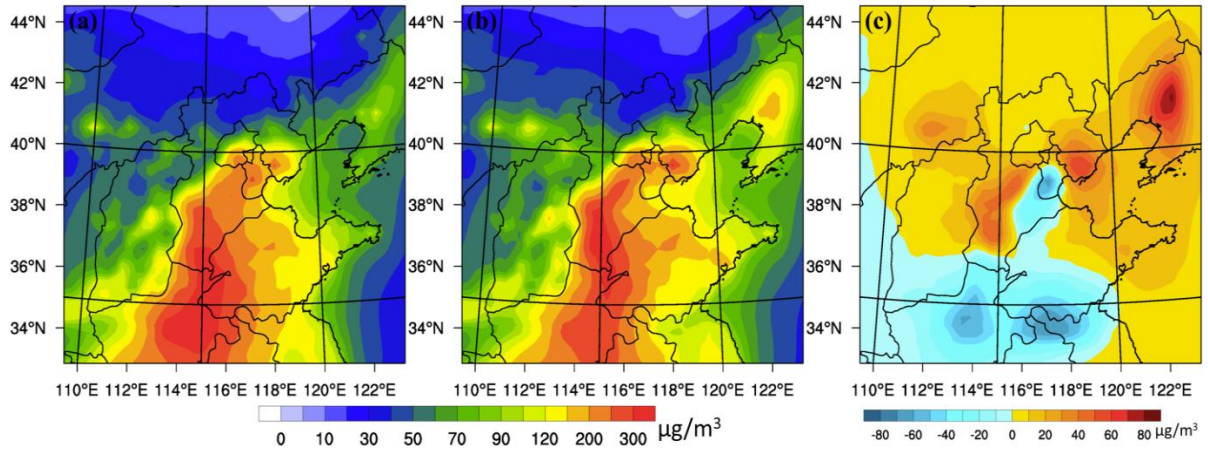


Figure 6.7. Monthly mean surface $PM_{2.5}$ in NODA case (a), DA case (b) and the differences (DA minus CTL) (c)

### 6.4.4 Impacts on estimates of anthropogenic radiative forcing

Figure 6.8 shows monthly averaged daytime (8:00 to 17:00) anthropogenic radiative forcing at the surface, inside the atmosphere and at the top of the atmosphere derived from CTL and DA cases. Forcing at the surface is negative over the entire domain and values are pronounced in the east and south regions. The domain mean forcing at the surface is about -26.9 $W/m^2$, and the domain forcing inside the atmosphere is comparable to it, but with a opposite sign (+24.2 $W/m^2$). The forcing at the top of the atmosphere has negative values in the east areas, including the East

China Sea, and is positive in west NCP, east Shanxi province and Inner Mongolia. The domain mean forcing at the TOA is about -2.7 W/m$^2$.

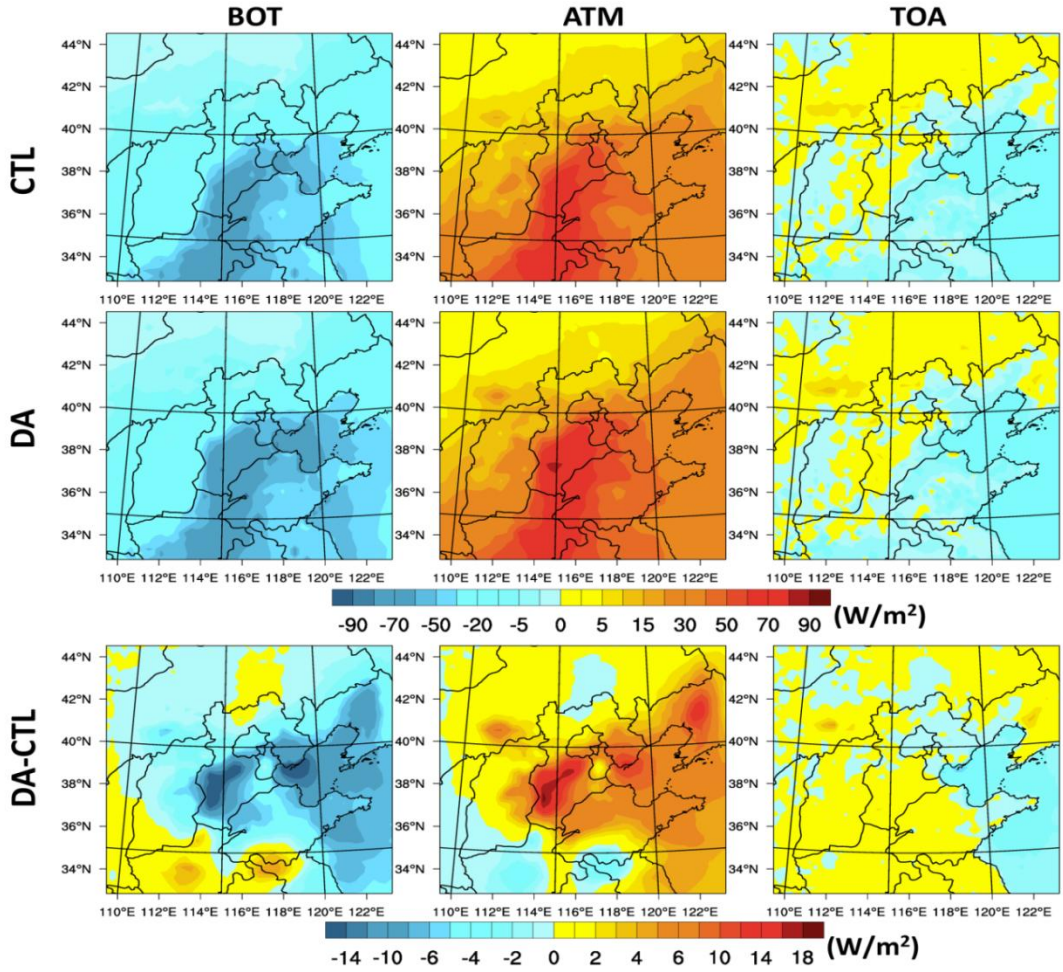


Figure 6.8. Monthly daytime all-skies anthropogenic radiative forcing (W/m$^2$) at the surface (BOT, positive values represent downward direction), inside the atmosphere (ATM, positive values indicate heating of the atmosphere) and at the top of the atmosphere (TOA, positive values denote downward direction) for CTL and DA cases; the last row refers to the differences between the CTL and DA cases

Due to the relatively large negative MBs shown in Table 6.1, the anthropogenic radiative forcing might have large uncertainties. To constrain this, we also derived anthropogenic radiative forcing with aerosols from the DA case, which has lower errors compared to observations. The patterns of forcing at the surface, inside the atmosphere and at the TOA are similar to the results from CTL case. Because of DA, radiative forcing at the surface decreases in most areas, but increases in the south domain regions, corresponding to the Changes shown in Figure 6.8. In CTL case, domain mean daytime forcing are -29.9W/$m^2$ at the surface, 27.0W/$m^2$ inside the atmosphere, and -2.9W/$m^2$ at the TOA. The domain mean changes of forcing at the surface, inside the atmosphere and at the TOA are -3.0, 2.8, and -0.2 W/$m^2$, respectively.

## 6.5 Summary

The capability of assimilating hourly surface $PM_{2.5}$ observations was added into the GSI 3DVAR system. This system with the WRF-Chem model was applied to reproduce the hazy month in January 2013. Two experiments were performed: a control experiment without DA and a DA experiment with aerosol analysis updated every 3h. The results show that surface $PM_{2.5}$ concentrations were significantly improved in terms of correlation coefficient, RMSE, MFB, MFE. The correlation coefficients between simulated and observed $PM_{2.5}$ averaged over all stations has been improved from 0.67 to 0.94. The DA system also improves $PM_{2.5}$ concentrations in the regions where observations were not assimilated. Due to DA, the monthly mean changes $PM_{2.5}$ concentrations can be over 80μg/$m^3$ in some areas.

The improved $PM_{2.5}$ concentrations due to DA have significant effects on anthropogenic aerosol radiative forcing. Due to DA, the domain mean changes of daytime forcing at the

surface, inside the atmosphere and at the TOA are -3.0, 2.8, and -0.2W/m$^2$, respectively. We estimated the daytime monthly mean anthropogenic aerosol radiative forcing to be -29.9W/m$^2$ at the surface, 27.0W/m$^2$ inside the atmosphere, and -2.9W/m$^2$ at the top of the atmosphere using the constrained model simulations.

This study proves that better initial conditions provided by DA can improve only short-term predictions since the impacts of errors in emission inventory or model will dominate after several hours. As the errors in emission inventory is the major cause of uncertainties in air quality modeling, particularly in polluted regions, like East Asia, it will be promising to improve air quality modeling by constrain uncertainties in emission inventory. In the future, better predictions of aerosol can be expected by using both adjusting initial conditions and constraining errors in emission inventory.

## 6.6 References


Adhikary, B., Kulkarni, S., Dallura, a., Tang, Y., Chai, T., Leung, L.R., Qian, Y., Chung, C.E., Ramanathan, V., Carmichael, G.R., 2008. A regional scale chemical transport modeling of Asian aerosols with data assimilation of AOD observations using optimal interpolation technique. Atmos. Environ. 42, 8600–8615. doi:10.1016/j.atmosenv.2008.08.031

Carmichael, G.R., Sandu, A., Chai, T., Daescu, D.N., Constantinescu, E.M., Tang, Y., 2008. Predicting air quality: Improvements through advanced methods to integrate models and measurements. J. Comput. Phys. 227, 3540–3571. doi:10.1016/j.jcp.2007.02.024

Chai, T., Carmichael, G.R., Sandu, A., Tang, Y., Daescu, D.N., 2006. Chemical data assimilation of Transport and Chemical Evolution over the Pacific (TRACE-P) aircraft measurements. J. Geophys. Res. Atmos. 111, 1–18. doi:10.1029/2005JD005883

Chai, T., Carmichael, G.R., Tang, Y., Sandu, A., Hardesty, M., Pilewskie, P., Whitlow, S., Browell, E. V., Avery, M. a., Nédélec, P., Merrill, J.T., Thompson, A.M., Williams, E., 2007. Four-dimensional data assimilation experiments with International Consortium for Atmospheric Research on Transport and Transformation ozone measurements. J. Geophys. Res. Atmos. 112, 1–18. doi:10.1029/2006JD007763

Chen, D., Liu, Z., Schwartz, C.S., Lin, H.-C., Cetola, J.D., Gu, Y., Xue, L., 2014. The impact of aerosol optical depth assimilation on aerosol forecasts and radiative effects during a wild fire event over the United States. Geosci. Model Dev. 7, 2709–2715. doi:10.5194/gmd-7-2709-2014

Chung, C.E., Ramanathan, V., Carmichael, G., Kulkarni, S., Tang, Y., Adhikary, B., Leung, L.R., Qian, Y., 2010. Anthropogenic aerosol radiative forcing in Asia derived from regional models with atmospheric and aerosol data assimilation. Atmos. Chem. Phys. 10, 6007–6024. doi:10.5194/acp-10-6007-2010

Elbern, H., Schmid, H., 1999. transport modeling l • j " } T. J. Geophys. Res. 104.

Elbern, H., Schmidt, H., 2001. Ozone episode analysis by four-dimensional variational chemistry data assimilation. J. Geophys. Res. 106, 3569. doi:10.1029/2000JD900448

Elbern, H., Schmidt, H., Ebel, A., 1997. for tropospheric chemistry modeling linear version of the model . The procedure is commonly. J. Geophys. Res. 102.

Elbern, H., Schmidt, H., Talagrand, O., Ebel, a., 2000. 4D-variational data assimilation with an adjoint air quality model for emission analysis. Environ. Model. Softw. 15, 539–548. doi:10.1016/S1364-8152(00)00049-9

Elbern, H., Strunk, a., Schmidt, H., Talagrand, O., 2007. Emission rate and chemical state estimation by 4-dimensional variational inversion. Atmos. Chem. Phys. Discuss. 7, 1725–1783. doi:10.5194/acpd-7-1725-2007

Gao, M., Guttikunda, S.K., Carmichael, G.R., Wang, Y., Liu, Z., Stanier, C.O., Saide, P.E., Yu, M., 2015. Health impacts and economic losses assessment of the 2013 severe haze event in Beijing area. Sci. Total Environ. 511, 553–561. doi:10.1016/j.scitotenv.2015.01.005

Gao, Y., Zhao, C., Liu, X., Zhang, M., Leung, L.R., 2014. WRF-Chem simulations of aerosols and anthropogenic aerosol radiative forcing in East Asia. Atmos. Environ. 92, 250–266. doi:10.1016/j.atmosenv.2014.04.038

Jiang, Z., Liu, Z., Wang, T., Schwartz, C.S., Lin, H.C., Jiang, F., 2013. Probing into the impact of 3DVAR assimilation of surface PM10 observations over China using process analysis. J. Geophys. Res. Atmos. 118, 6738–6749. doi:10.1002/jgrd.50495

Lin, C., Wang, Z., Zhu, J., 2008. An Ensemble Kalman Filter for severe dust storm data assimilation over China. Atmos. Chem. Phys. 8, 2975–2983. doi:10.5194/acp-8-2975-2008

Liu, Z., Liu, Q., Lin, H.C., Schwartz, C.S., Lee, Y.H., Wang, T., 2011. Three-dimensional variational assimilation of MODIS aerosol optical depth: Implementation and application to a dust storm over East Asia. J. Geophys. Res. Atmos. 116, 1–19. doi:10.1029/2011JD016159

Niu, T., Gong, S.L., Zhu, G.F., Liu, H.L., Hu, X.Q., Zhou, C.H., Wang, Y.Q., 2007. Data assimilation of dust aerosol observations for CUACE/Dust forecasting system. Atmos. Chem. Phys. Discuss. 7, 8309–8332. doi:10.5194/acpd-7-8309-2007

Pagowski, M., Grell, G. a., 2012. Experiments with the assimilation of fine aerosols using an ensemble Kalman filter. J. Geophys. Res. Atmos. 117, 1–15. doi:10.1029/2012JD018333

Pagowski, M., Grell, G. a., McKeen, S. a., Peckham, S.E., Devenyi, D., 2010. Three-dimensional variational data assimilation of ozone and fine particulate matter observations: Some results using the Weather Research and Forecasting-Chemistry model and Grid-point Statistical Interpolation. Q. J. R. Meteorol. Soc. 136, 2013–2024. doi:10.1002/qj.700

Saide, P.E., Carmichael, G.R., Liu, Z., Schwartz, C.S., Lin, H.C., Da Silva, a. M., Hyer, E., 2013. Aerosol optical depth assimilation for a size-resolved sectional model: Impacts of observationally constrained, multi-wavelength and fine mode retrievals on regional scale analyses and forecasts. Atmos. Chem. Phys. 13, 10425–10444. doi:10.5194/acp-13-10425-2013

Schutgens, N. a. J., Miyoshi, T., Takemura, T., Nakajima, T., 2009. Applying an ensemble Kalman filter to the assimilation of AERONET observations in a global aerosol transport model. Atmos. Chem. Phys. Discuss. 9, 23835–23873. doi:10.5194/acpd-9-23835-2009

Schwartz, C.S., Liu, Z., Lin, H.C., McKeen, S. a., 2012. Simultaneous three-dimensional variational assimilation of surface fine particulate matter and MODIS aerosol optical depth. J. Geophys. Res. Atmos. 117, 1–22. doi:10.1029/2011JD017383

Tombette, M., Mallet, V., Sportisse, B., 2008. $PM_{10}$ data assimilation over Europe with the optimal interpolation method. Atmos. Chem. Phys. Discuss. 8, 9607–9640. doi:10.5194/acpd-8-9607-2008

# CHAPTER 7 SUMMARY AND FUTURE WORK

## 7.1 Summary

Improvements in the understanding of the causes of winter haze events as well as the causes of increasing haze occurrences in the NCP, assessments of health and climate impacts of haze events, and advances in aerosol modeling via incorporating missing reactions and assimilating measurements were the main subjects of this thesis.

The first objective was to investigate the roles of meteorology, secondary aerosol formation, regional transport, and aerosol feedbacks in winter haze formation in the NCP. The best model configuration was found to represent the meteorology and concentrations of air pollutants during the January 2010 haze event. Various meteorology variables, including temperature, relative humidity, horizontal winds, and vertical mixing, during haze were characterized and it was found that the increases in temperature and relative humidity during haze were associated with moist warm southerly winds. The increasing ratios of primary aerosols, secondary inorganic aerosols and secondary organic aerosols from non-haze days to haze days were calculated and the role of cloud chemistry in this event was also quantified, which emphasized the importance of secondary aerosol formation and cloud chemistry in winter haze.

The contribution of regional transport to haze in Beijing was studied. A CO tracer model was built to study the role of regional transport and the FLEXPART model was used to study the transport pathways. It was found that non-local sources contributed about 47.8% to the $PM_{2.5}$ concentrations in Beijing in haze days and sources of the non-local contributions were primarily from south Hebei, Shandong and Henan provinces, which provides scientific basis to implement regional air pollution control strategies. The high aerosol loadings were shown to have important

feedbacks to decrease PBLH by more than 100 meters and increase $PM_{2.5}$ by about 20μg/$m^3$ in some areas.

The causes of increasing haze occurrences in the NCP are still unclear, which may be affected by both emission changes and meteorology changes. The responses of $PM_{2.5}$ concentrations to emission changes ($SO_2$, $NH_3$, $NH_4$, BC, and OC) and meteorology changes (temperature, relative humidity, and wind speeds) during winter haze were examined in objective two. The results suggest the increases in $SO_2$, OC and $NH_3$ emissions may be the main causes of increasing haze occurrences since surface sulfate and OC aerosols were estimated to increase by 30.8% and 26.5% due to emission changes from 1985 to 2010. Increasing $NH_3$ emissions also significantly increased $PM_{2.5}$ concentrations. Most previous similar air quality studies were conducted in Europe and the United States, and those results might not be suitable for controlling haze pollution in the NCP. The results in this objective provide some implications. Another novelty in objective two was investigating the impacts of meteorology changes on $PM_{2.5}$ concentrations using a fully online coupled model. All previous studies used offline models to conduct this kind of study, and the results might not be consistent with what is happening in the atmosphere due to the missing information in offline models. The results in objective two show that the increases in temperature lead to increases in sulfate, nitrate, and ammonium because of higher reaction rate, higher OH radicals and lower boundary layer heights, which is different from previous studies that omitted the impacts of higher temperature on wind fields and boundary layer heights. An increase in RH promoted more water aerosols and clouds, but caused decreases in dry $PM_{2.5}$ concentrations because of higher wet deposition rate, which is different than results from previous studies that found higher RH favors secondary inorganic aerosol formation.

In the third objective, the simulated $PM_{2.5}$ concentration from the WRF-Chem was used to evaluate health impacts and health-related economic losses due to severe haze events. This is the first known application of the WRF-Chem to assess short-term health risks of haze events. Previous similar studies are mostly based on observation data, but observations provide less spatial information of aerosols. Health impacts assessments show that the $PM_{2.5}$ concentrations in January were estimated to cause 690 (95% Confidence Interval (CI): (490, 890)) premature deaths, 45350 (95% CI: (21640, 57860)) acute bronchitis and 23720 (95% CI: (17090, 29710)) asthma cases in Beijing area, leading to about 253.8 (95% CI: (170.2, 331.2)) million US$ losses. This work connects haze pollution with health to stress the importance of implementing pollution control policies and protecting the public health.

The fourth objective was to improve the model performance in simulating sulfate during haze via incorporating heterogeneous chemistry. It was found that sulfate has been largely underestimated by current models compared with observations. Although the heterogeneous sulfate formation was added into some air quality models recently, like CMAQ, GEOS-Chem, the dependences of uptake coefficients were ignored or oversimplified. The novelty of this work is that the laboratory measured RH dependent $SO_2$ uptake coefficients were used. With included heterogeneous formation, model results agree better with observations, indicating that missing heterogeneous chemistry in current model may explain part of the underestimation of sulfate formation.

Although the model results were acceptable compared with observations based on acceptable air quality model performance metrics, errors still exist and were large in some days, which lead to large errors in health and climate effects estimates. Observed surface $PM_{2.5}$ concentrations were assimilated to constrain estimates of anthropogenic aerosol radiative forcing and the results

were shown in objective 5. The correlation coefficient between observations and model results was improved from 0.67 to 0.94. The data assimilation system was newly developed for the WRF-Chem model and it was first applied to constrain anthropogenic aerosol radiative forcing in China. The estimated daytime monthly mean anthropogenic aerosol radiative forcing was estimated to be -29.9W/$m^2$ at the surface, 27.0W/$m^2$ inside the atmosphere, and -2.9W/$m^2$ at the top of the atmosphere. The newly developed data assimilation system for the WRF-Chem model can also be used to improve $PM_{2.5}$ forecast to provide robust alerts for air pollution episodes, and be used to constrain estimates of health risks due to $PM_{2.5}$.

Based on the findings in this thesis, priorities should be given to control $SO_2$, $NH_3$, and OC emissions, which can be achieved by promoting the shift from coal/biofuel to cleaner energy, and by changing animal feeding and housing ways. In addition, more attention to greenhouse gases and absorbing aerosols is still necessary since absorbing aerosols play important roles in aerosol feedbacks, aerosol feedbacks can aggravate haze pollution, and increases in temperature may increase aerosol concentrations. The estimates of health and climate impacts due to haze emphasize the urgency and importance of controlling haze pollution. To protect the public health, it is of great importance to predict air pollution episodes, release alerts of incoming severe haze episodes, and take emergency measures to reduce pollution levels.

## 7.2 Future Work

In this thesis, the used CBMZ/MOSAIC mechanism is not able to simulate SOA. Even though some mechanism (such as MADE/SORGRAM) and some global and regional models consider the SOA, SOA in polluted atmospheres are still largely underestimated. This is probably because SOA involves numerous and complicated physical and chemical phenomena

(Lin et al., 2012). Recent studies have claimed that SOA is significant even under low pressure in winter haze (Huang et al., 2014). With the advance in understanding of SOA formation, more efforts should be made to improve modeling SOA during haze events.

In the chapter 3, we explored the sensitivity of $PM_{2.5}$ to emission changes using detailed $SO_2$, BC and OC emissions in 1985, inferred $NH_3$ and $NO_x$ emissions. Emissions for other species were taken from inventory for 2010. In the future, with available comprehensive historical emissions, we can obtain better relationships between emission changes and $PM_{2.5}$ concentrations.

In chapter 4, we evaluated the health impacts of the 2013 haze event using the $PM_{2.5}$ fields from the WRF-Chem model. Although the performance of WRF-Chem in simulating $PM_{2.5}$ was good compared with measurements, there were still large uncertainties. With more and more surface and satellite measurements are becoming available, we can assess the health impacts using the $PM_{2.5}$ fields that corrected by assimilating measurements from multiple platforms. Furthermore, the contribution of each emission sector (industry, power, agriculture, residential, and transportation) on human health can be further studied in the future.

In chapter 6, we only assimilated surface $PM_{2.5}$ concentrations because few satellite measurements were available during haze event. The newly released Deep Blue (DB) retrievals provide much higher sampling frequency during heavy pollution conditions (Tao et al., 2015). In the future, improving modeling aerosols in haze pollution will benefit from this dataset. Besides, the influences of aerosols on radiation vary between different aerosol species. For example, sulfate affects climate through light-scattering properties, black carbon mainly absorbs light, and organic carbon primarily scatters light (Nocakov et al., 2015). With more observations of aerosol

species becoming available in China, we can assimilate individual aerosol specie to constrain estimates of climate effects. Furthermore, the contributions of different anthropogenic emission sectors, such as power, industry, transportation, residential and agriculture, to the total anthropogenic radiative forcing can be additionally investigated in the future, which will provide useful suggestions for air pollution control from climate effects aspect.

The large uncertainties in emission inventory remarkably affect the aerosol modeling, which can be improved by using inverse modeling. Some inverse modeling methods and the adjoint model of WRF-Chem have been developed (Guerrette and Henze, 2015; Saide et al., 2015). In the future, we can apply these techniques to improve aerosol modeling by reducing uncertainties in emission inventory.

## 7.3 Reference


Gao, M., Carmichael, G.R., Wang, Y., Saide, P.E., Yu, M., Xin, J., Liu, Z., Wang, Z., 2015a. Modeling study of the 2010 regional haze event in the North China Plain. Atmos. Chem. Phys. Discuss. 15, 22781–22822. doi:10.5194/acpd-15-22781-2015

Gao, M., Guttikunda, S.K., Carmichael, G.R., Wang, Y., Liu, Z., Stanier, C.O., Saide, P.E., Yu, M., 2015b. Health impacts and economic losses assessment of the 2013 severe haze event in Beijing area. Sci. Total Environ. 511, 553–561. doi:10.1016/j.scitotenv.2015.01.005

Guerrette, J.J., Henze, D.K., 2015. Development and application of the WRFPLUS-Chem online chemistry adjoint and WRFDA-Chem assimilation system. Geosci. Model Dev. 8, 1857–1876. doi:10.5194/gmd-8-1857-2015

Huang, R.-J., Zhang, Y., Bozzetti, C., Ho, K.-F., Cao, J.-J., Han, Y., Daellenbach, K.R., Slowik, J.G., Platt, S.M., Canonaco, F., Zotter, P., Wolf, R., Pieber, S.M., Bruns, E. a., Crippa, M., Ciarelli, G., Piazzalunga, A., Schwikowski, M., Abbaszade, G., Schnelle-Kreis, J., Zimmermann, R., An, Z., Szidat, S., Baltensperger, U., Haddad, I. El, Prévôt, A.S.H., 2014.

High secondary aerosol contribution to particulate pollution during haze events in China. Nature. doi:10.1038/nature13774

Lin, G., Penner, J.E., Sillman, S., Taraborrelli, D., Lelieveld, J., 2012. Global modeling of SOA formation from dicarbonyls, epoxides, organic nitrates and peroxides. Atmos. Chem. Phys. 12, 4743–4774. doi:10.5194/acp-12-4743-2012

Novakov, T., Menon, S., Kirchstetter, T.W., Koch, D., Hansen, J.E., 2005. Aerosol organic carbon to black carbon ratios: Analysis of published data and implications for climate forcing. J. Geophys. Res. 110, 1–13. doi:10.1029/2005JD005977

Saide, P.E., Peterson, D. a., Silva, A. Da, Anderson, B., LukeD.Ziemba, Diskin, G., Sachse, G., Hair, J., Butler, C., Fenn, M., Jimenez, J.L., Campuzano-Jost, P., Perring, A.E., JoshuaP.Schwarz, Markovic, M.Z., Russell, P., Redemann, J., Shinozuka, Y., Streets, D.G., Yan, F., Dibb, J., Yokelson, R., Toon, O.B., Hyer, E., Carmichael, G.R., 2015. Revealing important nocturnal and day-to-day variations in fire smoke emissions through a multiplatform inversion. Geophys. Res. Lett. 3609–3618. doi:10.1002/2015GL063737.Received

Tao, M., Chen, L., Wang, Z., Tao, J., Che, H., Wang, X., Wang, Y., 2015. Comparison and evaluation of the MODIS Collection 6 aerosol data in China. J. Geophys. Res. Atmos. 6992–7005. doi:10.1002/2015JD023360.Received